

Aus dem Institut für Schlaganfall- und Demenzforschung
Klinikum der Universität München, Großhadern
Direktor: Prof. Dr. Martin Dichgans

Alarmin-induced atherosclerosis progression after stroke

Dissertation

Zum Erwerb des Doktorgrades der Naturwissenschaften
an der medizinischen Fakultät der
Ludwig-Maximilians-Universität zu München

vorgelegt von
Stefan Roth
aus Stuttgart
2018

Mit Genehmigung der Medizinischen Fakultät
der Universität München

Berichterstatter: PD Dr. Christof Haffner

Mitberichterstatter: Prof. Dr. Alexander Faußner

Dekan: Prof. Dr. med. dent. Reinhard HICKEL

Tag der mündlichen Prüfung: 02.10.2018

Für
Sabine und Maja

AFFIDAVIT

Roth, Stefan

Name, Vorname

Ich erkläre hiermit an Eides statt,
dass ich die vorliegende Dissertation mit dem Thema

„Alarmin-induced atherosclerosis progression after stroke“

selbstständig verfasst, mich außer der angegebenen keiner weiteren Hilfsmittel bedient und alle Erkenntnisse, die aus dem Schrifttum ganz oder annähernd übernommen sind, als solche kenntlich gemacht und nach Herkunft unter Bezeichnung der Fundstelle einzeln nachgewiesen habe.

Ich erkläre des Weiteren, dass die hier vorgelegte Dissertation nicht in gleicher oder in ähnlicher Form bei einer anderen Stelle zur Erlangung eines akademischen Grades eingereicht wurde.

München, 30.10.2018

Ort, Datum

Stefan Roth

Stefan Roth

TABLE OF CONTENTS

Affidavit	4
Table of Contents	5
Abbreviations	6
Publication list.....	7
1 Introduction	9
1.1 Stroke.....	9
1.1.1 Epidemiology	9
1.1.2 Etiology	9
1.1.3 Therapy of ischemic stroke	10
1.1.4 The systemic immune response after stroke.....	11
1.2 Atherosclerosis	14
1.2.1 Pathology.....	14
1.2.2 The role of the immune system in atheroprogession.....	15
1.2.3 Animal models of atherosclerosis	18
2 Project design	20
3 Summaries	21
3.1 Summary	21
3.2 Zusammenfassung	25
4 Research articles.....	28
4.1 DAMP signaling is a key pathway inducing immune modulation after brain injury.....	28
4.2 Brain-released alarmins and stress response synergize in accelerating atherosclerosis progression after stroke.	45
5 References	90
6 Acknowledgements	95

ABBREVIATIONS

AP-1	Activator protein 1
ApoB100	Apolipoprotein B-100
ApoE	Apolipoprotein E
CCL2	c-motif chemokine ligand 2
CCR2	c-motif chemokine receptor 2
CD	Cluster of differentiation
CX3CR1	C-X3-C motif chemokine receptor 1
DAMP	Damage/Danger-associated molecular pattern
HF diet	High fat diet
HMGB1	High mobility group box 1 protein
IFN- γ	Interferon gamma
IL-1 / 6 / 12	Interleukin 1 / 6 / 12
IRF	Interferon regulatory factor
LAA	Large-artery atherosclerosis
LDL	Low-density lipoprotein
Ly6C	Lymphocyte antigen 6 complex
M-CSF	Macrophage colony-stimulating factor
MMP	Matrix metalloproteases
MRI	Magnetic resonance imaging
NF κ B	Nuclear factor 'kappa-light-chain-enhancer' for activated B cells
OxLDL	Oxidized low-density lipoprotein
PRR	Pattern recognition receptor
Rag 1 / 2	Recombination activating gene 1 / 2
RAGE	Receptor for advanced glycation endproducts
SMC	Smooth muscle cell
SNS	Sympathetic nervous system
TNF- α	Tumor necrosis factor alpha
tPA	Tissue plasminogen activator
VCAM-1	Vascular cell adhesion molecule 1
VLA-4	Very late antigen 4
VLDL	Very low-density lipoprotein
WT	Wild type

PUBLICATION LIST

Modeling stroke in mice: permanent coagulation of the distal middle cerebral artery.

Llovera G*, **Roth S***, Plesnila N, Veltkamp R, Liesz A.; *J Vis Exp.* 2014 Jul 31;(89):e51729. doi: 10.3791/51729.

DAMP signaling is a key pathway inducing immune modulation after brain injury.

Liesz A, Dalpke A, Mracsko E, Antoine DJ, **Roth S**, Zhou W, Yang H, Na SY, Akhisaroglu M, Fleming T, Eigenbrod T, Nawroth PP, Tracey KJ, Veltkamp R.
J Neurosci. 2015 Jan 14;35(2):583-98. doi: 10.1523/JNEUROSCI.2439-14.2015.

Acquired Immunoglobulin G deficiency in stroke patients and experimental brain ischemia.

Liesz A, **Roth S**, Zorn M, Sun L, Hofmann K, Veltkamp R.
Exp Neurol. 2015 Sep;271:46-52. doi: 10.1016/j.expneurol.2015.04.021. Epub 2015 May 7

Results of a preclinical randomized controlled multicenter trial (pRCT): Anti-CD49d treatment for acute brain ischemia.

Llovera G, Hofmann K, **Roth S**, Salas-Pérdomo A, Ferrer-Ferrer M, Perego C, Zanier ER, Mamrak U, Rex A, Party H, Agin V, Fauchon C, Orset C, Haelewyn B, De Simoni MG, Dirnagl U, Grittner U, Planas AM, Plesnila N, Vivien D, Liesz A.
Sci Transl Med. 2015 Aug 5;7(299):299ra121. doi: 10.1126/scitranslmed.aaa9853.

HMGB1 as a key mediator of immune mechanisms in ischemic stroke.

Singh V, **Roth S**, Veltkamp R, Liesz A.
Antioxid Redox Signal. 2016 Apr 20;24(12):635-51. doi: 10.1089/ars.2015.6397. Epub 2015 Nov 30.
Review.

Stroke research at the crossroads – where are we heading?

Roth S, Liesz A.
Swiss Med Wkly. 2016 Jul 11;146:w14329. doi: 10.4414/smw.2016.14329. eCollection 2016. Review.

Microbiota dysbiosis controls the neuroinflammatory response after stroke.

Singh V*, **Roth S***, Llovera G, Sadler R, Garzetti D, Stecher B, Dichgans M, Liesz A.
J Neurosci. 2016 Jul 13;36(28):7428-40. doi: 10.1523/JNEUROSCI.1114-16.2016.

Inadequate food and water intake determine mortality following stroke in mice.

*Lourbopoulos A, Mamrak U, **Roth S**, Balbi M, Shrouder J, Liesz A, Hellal F, Plesnila N.*

J Cereb Blood Flow Metab. 2017 Jun;37(6):2084-2097. doi: 10.1177/0271678X16660986. Epub 2016 Jan 1.

Brain-released alarmins and stress response synergize in accelerating atherosclerosis progression after stroke.

***Roth S**, Singh V, Tiedt S, Schindler L, Huber G, Geerlof A, Antoine DJ, Anfray A, Orset C, Gauberti M, Fournier A, Holdt LM, Erlandsson Harris H, Engelhardt B, Bianchi ME, Vivien D, Haffner C, Bernhagen J, Dichgans M, Liesz A*

Sci Transl Med. 2018 Mar 14;10, 432. doi: DOI: 10.1126/scitranslmed.aao1313

*(*authors contributed equally to the manuscript)*

1 INTRODUCTION

1.1 Stroke

A stroke is caused by the interruption of the blood supply to the brain, usually because a blood vessel bursts (hemorrhagic) or is blocked by a clot (ischemic). Approximately 85 % of all strokes are ischemic and 15 % are hemorrhagic. This event cuts off oxygen and nutrients supply, causing damage to the brain tissue. The most common symptom of a stroke is sudden weakness or numbness of the face, arm or leg, most often on one side of the body. Other symptoms include: confusion, difficulty in speaking or understanding speech; difficulty seeing with one or both eyes; difficulty walking, dizziness, loss of balance or coordination; severe headache (hemorrhagic) with no known cause; fainting or unconsciousness.

The effects of a stroke depend on which part of the brain is injured and how severely it is affected. (*Definition by World Health Organization, http://www.who.int/topics/cerebrovascular_accident/en/*).

1.1.1 Epidemiology

In 2010, the absolute number of first-ever strokes worldwide was 16.9 million, causing a total of approximately 5.9 million deaths¹. In the 2017 update of the heart disease and stroke statistics², stroke ranks No. 5 among all causes of death behind heart diseases, cancer, chronic lower respiratory disease and unintentional injuries. Stroke has a global epidemiology; about 85 % of all stroke deaths are registered in low- and middle income countries³. Moreover, the age-standardized incidence of stroke significantly decreased in high-income countries, whereas it is still increasing in low- and middle-income countries⁴. In 2010, stroke was the third most common cause of disability-adjusted life-years (102 million)⁵. Compared to 1990 this is a significant increase and prognosis is still rising. In addition, 5.2 million strokes occurred in children (aged <20 years old) and young to mid-aged adults (<64 years). In Europe, the total annual costs imposed by stroke patients were estimated to be €64.1 billion in 2010⁶. Recurrent stroke events are an additional burden. In 2002, a study from South Carolina started which (USA) showed a recurrence rate of 5 % after 6 months, 8 % after 1 year and 18,1 % after 4 years⁷. Recurrent stroke is highly associated with greater numbers of risk factors and higher incidence of large-vessel atherosclerosis than the first stroke^{8,9}. The stroke incidence and costs will further increase due to aging of the population¹⁰.

1.1.2 Etiology

The most common forms of stroke are ischemic stroke and the hemorrhagic stroke. About 15 % are hemorrhagic, initialized by a ruptured vessel and resulting in extravasation of blood. Hemorrhagic stroke is sub classified in intracranial hemorrhagic (ca. 10 %) and subarachnoid hemorrhagic stroke (ca. 5 %). Of all strokes 85 % are classified as ischemic¹¹. An ischemic stroke can be the result of an

embolus or a local thrombus, which can cause a narrowing or even occlusion of a supply artery of the brain. Based on Trial of Org 10172 in Acute Stroke Treatment (TOAST) criteria¹² five different types of ischemic stroke can be classified: 1) large-vessel disease, 2) cardioembolism, 3) small-vessel disease, 4) stroke of other determined etiology, and 5) stroke of undetermined etiology (Fig. 1). For large-vessel disease, one of the supplying brain arteries is occluded by lipid-laden atherosclerotic plaque or narrowed by a severe stenosis. Cardioembolism is induced in much the same way like atherothrombosis, however the blood clot originates from the heart, for example as a result of supraventricular arrhythmias due to atrial fibrillation. Small-vessel derived strokes are classically small (<1.5cm) and depending on the location within brain, usually lacunar syndromes.

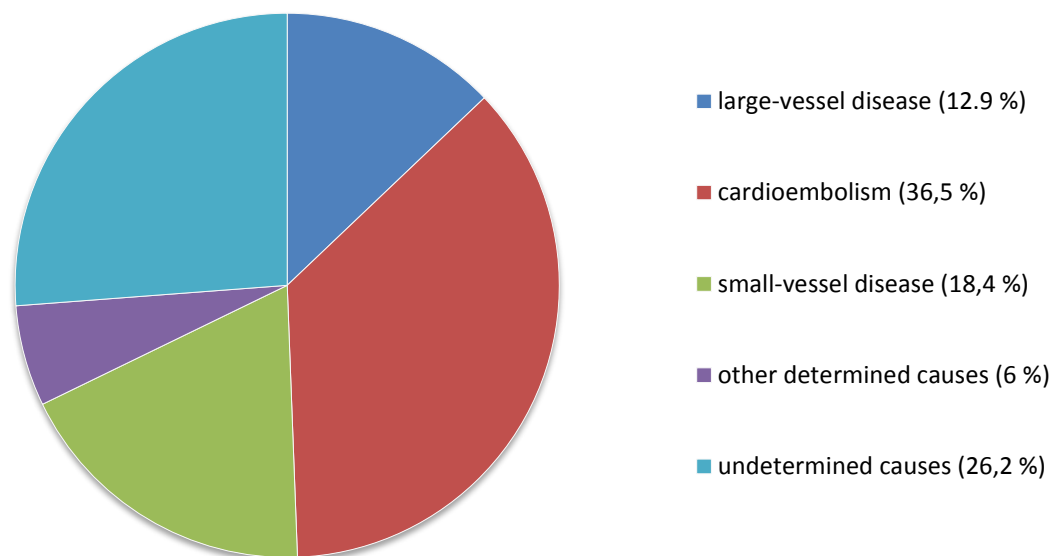


Figure 1. Ischemic stroke subclassification (Modified from Gomes J. and Wachsman A.M. *Handbook of Clinical Nutrition and Stroke*, Springer Science 2013).

1.1.3 Therapy of ischemic stroke

Although the medical and economic burden of stroke is enormous, thrombolysis with tissue plasminogen activator (tPA)¹³ and mechanical vascular recanalization^{14,15} are currently the only clinically approved therapies for ischemic stroke. Additionally, well known limitations and risks including a short time window, coagulation abnormalities, intracranial hemorrhage and further contraindications, make these therapeutic options only accessible for a small percentage of stroke patients^{10,16}. Secondary prevention after acute treatment against recurrent ischemic events is provided with antiplatelet drugs, for example aspirin, statins against hypercholesterolemia and anticoagulants. Moreover, mechanical endarterectomy for symptomatic carotid artery stenosis is an option. However, prognosis for stroke patients remains poor and necessity for effective stroke treatment remains urgent. To overcome this lack of treatments, translational stroke research mainly focused on neuroprotective approaches in the acute phase after stroke for the last two decades. In total, more than 1,000 possible neuroprotective agents and compounds have been tested, *in vitro* and in animal models. Although promising results were achieved in this experimental setup, the approximately 50 compounds reaching

clinical trials did not show any improvement in the patient^{10,17}. Possible reasons for the failure are of either methodological or translational nature. The inappropriate selection of experimental animals in terms of physiology, genetic background, sex and age play an important role. Additionally, design of the study including dosage of drugs and administration route are as pivotal as appropriate statistics of experimental studies¹⁸. In particular, this phenomenon was discussed as “translational roadblock” in stroke research and started to lead scientists away from acute neuroprotective treatment towards subsequent processes in the immune system and associated phenomena like comorbidities and tissue regeneration.

1.1.4 The systemic immune response after stroke

Inflammation is an essential element of stroke pathology. Ischemia-induced brain tissue damage activates astrocytes and local immune cells like microglia¹⁹. Continuous crosstalk of local immune cells in the brain and the increased expression of adhesion molecules and chemokines lead to recruitment of peripheral immune cells. Inflammatory signaling is instrumental in all stages after ischemia in brain and plays an important role from early damage associated events until the late processes underlying post-ischemic tissue repair^{20,21,22}.

Stroke not only inflicts inflammatory processes in the brain, it also induces sterile immune responses systemically. Release of endogenous alarmins from necrotic cerebral cells is one initiator of peripheral immune responses. Alarmins – also referred to as damage/danger-associated molecular patterns (DAMPs) – represent a plethora of different molecules. The heterogeneous group of alarmins includes various proteins but also DNA and ATP, which are all passively released from necrotic tissue.

An example for a prototypic alarmin is the high mobility group box 1 protein (HMGB1). HMGB1 is the most abundant non-histonic nuclear protein and a highly conserved molecule²³. Under healthy conditions HMGB1 binds to the minor groove of linear DNA and assists the binding of transcription factors²⁴. However, HMGB1 is immediately released from the nucleus to the extracellular space when cells undergo necrotic cell death. Once released, the reduction/oxidation-state of HMGB1 is detrimental for its function. Oxidation of the cysteines on amino acid position 23, 45 and 106 makes the protein either chemotactic (=all-thiol HMGB1)²⁵, cytokine-inducing (=disulfide HMGB1)²⁶ or as fully oxidized protein (=sulfonyl HMGB1)²⁷ even resolving the inflammation. Disulfide HMGB1, which we found predominately in murine and human stroke plasma 24 to 48 h after ischemia^{28,29}, has a high affinity for pattern recognition receptors (PRRs)²¹. In the repertoire of PRRs the receptor for advanced glycation endproducts (RAGE) and toll-like receptors 2 and 4 (TLR2 and 4) are the most abundant binding partners³⁰. HMGB1-RAGE, -TLR2 or -TLR4 interactions immediately activate pro-inflammatory intracellular signaling cascades. Downstream, the cascade NFκB translocates to the nucleus and initiates expression of pro-inflammatory cytokines such as IL-1β, IL-6, TNF-α and additional HMGB1.

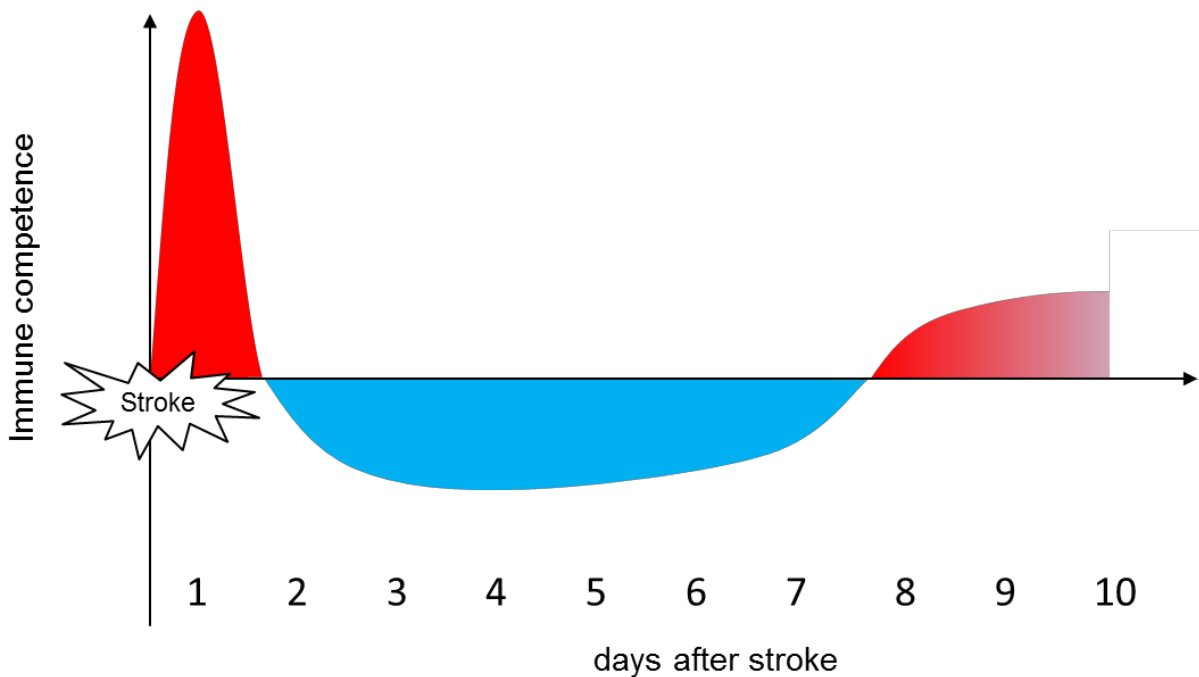


Figure 2. Different stages of peripheral immune competence after stroke. Stroke is an initial event for a complex sterile peripheral immune cascade. Acute (over)activation of the immune system is followed by a subacute immunosuppression phase, which provides ground for infections like pneumonia. Interestingly, in the chronic phase the immune competence strengthens again and stays in a state of chronic low-grade inflammation.

Once alarmins reach the blood stream they induce not only inflammation in brain but a pronounced peripheral immune response. This peripheral immune response is a multiphasic cascade including an early inflammatory activation phase followed by subacute immunosuppression and a chronic low-grade inflammation (**Figure 2**).

The systemic acute inflammatory phase is characterized by a fast and pronounced reaction to the brain damage. High levels of pro-inflammatory cytokines such as IL-1, IL-6 and TNF- α are present in the plasma of mice and stroke patients already hours after stroke²⁸. Additionally, stroke-induced sympathetic innervation activates bone marrow and induces emigration of myeloid cells into circulation. We and others³¹ found decreased numbers of myeloid cells in bone marrow already 24h after stroke. These bone marrow-derived cells migrate to the spleen²⁹, where expression levels of TNF- α and IL-6 are highly elevated³². Moreover, splenic monocytic cells provide high levels of major histocompatibility complex class II (MHCII). Those protein complexes provide antigen-information for splenic T and B cells initiating the adaptive immune response.

The stage of (over)activation of the peripheral immune response is followed by subacute immunosuppression. A well-established concept for secondary immunosuppression is a sympathetic activation and a catecholamine-mediated defect³³ leading to massive T cell death. This suppressive phenomenon provides space for secondary comorbidities, like pneumonia and urinary tract infections, which are difficult to control and cause death after cerebral ischemia³⁴. Blockage of beta-adrenoreceptors in experimental stroke showed a drastic reduction of bacterial infections and

subsequently, reduction of mortality in mice³³. Another current concept for immunosuppression is an “exhausted phenotype” presented by immune cells. This phenotype is defined by a reduced cytokine production and a decrease in MHCII expression. Moreover, severe lymphoid cell death can be found in spleen, blood and thymus. Herein, the detailed mechanisms are still under investigation²¹.

For the following chronic phase (> 10 days) after cerebral ischemia, recent evidences from my work^{29,35} as well as publications from other research groups³⁶ suggest again immunological changes (**Figure 2**). Severe stroke induces long-term alteration of the immune system due to high levels of HMGB1 and cytokines such as IL-6. These were also found in stroke patients up to one year after the initial ischemic event³⁶. In the context of stroke recurrence and common inflammatory comorbidities such as atherosclerosis, this provides a whole new perspective for stroke patient treatment.

1.2 Atherosclerosis

Atherosclerosis is the main cause of vascular diseases including coronary artery disease and cerebrovascular events. It slowly progresses in lesion formation and luminal narrowing of arteries. The underlying pathology is a complex process involving a chronic inflammatory state of the arterial wall at predilection sites with blood flow turbulences such as arterial branches³⁷. Consequently, plaque rupture and thrombosis are the most common causes leading to peripheral artery disease, acute coronary syndrome, and stroke³⁸.

1.2.1 Pathology

The initial event in atherogenesis is a dysfunction in the vascular endothelium, structural alterations and surface presentation of scavenger receptors and proteoglycans³⁹. These receptors lead to an accumulation of very low and low-density lipoproteins (VLDL, LDL) in the sub endothelial space. Moreover, binding of circulating cholesterol via apolipoprotein B100 (ApoB-100, containing LDL) to the proteoglycans has a key role of intimal retention. Subsequently, this leads to oxidative modification of the lipoproteins via reactive oxygen species and enzymes such as myeloperoxidase³⁸. Oxidized LDL (oxLDL) initiates two critical changes in the vascular micro-milieu. First, it inhibits the production of endogenous nitric oxide, an important mediator of vasodilation⁴⁰. Second, oxLDL activates the expression of adhesion molecules and chemokines by endothelial cells via multiple receptors such as the lectin-like oxidized low-density lipoprotein receptor-1⁴¹ and PRRs. The amplified expression of adhesion molecules drives the intimal infiltration of immune cells. Consequently, this sequence of events results in an early stage of fatty streak lesions which mainly consist of monocytes and macrophages accumulating intracellular lipids known as foam cells. Continuous accumulation of apoptotic cells and cholesterol crystals induces the formation of a necrotic core (**Figure 3**). In this stage, lesions are covered by a fibrous cap, composed of smooth muscle cells (SMCs) and collagen structures⁴². Increased secretion of matrix metalloproteases and replacement of SMCs in the fibrous cap with macrophages leads to the thinning of the fibrous cap. Ultimately, these morphological changes in the composition of the plaque increase the vulnerability for plaque ruptures⁴³⁻⁴⁵.

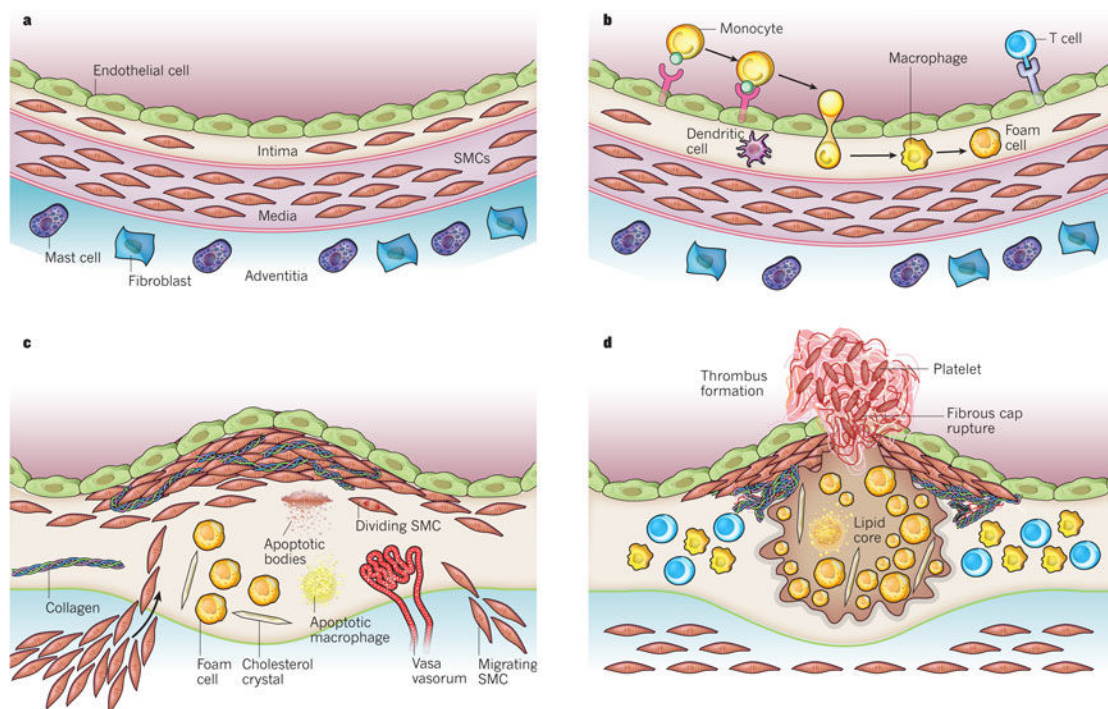


Figure 3. Stages in the development of atherosclerotic lesions (adapted from Libby P and Hansson GK, 2011 Nature).

a. Under healthy conditions there are three arterial layers, the intima, media and adventitia. The intima has direct contact with the blood via a monolayer of endothelial cells. The media is a complex extracellular matrix which embeds SMCs. The outer layer, adventitia, inhabits mast cells and fibroblasts but also contains nerve endings and supplying microvessels. **b.** The initiation of atherosclerosis include adhesion of blood-derived leukocytes to the activated endothelium and migration to the intima; maturation and proliferation of monocytes/macrophages and the uptake of lipids drive the atheroprogession further forward. **c.** Migration of SMCs from the media to the intima and production of matrix macromolecules such as collagen are involved in further lesion growth. Macrophages and SMCs can undergo apoptosis in advanced lesions and debris derived from dead cells can accumulate in the lesion center as a necrotic core. **d.** Thrombosis can arise when a plaque ruptures. The fracture of the fibrous cap enables the contact of blood coagulation components and tissue factor from the plaque. The thrombus can occlude a vessel leading to ischemia of the posterior area.

1.2.2 The role of the immune system in atheroprogession

Atherosclerosis is an inflammatory disease which is correlated to hyperlipidemia^{46,47}. The immune system plays a major role in atherogenesis. The endothelium of healthy and atherosclerotic vessels expresses PRR, including Toll-like receptors and the receptor for RAGE. A broad spectrum of ligands can bind to PRRs. Ligation of modified or oxidized LDL to PRRs activates the pro-inflammatory signal pathways. Most abundant transcription factors in this inflammatory response⁴³ are NFκB, IRF and AP-1. They mediate the expression of a series of genes encoding pro-inflammatory mediators such as cytokines and chemokines. Studies with PRR or intracellular signaling knockout mice showed altered atheroprogession compared to wildtype mice^{48,49}. In addition to LDL, HMGB1 activates the endothelium as well and induces thereby the secretion of pro-inflammatory mediators⁵⁰.

These mediators can then subsequently attract circulating immune cells to the vascular lesions. Amongst others, chemokines such as the CC-chemokine ligand 2 (CCL2) play an important role in the recruitment and migration of monocytes into the vessel wall. Circulating monocytes express the receptor for CC-chemokine 2 (CCR2) on their membrane. Absence of either CCL2 or a knockout for its receptor CC-chemokine receptor 2 (CCR2) showed a decrease in early atheroprogession⁵¹. The

CCR2-CCL2 interaction is not only known to play a role in atheroprotection but is also a key driver of immune cell migration to the ischemic brain⁵².

Moreover, the activated endothelium expresses membrane-bound adhesion molecules such as vascular cell adhesion molecule 1 (VCAM1) and selectins^{50,53}. On the other side, immune cells express the very late antigen-4 (VLA-4) which is the most abundant ligand for VCAM1⁵⁴. In the initiation phase of atherosclerosis this interaction plays an important role. Adhesion molecule-immune cell interactions enable myeloid and lymphoid immune cells to enter the arterial wall (**Figure 4**)^{55,56}.

The majority of the early invading immune cells are monocytes which can in mice be characterized by the expression of lymphocyte antigen 6 complexes (Ly6C). Approximately 80 % of blood monocytes are expressing high levels of Ly6C (Ly6C^{high}). Ly6C^{high} monocytes are short-lived myeloid cells with pro-inflammatory functions. This subpopulation invades into inflamed tissue and differentiates into dendritic cells or macrophages⁵⁶ (**Figure 4**). Ly6C^{high} monocytes have been shown to egress the bone marrow via upregulation of CCR2 and to be attracted to inflammatory sites⁵⁷. The other 20 % of monocytes are expressing only low levels of Ly6C (Ly6C^{low}). Moreover, this population expresses low levels of CCR2 but high levels of CX3CR1. They crawl along the luminal surface and are therefore referred to as patrolling⁵⁸. Under the influence of inflammatory mediators, they extravasate and phagocytose pathogens.

In contrast, human monocytes do not express Ly6C but are classified on the basis of CD14 and CD16 expression. CD14^{high}CD16^{neg} monocytes are comparable to the murine Ly6C^{high} monocyte population; they express high levels of CCR2 and are the most prevalent subset⁵⁹. CD16⁺ monocytes comprise the counterpart to Ly6C^{low} monocytes. This subpopulation is called “non-classical monocytes” and shows patrolling behavior comparable to murine Ly6C^{low} monocytes⁵⁸.

The presence of costimulatory factors such as the macrophage colony-stimulating factor (M-CSF) initiates the differentiation of monocytes to macrophages⁶⁰. In established atherosclerotic lesions resident macrophages have been shown to be mainly derived from proliferation but not *de novo* infiltration⁶¹. During the inflammation-driven atheroprotection the initial fatty streak lesion matures into an atherosclerotic plaque with necrotic core region (**Figure 3**). Continuous infiltration and proliferation of immune cells enhance the lesion. Moreover, death of macrophages and foam cells lead to the formation of a necrotic core. This region contains extracellular lipids, cholesterol crystals and cell debris and is surrounded by a fibrous cap which stabilizes the plaque^{56,62}. Further progression of plaque pathology with increased secretion of matrix metalloproteinases and cytokines can cause thinning of the fibrous cap and lead to plaque destabilization⁶³.

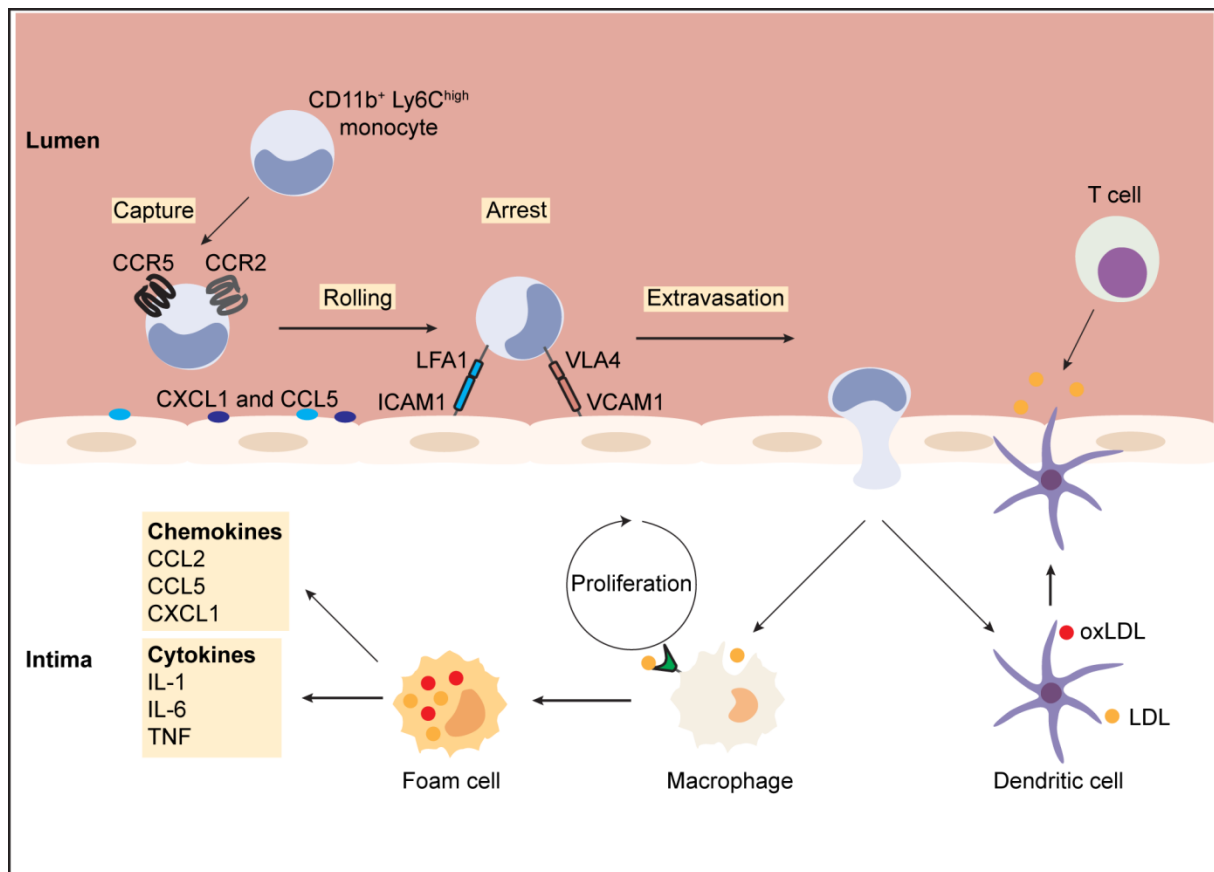


Figure 4. Monocyte recruitment and accumulation in plaques (modified from Moore, K.J. et al., *Nature Reviews Immunology*, 2013). The endothelial expression of chemokines (CCL2, CXCL1 etc.) and adhesion molecules (ICAM1, VCAM1) due to hyperlipidemia lead to monocyte recruitment into the early fatty streak formations. Especially Ly6C^{high} monocytes infiltrate the plaque. Chemokine – chemokine receptor interactions, like CCL2 – CCR2 interactions, play a pivotal role in attracting monocytes to the lesions. Binding of endothelial adhesion molecules, especially ICAM1 and VCAM1, facilitate the arrest and finally extravasation of the cells into the intima. Monocytes can differentiate into macrophages and dendritic cells. Macrophages take up oxidized or naïve LDL via phagocytosis or scavenger receptor-mediated pathways, resulting in the formation of foam cells. These foam cells secrete pro-inflammatory cytokines (IL-6, IL-1 β and TNF- α) and chemokines, amplifying the inflammatory response^{64,65}.

In addition, cells of the adaptive immune system are present in atherosclerotic lesions (**Figure 3**). Studies with adaptive immunity-deficient atherosclerotic mouse models demonstrated a substantial role of T and B cells in atherosclerosis. *ApoE*^{-/-} mice crossed with lymphocyte-deficient mice lacking recombination-activating gene 1 or 2 (*Rag1*^{-/-} or *Rag2*^{-/-}) showed significantly less plaque progression, compared to *ApoE*^{-/-} mice^{43,66}. In contrast to monocytes, T cells are less abundant in atherosclerotic plaques and contribute mainly to the later stages of atheroprogession via secretion of pro-inflammatory mediators^{67,68}. T cells recognize antigens in form of a complex of a foreign peptide bound to a MHC molecule. These antigens are presented by an antigen-presenting cell such as dendritic cells, which present antigens to T cells in the arterial wall⁶⁹. However, the initial site of antigen presentation in atherosclerosis is unknown.

CD4⁺ T_{helper} and CD8⁺ T_{cytotoxic} cells are found in human lesions, but T_{helper} cells dominate in numbers⁷⁰. Similar to that, in *ApoE*^{-/-} and *LDLR*^{-/-} mice CD4⁺ T cells are the predominant subset in atherosclerotic lesions⁷¹. From human plaques it is known that T helper type 1 cells are drivers for

pathogenic effects⁷². Interferon gamma (IFN γ), signature cytokine of T_h1 cells is correlated with higher MHC class II expression, enhanced protease and chemokine secretion, adhesion molecule presence and reduced fibrous cap formation⁴³. On the other hand, IFN- γ deficiency leads to a reduction in lesion lipid accumulation and cellularity⁷³. A similar effect was shown after inhibition of IL-12, another T_h1-associated cytokine. While the early plaque progress decreased, there was no beneficial effect observed in established lesions⁷⁴. In addition, deletion of T_h1 transcription factor T-bet leads to significant reduction in lesion development^{43,75}. Taken together, T_h1 cells play a crucial role in the development of plaques. For the pro-inflammatory subset of T_h17 cells the role in atherosclerosis is unclear. The signature cytokine IL-17 was detected in human atherosclerotic plaques⁷⁶, however, the experimental approaches to date provided controversial results. The subset of regulatory T cells (T_{reg}) shows atheroprotective effects in experimental studies. In this context, the most frequently described T cells are FoxP3⁺ T cells. They have been found in human and murine plaques in low numbers. Transfer of wildtype FoxP3⁺ T cells into atherosclerotic mice have been reported to be atheroprotective. They are known to produce IL-10 and transforming growth factor beta (TGF- β), which both have atheroprotective effects in mouse models⁷⁷.

Studies on B cells have revealed controversial findings, showing atheroprotective as well as atheropromotive effects of B cells. One prominent example for a successful B cell-target treatment in experimental atherosclerosis was the depletion with an antibody against CD20 in atherosclerosis. This study demonstrated reduced lesion progression after depletion⁷⁸. Moreover, this and other studies indicated that only B-2 and not B-1 (CD20⁺) cells are atheroprotective^{79,80,81}. Taken together, the innate and adaptive immune responses are essential drivers for atherosclerotic development. Due to this fact, they also represent key targets for therapeutic approaches.

1.2.3 Animal models of atherosclerosis

An optimal animal model of atherosclerosis should develop various stages of the disease including fatty streaks, infiltration of immune cells, accumulation of foam cells, vulnerable and stable plaques as well as relevant complications such as calcification, ulceration, hemorrhage, plaque rupture, thrombosis, stenosis and the formation of aneurysms. Efforts are being made to develop animal models that replicate human atherosclerosis, however, each of the current animal models have some limitations⁸².

Mice are the most widely used species for experimental studies on atherosclerosis. While large animal models have also been developed in rabbits, pigs and non-human primates, the ease of breeding and availability of genetic modifications in mice make them in most cases the favorite species of choice⁸². The two most frequently used models of genetically-induced atherosclerosis in mice are *LDLR*^{-/-} and *ApoE*^{-/-} mice. *LDLR*^{-/-} mice have a knockout in the low density lipoprotein receptor, a membrane-based receptor that recognizes apolipoprotein B100, which is placed in the phospholipid layer of

LDL⁸³. These mice are mildly hypercholesterolemic on normal diet; however high-fat diet increases cholesterol levels remarkably. The severity of disease correlates significantly with blood cholesterol levels^{84,85}. *ApoE*^{-/-} mice have a knockout in the apolipoprotein E. In mice, there is only one ApoE isoform being essential for catabolizing lipoproteins and triglycerides. Plasma cholesterol is mostly carried on lipoprotein remnants and rather than LDL, the “offending” guy in human atherosclerosis⁸². From birth on *ApoE*^{-/-} mice are hypercholesterolemic and develop spontaneous lesions under chow diet. When fed with a HF diet mice are severely hypercholesterolemic and develop more lesions⁸⁶. Moreover, *ApoE*^{-/-} mice develop severe, reproducible plaques with complex immune cell interactions within 8 weeks of HF diet⁸⁷. Nevertheless, both models do not result in spontaneous plaque rupture, which is a limitation to further investigate consequences of atherosclerosis like myocardial infarction and stroke. To overcome these limitations, mouse models with unstable or even rupturing plaques have been developed. One possibility is a tandem stenosis of the common carotid artery in *ApoE*^{-/-} mice fed with HF diet³⁷. Another possibility is an additional gene modification. As an example, genetically modified *ApoE*^{-/-} mice in which matrix metalloproteinases (MMP) expression of macrophages is upregulated show increased plaque instability⁸⁸. And finally, the acceleration of plaque destabilization with chronic angiotensin II infusion also leads to a higher number of rupture sites in the fibrous cap⁸⁹.

2 PROJECT DESIGN

Acute brain lesions induce multiphasic alterations of the peripheral immune response comprising early activation and subsequent immunosuppression. In this project, we focused on soluble pro-inflammatory mediators—referred to as alarmins—as potential mediators of post-stroke systemic inflammation. Alarmins are released from necrotic brain tissue and represent a potent mode of brain-immune communication. Previous studies indicated a correlation between cerebral lesion volume and the extent of systemic immune alterations⁹⁰. High mobility group box protein 1 (HMGB1) is a prototypic alarmin with strong pro-inflammatory functions. HMGB1 is passively secreted from the necrotic tissue after ischemia^{19,91}. Levels of HMGB1 are reported to be elevated immediately after ischemic injury and to last for more than one year in stroke patients with severe stroke³⁶. However, it was previously unknown whether post-stroke chronic inflammation has an impact on common inflammatory comorbidities. Atherosclerosis is not only one of the most prevalent prominent comorbidities in stroke patients but also a common etiology of recurrent stroke events^{8,9}. Atherosclerosis has a complex inflammatory pathology initialized by a dysbalance in the lipid metabolism increasing the invasion of leukocytes to the arterial wall. This influx of immune cells results in a chronic pro-inflammatory milieu and subsequently in atherosclerotic plaques. Established atherosclerosis can lead to stenosis or to a plaque rupture causing a thrombus formation. Both can result in a blockage of brain-supplying arteries causing stroke.

The hypothesis of this project was to test alarmin-mediated immune activation in experimental stroke and investigate the impact of this pathway on the progression of atherosclerosis after stroke induction. We used an experimental approach in established mouse models of stroke and atherosclerosis to investigate the following specific aims:

- A) How do alarmins affect the systemic immune interaction after experimental stroke?

Manuscript 1

- B) What are possible signal pathways activating immune cells?

Manuscript 1 & 2

- C) Does post-stroke systemic inflammation accelerate atherosclerosis progression?

Manuscript 2

3 SUMMARIES

3.1 Summary

Stroke is one of the top 5 reasons for death in developed industrial countries. Approximately 6 million people die due to stroke or its consequences. Moreover, stroke is the most frequent reason for disability in high-aged populations. Approximately 85 % of all strokes are ischemic and only 15 % are caused by intracerebral hemorrhage. The main reasons for ischemic stroke are a heart embolism, microangiopathies or a thromboembolic event in a distal brain artery caused by vessel stenosis (macroangiopathy). After stroke itself mortality is also influenced by infections in the subacute phase and recurrent ischemic events. The risk of a recurrent stroke event is up to 30 % within the first 5 years after stroke, about nine times the risk of stroke in general population⁹². Especially macroangiopathy was correlated with the highest recurrence rate after the first stroke.

After stroke, complex neuroimmunological alterations take place in the brain including the clearance of debris, building of a scar formation and a long-term regeneration of lost tissue. Moreover, a multiphasic immune cascade can be observed in the peripheral immune system. Within this project we found that passive secretion of alarmins—soluble mediators of neural cell death— can cause systemic immune alterations after ischemia. Alarmins implement a plethora of different molecules including different proteins, ATP and also DNA. In this context, the high mobility group box 1 protein (HMGB1) should be highlighted. A non-histonic nuclear protein which, once secreted to extracellular space, shows cytokine-like properties. HMGB1 is well known to interact with Pattern Recognition Receptors (PRR). In particular, it shows high affinity to the receptor of advanced glycation endproducts (RAGE). In general, PRRs are highly abundant on innate immune cells. The HMGB1-RAGE interactions can activate intracellular signal cascades and thereby, activate these immune cells. An acute activation of the peripheral immune system can be detected almost immediately after stroke. Within the following days, the immune system breaks down and shows a subacute immunosuppression. We and others found strong evidences that the immune system modulates a chronic low grade inflammation after this suppressive phase. This can be seen in increased serum levels of pro-inflammatory markers such as HMGB1, IL-6 and TNF- α .

The goal of my thesis was to investigate (1) how alarmins affect the systemic immune alterations after experimental stroke and (2) which signal pathways are involved in activation of immune cells. Moreover, we were interested in (3) how post-stroke immune alterations can affect one of the most common comorbidity of stroke, atherosclerosis.

We were able to show increased HMGB1 serum concentrations almost immediately after experimental stroke in mice. In addition, a similar pattern of increased HMGB1 levels was found in stroke patients' serum. A mass spectrometry analysis of murine serum after stroke demonstrated a change from a fully reduced state to the disulfide form of HMGB1 within 24 h after stroke. This highly reactive Redox

form of HMGB1 can be associated with the early activation of the innate and adaptive immune system in rodent and humans. Neutralization of circulating HMGB1 by monoclonal antibodies ameliorated pro-inflammatory cytokine expression in the spleen. The inflammatory response after stroke was also reflected by behavioral changes. Besides the focal deficits attributable to brain tissue loss, stroke mice were highly immobile and showed a disturbed circadian rhythm. These behavioral domains are commonly known to represent “cytokine-induced sickness behavior”. Correspondingly, neutralization of pro-inflammatory cytokines via antibody treatment improved overall activity and circadian rhythm disturbances. In RAGE knockout mice, behavioral deficits were also less prominent compared to WT stroke mice.

In the subacute phase, we found an expansion of splenic innate immune cells and at the same time a decrease in adaptive immune cells counts. T cell counts were particularly decreased in blood and spleen during the subacute phase after stroke. Inhibition of HMGB1, knockout of RAGE and other PRRs resulted in a less immunosuppressive phenotype.

In conclusion, immediately after stroke elevated levels of HMGB1 can be found in serum of mice and patients. These elevated levels of HMGB1 lead to an acute activation of the peripheral immune system by binding to PRRs such as RAGE. High levels of cytokines induce a behavioral phenotype known as “cytokine-induced sickness behavior” in mice, including immobility and disturbed circadian rhythm. Subsequently, the subacute phase is characterized by an exhausted immune system and a substantial reduction in T lymphocyte counts.

After characterization of the acute and subacute phase after stroke, we focused our investigation on the chronic low-grade inflammation. We hypothesized that chronic systemic inflammation after stroke might affect the pathophysiology of inflammatory comorbidities of stroke patients such as atherosclerosis—one of the most common comorbidities in elderly patients and a main etiology of cerebrovascular events. Hence, we were interested in how post-stroke peripheral immune alterations can affect atherosclerosis. Therefore, we used a well-established atherosclerosis mouse model (*ApoE*^{-/-}). Mice were fed a high-fat diet (“western style diet”) to induce atherosclerosis. After 8 weeks of high-fat diet, an experimental stroke was induced and we analyzed the atherosclerotic outcome one month after. We found increased plaque loads in aorta and aortic valve regions. Moreover, the myeloid cell numbers in atherosclerotic plaques were elevated. Histological analysis revealed fibrous cap thinning and evidences were found for plaque ruptures in *ApoE*^{-/-} mice after stroke. *De novo* infiltration of myeloid cells was observed to be the key driver for increased myeloid cell counts in plaques. Already 3 d after stroke, increased levels of CC-chemokine ligand 2 (CCL2) and its receptor (CCR2) were detectable in the aorta. Furthermore, we detected an activation of the vascular endothelium by soluble mediators. We found high levels of vascular adhesion molecule 1 (VCAM1) in the aortic region after stroke, using an *in vivo* MRI approach. VCAM1 plays a pivotal role in leukocyte extravasation into the

arterial wall. HMGB1 levels were still elevated in mice more than one month after stroke. At the same time, we observed murine and patients' blood-derived monocytes still being activated. With an *in vivo* antibody-specific inhibition of HMGB1 and a systemic RAGE knockdown using small interfering RNA in mice, we were able to show that particularly the HMGB1-RAGE interaction played an important role in post-stroke atheroprogession. Besides post-stroke alarmins, we found a sympathetic activation of the bone marrow after stroke. Thus, we found an egress of CCR2⁺ monocytes from the bone marrow already 24 h after ischemia. Labeling myeloid cells with fluorescent nanocrystals enabled us to investigate trafficking of myeloid cells after stroke and revealed the translocation of myeloid cells to the spleen within 24h after stroke. In addition, we were able to inhibit cell egress from the bone marrow using adrenergic beta-receptor blockers. Lastly, we approached atheroprogession after stroke with a combined treatment approach (Beta-blocker + alarmin inhibitor) in order to dissect the differential contribution of the sympathetic stress response and alarmin-mediated pathways. These experiments revealed a synergistic effect of both cascades (stress and alarmins) with their blockage leading to significant amelioration of post-stroke atheroprogession.

In summary, this project gave strong evidences that alarmins—passively secreted by dying neural cells—immediately activate the peripheral immunity after stroke (**Figure 5**). A multiphasic cascade is initiated which includes an acute immune (over)activation, followed by a subacute immunosuppression and a chronic low-grade inflammation. Furthermore, peripheral immune alterations have a substantial impact on the progression of atherosclerosis after stroke. We detected that stress response and alarmins synergize in post-stroke atheroprogession.

Our studies were able to reveal some of the mechanisms involved in post-stroke atheroprogession and tested potential therapeutic targets. Nevertheless, further investigations are needed to fully understand the whole process in the complex interaction of post-stroke sterile inflammation, atheroprogession and recurrent ischemic events.

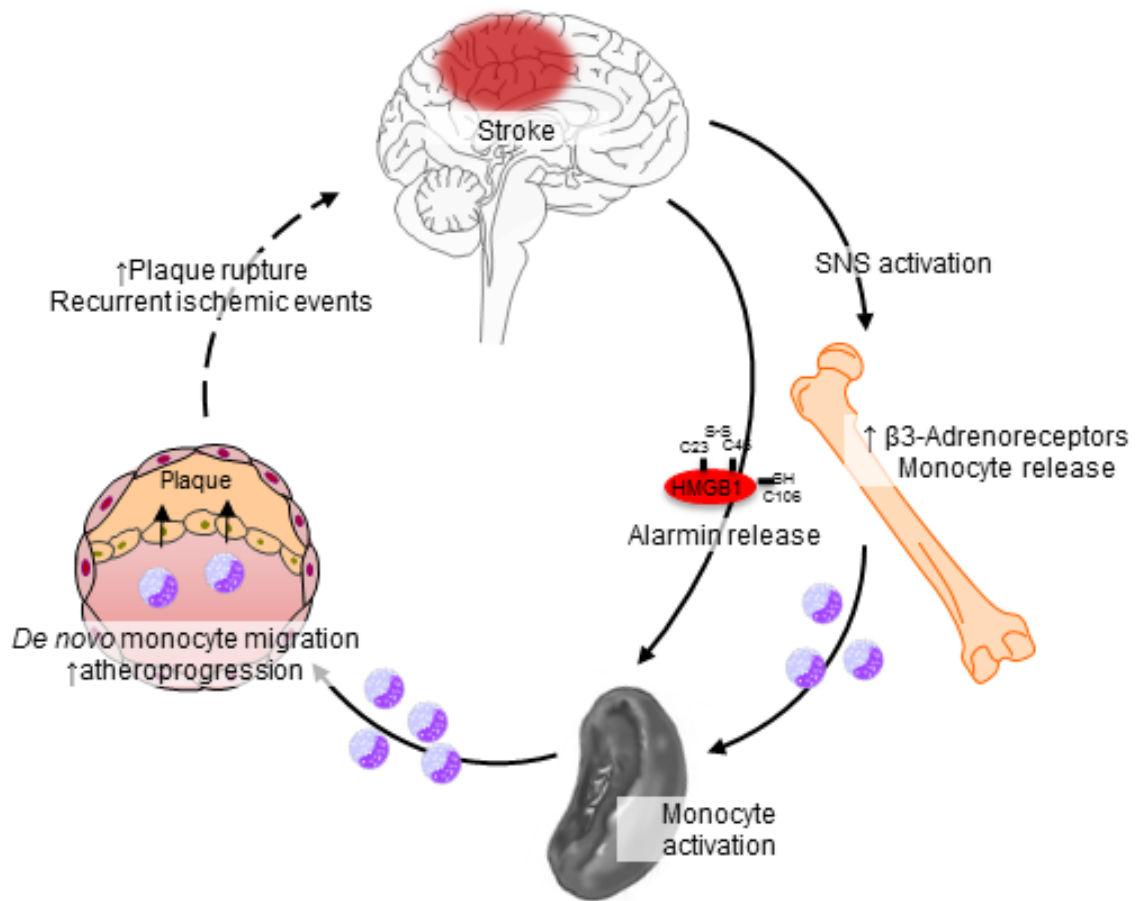


Figure 5. Schematic overview. Stroke-induced neural cell death leads to a release of alarmins, in particular HMGB1. At the same time, increased sympathetic nervous system (SNS) activation after stroke induces release of monocytes from the bone marrow. These cells can be found in the spleen where they get into contact with HMGB1 and other brain-derived alarmins and get activated. Activated monocytes interact with increased chemokine levels and adhesion molecules on the endothelium of vessels. This leads to a *de novo* migration of monocytes into established atherosclerotic plaques. Atheroprotection gets accelerated and plaques become more prone to rupture. This can ultimately induce recurrent ischemic cerebrovascular events.

3.2 Zusammenfassung

Schlaganfall ist einer der 5 häufigsten Todesursachen in entwickelten Industrienationen. Jedes Jahr sterben weltweit schätzungsweise 6 Millionen Menschen an den Folgen eines Hirninfarktes. Zusätzlich ist Schlaganfall die häufigste Ursache für eine im höheren Alter erworbene Behinderung. Von allen Schlaganfällen sind etwa 85% ischämisch und nur etwa 15% intrazerebrale Blutungen. Die Hauptgründe für den ersten ischämischen Schlaganfall eines Patienten sind unter anderem Verschlüsse distaler Hirngefäße aufgrund von Gefäßstenosen (Makroangiopathie), Herzembolien oder Mikroangiopathien. Neben der akuten Lebensgefahr durch Schlaganfall spielen auch die hohen Rezidivraten nach einem ersten Schlaganfall eine wichtige Rolle. Das Risiko auf einen erneuten Schlaganfall ist bis zu 30 % höher in Schlaganfallpatienten, verglichen mit gleichaltrigen Patienten ohne Schlaganfall. Besonders hohe Rezidivraten korrelierten in mehreren Studien explizit mit Makroangiopathie.

Nach Schlaganfall ist neben komplexen neuroimmunologischen Alterationen auch eine multiphasische Immunreaktion des peripheren Immunsystems zu beobachten. Im Rahmen dieser Arbeit konnte gezeigt werden, dass die passive Sekretion von Alarminen—lösliche Botenstoffe nach neuralem Zelltod—als Schlüsselmediatoren dieser systemischen Immunalteration auftreten. Aus dem breiten Spektrum der Alarmine hervorzuheben ist hier das high mobility group box protein 1 (HMGB1). Hierbei handelt es sich um ein Nicht-Histon-Protein im Zellkern, welches nach Sekretion in den extrazellulären Raum Zytokin-ähnliche Eigenschaften annimmt. HMGB1 interagiert mit sogenannten Pattern recognition receptors (PRR) und zeigt insbesondere für den Receptor of advanced glycation endproducts (RAGE) eine hohe Affinität. Generell sind PRRs in großer Zahl auf Zellen der angeborenen Immunabwehr exprimiert. Die HMGB1-RAGE Interaktionen können intrazelluläre Signalkaskaden aktivieren und sorgen so für eine Aktivierung der Immunzellen. Nur Stunden nach Auftreten des Infarkts kommt es bereits zu einer akuten Aktivierung des peripheren Immunsystems, welche in den darauffolgenden Tagen von einer subakuten Immunsuppression abgelöst wird. Aktuelle Forschungsarbeiten zeigen zudem ein Wiedererstarken des peripheren Immunsystems in Form einer chronischen Entzündungsreaktion, dies konnte bereits zuvor anhand von erhöhten Serumwerten für Entzündungsmarker (HMGB1, TNF- α , IL-6) gezeigt werden.

Ziel der vorliegenden Arbeit war es herauszufinden, (1) wie Alarmine die systemischen Immunreaktionen nach Schlaganfall modulieren und (2) welche Signalkaskaden in Immunzellen hierbei eine Rolle spielen. Zudem wollten wir herausfinden, (3) ob der chronische Entzündungsstatus nach Schlaganfall Auswirkungen auf die Progression von Atherosklerose hat.

Wir konnten im experimentellen Mausmodell zeigen, dass bei großen Infarkten bereits 30 Minuten nach Schlaganfall hohe Konzentrationen von HMGB1 im Serum zu finden sind. Serumanalysen von Schlaganfallpatienten ergaben ebenfalls hohe HMGB1-Werte innerhalb von wenigen Stunden nach Schlaganfall. Massenspektrometrie von murinem Serum nach Schlaganfall zeigte, dass innerhalb eines

Tages hauptsächlich die hochaktive Disulfidform von HMGB1 zu finden war. Dies ging einher mit einer frühen Aktivierung der angeborenen und adaptiven Immunität (stark erhöhte IL-6 und TNF- α Werte). In der Maus konnte die Immunaktivierung durch Antikörper-vermittelte Neutralisation von HMGB1 merklich abgeschwächt werden.

Der aktivierte Immunstatus zeigte sich auch im Verhalten der Mäuse. Tiere mit Schlaganfall waren deutlich inaktiver und zeigten im Vergleich zu scheinoperierten Tieren einen gestörten zirkadianen Rhythmus. Neutralisation pro-inflammatorischer Zytokine führte zu einer sichtlichen Verbesserung des zirkadianen Rhythmus und der allgemeinen Aktivität der Mäuse. Wurde der für HMGB1 hochaffine Rezeptor RAGE in Mäusen genetisch ausgeschaltet, so konnte man ebenfalls eine Verbesserung der Aktivität feststellen.

Nach der akuten Aktivierung konnte in der subakuten Phase eine Expansion angeborener Immunzellen beobachtet werden. Dies ging einher mit einer Reduzierung der adaptiven Immunität, vor allem in der Milz. Die Anzahl der T Zellen in der Milz nach Schlaganfall verminderte sich um über die Hälfte der ursprünglichen Zellzahl. Auch hier zeigte eine Inhibition von HMGB1 bzw. ein Knockout von RAGE und anderen PRRs eine deutliche Verbesserung des Immunstatus.

Zusammenfassend lässt sich sagen, dass unmittelbar nach Schlaganfall stark erhöhte HMGB1 Konzentrationen im Blut von Mäusen und Patienten zu finden sind. Dies führt über die Aktivierung von PRRs, vor allem RAGE, zu einer rapiden Überaktivierung des peripheren Immunsystems. Die hohen Zytokinkonzentrationen äußern sich im Verhalten der Tiere, was bis zu Störungen des zirkadianen Rhythmus führt. In der anschließenden, subakuten Phase nach Schlaganfall führt eine Erschöpfung des Immunsystems zu einem massiven Lymphozyten-Verlust.

Nach Charakterisierung der akuten und subakuten Phase nach Schlaganfall war die chronische Phase der schlaganfallinduzierten Immunantwort zentraler Gegenstand weiterer Nachforschungen. Wir stellten die Hypothese auf, dass die chronische Entzündung nach Schlaganfall die Pathophysiologie entzündlicher Komorbiditäten, wie zum Beispiel Atherosklerose (eine der häufigsten Komorbiditäten in älteren Patienten und Hauptursache für zerebrovaskuläre Vorfälle) beeinflusst. Hierzu verwendeten wir ein etabliertes Mausmodell für Atherosklerose (*ApoE*^{-/-}). Mithilfe einer kalorienreichen Diät („Western Style Diet“) induzierten wir fortgeschrittene atherosklerotische Plaques. Einen Monat nach Induktion eines experimentellen Schlaganfalls fanden wir einen Anstieg der Plaquelast in Aorten und den Aortenklappen in den *ApoE*^{-/-} Mäusen. Damit einhergehend war die myeloide Zellzahl in Aorten stark erhöht. Histologische Färbungen zeigten ausgedünnte fibröse Kappen um die Plaques und wir fanden Anzeichen für Rupturen einzelner Plaques. Als Grund für die erhöhte Zellzahl im Plaque konnten wir eine *de novo* Infiltration von Monozyten feststellen. In diesem Prozess spielt zum einen der CC-Chemokin Ligand 2 (CCL2) und dessen Rezeptor (CCR2) eine essentielle Rolle. Des Weiteren führt die Aktivierung des vaskulären Endotheliums durch Plasmamediatoren nach Schlaganfall zu der

Neueinwanderung von Immunzellen. Mithilfe von *in vivo* Magnetresonanztomografie konnten wir beobachten, dass nach Schlaganfall mehr VCAM1 vom aortalen Endothel exprimiert wird. Außerdem konnten wir zeigen, dass insbesondere HMGB1 in Interaktion mit RAGE eine wesentliche Rolle in der Immunaktivierung spielt. Zusätzlich detektierten wir erhöhte HMGB1 Konzentration einen Monat nach Schlaganfall in Mäusen. Sowohl in Patientenblut als auch in der Maus fanden wir bis zu 3 Monaten nach Schlaganfall eine erhöhte Monozytenaktivität. Inhibition mithilfe eines Antikörpers gegen HMGB1 und systemischer knock down von RAGE mittels siRNA zeigten jeweils Abschwächung der Atheroprogression.

Neben der Alarminsekretion ins Blut führt Schlaganfall ebenfalls zu einer sympathischen Innervation was zur Aktivierung des Knochenmarks führt. Bereits 24 Stunden nach Schlaganfall stellten wir vermehrte Migration von myeloiden Immunzellen aus dem Knochenmark in die Milz fest. Diesen Prozess konnten wir durch Injektion fluoreszierender Nanokristalle in das Knochenmark nach Schlaganfall darstellen und mithilfe von Beta Blockern inhibieren.

Eine kombinierte Hemmung der sympathischen Innervation und der Alarmine mithilfe eines Beta-Blockers und der löslichen Form von RAGE als Alarminrezeptor führte zu einer starken Reduktion der myeloiden Zellzahlen in der Aorta und verminderter Aktivierung der Monozyten. Zusätzlich konnte eine verminderte Plaquelast in den Aortenklappen festgestellt werden.

Somit konnten wir in dieser Studie zeigen, dass Alarmine unmittelbar nach Schlaganfall das periphere Immunsystem aktivieren. Es kommt zu einer multiphasischen Kaskade aus akuter Immunaktivierung, subakuter Immunsuppression und erneuter chronischer Aktivierung des peripheren Immunsystems (**Figure 5**). Die chronische Entzündungsphase wirkt sich negativ auf die Komorbidität Atherosklerose aus. Indikator dafür war eine erhöhte Plaquelast und eine gesteigerte Plaquevulnerabilität. Wir konnten zeigen, dass ein Synergismus aus sympathetischer Aktivierung und Alarminsekretion die Atheroprogression vorantreibt. Wir konnten anhand der Ergebnisse dieser Studie Teile der beteiligten Mechanismen der Atheroskleroseprogression nach Schlaganfall erstmals aufzeigen und als neuartige therapeutische Ziele testen. Trotz der neuen Erkenntnisse werden aber weitere Studien nötig sein, um die genauen Prozesse der post-ischämischen Immunantwort, Atheroprogression und rezidivierender Schlaganfälle zu verstehen.

4 RESEARCH ARTICLES

4.1 DAMP signaling is a key pathway inducing immune modulation after brain injury.

Acute brain ischemia leads to complex neuronal immune cascades. Also in the periphery sterile brain injury induces profound alterations of the immune compartment. An early systemic immune activation within hours after stroke is followed by the opposing phenomena of subsequent immunosuppression. Animal models for experimental brain ischemia as a paradigm of acute brain lesions and additionally a large cohort of stroke patients were analyzed.

Our results indicate that the cytokine-inducing, fully reduced isoform of high mobility group box protein 1 (HMGB1) is released from the ischemic brain in the hyperacute phase of stroke in mice and patients. Cytokine secretion of activated immune cells in the periphery in response to the brain injury induces a severe sickness behavior, which affected even the circadian rhythm of the rodent. This could be abrogated by inhibition of the HMGB1-RAGE pathway or direct cytokine neutralization. Subsequently, HMGB1-release induced monocyte mobilization and splenic proliferation of bone marrow-derived innate immune cells, inhibiting the peripheral adaptive immune response. Finally, HMGB1-RAGE interaction resulted in an exhaustive phenotype of monocytes and lymphopenia, a hallmark of subacute immunosuppression after large stroke.

This study introduces the HMGB1-RAGE signaling pathway as one of the key mechanisms explaining the complexity of post-ischemic brain-periphery immune interactions.

Author contribution: performing and analyzing experiments, correction of the manuscript

(Copyright permission under the terms of “the creative commons attribution-noncommercial-share alike 3.0”)

DAMP Signaling is a Key Pathway Inducing Immune Modulation after Brain Injury

Arthur Liesz,^{1,2,3} Alexander Dalpke,⁴ Eva Mracsko,¹ Daniel J. Antoine,⁵ Stefan Roth,^{2,3} Wei Zhou,¹ Huan Yang,⁶ Shin-Young Na,¹ Mustafa Akhilaroglu,^{1,7} Thomas Fleming,⁸ Tatjana Eigenbrod,⁴ Peter P. Nawroth,⁸ Kevin J. Tracey,⁶ and Roland Veltkamp^{1,9}

¹Department of Neurology, University Heidelberg, 69120 Heidelberg, Germany, ²Institute for Stroke and Dementia Research, Klinikum der Universität München, 81377 Munich, Germany, ³Munich Cluster for Systems Neurology, 80336 Munich, Germany, ⁴Department of Infectious Diseases, Medical Microbiology and Hygiene, University Heidelberg, 69120 Heidelberg, Germany, ⁵MRC Centre for Drug Safety Science, Molecular & Clinical Pharmacology, University of Liverpool, Liverpool L69 3GE, United Kingdom, ⁶Laboratory of Biomedical Sciences, Feinstein Institute for Medical Research, Manhasset, New York 11030, ⁷Department of Physiology, School of Medicine, Dokuz Eylul University, Inciralti, Izmir, 35340, Turkey, ⁸Department of Internal Medicine, University Heidelberg, 69120 Heidelberg, Germany, and ⁹Division of Brain Sciences, Imperial College London, London SW7 2AZ, United Kingdom

Acute brain lesions induce profound alterations of the peripheral immune response comprising the opposing phenomena of early immune activation and subsequent immunosuppression. The mechanisms underlying this brain-immune signaling are largely unknown. We used animal models for experimental brain ischemia as a paradigm of acute brain lesions and additionally investigated a large cohort of stroke patients. We analyzed release of HMGB1 isoforms by mass spectrometry and investigated its inflammatory potency and signaling pathways by immunological *in vivo* and *in vitro* techniques. Features of the complex behavioral sickness behavior syndrome were characterized by homecage behavior analysis. HMGB1 downstream signaling, particularly with RAGE, was studied in various transgenic animal models and by pharmacological blockade. Our results indicate that the cytokine-inducing, fully reduced isoform of HMGB1 was released from the ischemic brain in the hyperacute phase of stroke in mice and patients. Cytokines secreted in the periphery in response to brain injury induced sickness behavior, which could be abrogated by inhibition of the HMGB1-RAGE pathway or direct cytokine neutralization. Subsequently, HMGB1-release induced bone marrow egress and splenic proliferation of bone marrow-derived suppressor cells, inhibiting the adaptive immune responses *in vivo* and *in vitro*. Furthermore, HMGB1-RAGE signaling resulted in functional exhaustion of mature monocytes and lymphopenia, the hallmarks of immune suppression after extensive ischemia. This study introduces the HMGB1-RAGE-mediated pathway as a key mechanism explaining the complex postischemic brain-immune interactions.

Key words: alarmins; HMGB1; immunomodulation; myeloid-derived suppressor cell; RAGE; stroke

Introduction

Acute brain injuries, including stroke, induce profound alterations of the peripheral immune system (Chamorro et al., 2012), which contribute substantially to morbidity and mortality of pa-

tients. The best described component of these systemic immune alterations is an acquired immune deficiency in the subacute phase after ischemic stroke, which predisposes patients to infections (Meisel et al., 2005). The main features of this syndrome are an inactivation of circulating monocytes and lymphopenia (Liesz et al., 2009; Urra et al., 2009b). On the other hand, activation of the peripheral immune system preceding the immunosuppressive syndrome has also been consistently described (Offner et al., 2006a). This sterile inflammatory response includes the massive release of proinflammatory cytokines from systemic innate immune cells within hours after the brain lesion (An et al., 2014). Yet, the pathophysiological impact of this early immune activation as well as its mediators are unknown.

In view of the extensive impact of the perturbed peripheral immune system on the damaged brain as well as on systemic infectious complications, the identification of the signaling pathways underlying systemic immune modulation is of great translational relevance. Previous reports have suggested a role of the autonomic nervous system in mediating subacute immunosuppression after acute brain injuries because elevated catechol-

Received June 15, 2014; revised Oct. 7, 2014; accepted Oct. 29, 2014.

Author contributions: A.L. and R.V. designed research; A.L., A.D., E.M., D.J.A., S.R., W.Z., M.A., and T.E. performed research; T.F., P.P.N., and K.J.T. contributed unpublished reagents/analytic tools; A.L., A.D., E.M., D.J.A., H.Y., S.-Y.N., M.A., T.E., P.P.N., and R.V. analyzed data; A.L. and R.V. wrote the paper.

This work was supported by the German Research Foundation DFG VE196/3-1 to R.V. and the Else-Kröner-Fresenius Foundation 2012/A118 to A.L., D.J.A. was supported by the Medical Research Council and a Wellcome Trust research fellowship. P.P.N. received funding by the German research foundation (Deutsche Forschungsgemeinschaft) for the collaborative research clusters (SFB) 1118 and 938. The authors thank the participating patients for their contribution to this study and Simone Karcher, Sabrina Heide, and Rene Karayilan for their technical support.

The authors declare no competing financial interests.

Correspondence should be addressed to either of the following: Dr. Arthur Liesz, Institute for Stroke and Dementia Research, University Hospital Munich, Max-Lebsche-Platz 30, 81377 Munich, Germany. E-mail: Arthur.Liesz@med.uni-muenchen.de; or Dr. Roland Veltkamp, Imperial College, Charing Cross Hospital, Fulham Palace Road, London SW7 2AZ, United Kingdom, E-mail: Roland.Veltkamp@imperial.nhs.uk.

DOI:10.1523/JNEUROSCI.2439-14.2015

Copyright © 2015 the authors 0270-6474/15/350001-16\$15.00/0

amine levels were observed in some of the previous experimental stroke studies. Blocking of adrenoreceptors reversed aspects of poststroke immunodepression, including susceptibility to bacterial infections in experimental stroke (Prass et al., 2003; Meisel et al., 2005). However, recent clinical (Liesz et al., 2013a) as well as experimental (Mracsko et al., 2014) studies have yielded mixed results regarding the implications of catecholamines in immunodepression.

Therefore, we focused in this study on soluble mediators released from the necrotic brain tissue as an alternative pathway in poststroke brain-immune interaction. Previous studies suggested a strong correlation between the volume of damaged brain tissue and the extent of systemic immune alterations, regardless of infarct location (Gendron et al., 2002; Hug et al., 2009). Accordingly, we speculated that soluble mediators would be released from dying neurons in proportion to the extent of necrotic tissue. As a prototypic alarmin, high mobility group box 1 (HMGB1) is a nuclear protein, which is released from necrotic cells with high inflammatory potency (Lotze and Tracey, 2005). As such, HMGB1 can act itself as a cytokine or amplify the binding of cytokines and nucleosomes to Toll-like receptors (TLRs) (Bianchi, 2009). The receptor of advanced glycation end-products (RAGE) has been identified as a key receptor (in addition to TLR2 and TLR4) for HMGB1, mediating activation pathways to a variety of cell types in an organ-specific manner (Lotze and Tracey, 2005).

Our study introduces the signaling of brain-released alarmins, such as HMGB1, through RAGE as an important link between acute brain injury and systemic immune alterations. We demonstrate a biphasic scenario where this signaling cascade initially activates peripheral monocytes and dendritic cells, resulting in a massive release of proinflammatory cytokines. Subsequently, initial (over)activation of the peripheral immune system results in exhaustion of monocytes and recruitment of immature monocytes. Suppressive signaling by the altered monocyte population leads to apoptosis of lymphocytes, the hallmark of poststroke immunosuppression.

Materials and Methods

Animals. The study was conducted in accordance with national guidelines for the use of experimental animals, and the protocols were approved by the governmental committee (Regierungspraesidium Karlsruhe, Germany). Animal experiments were designed, performed, and data reported according to the ARRIVE guidelines (Kilkenny et al., 2010). We used age-matched, male mice (C57BL/6J, 10–12 weeks, 23–25 g body weight, Charles River Laboratories). *RAGE*^{-/-} (Lilienstiel et al., 2004) and *MyD88*^{-/-} (Adachi et al., 1998) mice were bred in the core animal facility of the University of Heidelberg under specified pathogen-free conditions.

Patient recruitment and blood sampling. Blood samples used for analysis in this study were collected during a previous study (Liesz et al., 2013a) conducted between October 2011 until November 2012. In brief, inclusion criteria were study enrollment within 24 h after symptom onset. Exclusion criteria were recent clinical infection (fever, cough, antibiotic treatment, laboratory markers) within 14 d before admission, a chronic immunological disorder, preexisting immunosuppression, cancer, and pregnancy. Blood samples from 104 patients obtained within 24 h after symptom onset were analyzed. Patient characteristics are depicted in Tables 1 and 2. Stroke patients received routine cranial imaging by CT (Somatom Sensation 16) and/or 3T MRI (Trio and/or Verio; all Siemens Medical Systems) to detect ischemic brain lesions. Volume was calculated by integrating areas on each image multiplied by section diameter using a Syngo Multimodality workplace with syngoMMWP-software (version VE31A, Siemens). For the control group, patients were included that presented at the Department of Ophthalmology for pre-

Table 1. Patient characteristics of stroke and control patients for HMGB1 blood analysis

	Controls	Stroke patients	<i>p</i>
Total patients per group	20	104	
Age (years)	69.3 ± 9.2	73.2 ± 10.4	0.241
NIHSS on admission	0	11.7 ± 6.4	—
Median stroke volume (ml)	NA	29.4	—
Laterality (right/left)	NA	53/51	—
Blood samples (<i>n</i>) obtained within 24 h after symptom onset	NA	104	—
Blood samples (<i>n</i>) obtained within 72 h after symptom onset	NA	153 ^a	—
Mean time: symptom onset to first blood sampling (hours)	NA	10.7 ± 5.2	—
Comorbidities			
Hypercholesterolemia	6 (30%)	27 (26%)	0.998
Arterial hypertension	17 (85%)	72 (69%)	0.151
Diabetes	7 (35%)	30 (29%)	0.581
Premedication			
β-AR blocker	7 (35%)	39 (38%)	0.832
Oral anticoagulation ^b	4 (20%)	17 (16%)	0.689
Antithrombotics ^c	8 (27%)	17 (24%)	0.167
Sympathicoactive medication ^d	3 (15%)	7 (7%)	0.069

^aForty-nine patients were measured twice (at hospital admission and at day 3 after stroke onset).

^bPhenprocoumon, rivaroxaban.

^cAspirin, aspirin + dipyridamole, clopidogrel.

^dClonidin, oxybutinin, inhalable β2-AR agonists, doxazosin, terazosin.

Table 2. Patient characteristics of stroke and control patients for MDSC FACS (Fig. 3D)

Patient	Age (years)	Hypertension	Diabetes	Lesion localization	NIHSS	Lesion volume (cm ³)
Control 1	67	+	—	NA	NA	NA
Control 2	91	+	—	NA	NA	NA
Control 3	86	—	+	NA	NA	NA
Control 4	84	+	+	NA	NA	NA
Control 5	31	—	—	NA	NA	NA
Control 6	64	+	—	NA	NA	NA
Stroke 1	69	+	—	MCA, R	18	143
Stroke 2	76	+	+	MCA, R	33	317
Stroke 3	87	+	—	MCA, R	24	214
Stroke 4	43	—	—	ACA + MCA, L	19	293
Stroke 5	64	—	—	MCA, L	22	184
Stroke 6	73	+	+	MCA, R	18	174

NA, Not applicable; ACA, anterior cerebral artery; R, right; L, left.

surgical screening for cataract operation. Patients were selected to be in the same range for age and gender of patients with cerebrovascular disorders. All procedures were performed after written informed consent was obtained by the patient or a legal representative.

Animal experiments. Animals received intraperitoneal injection of 100 μg monoclonal anti-HMGB1 antibodies (clone 2g7) (Qin et al., 2006) 30 min before ischemia induction or an isotype control antibody (BioX-Cell); 100 μg soluble RAGE (full-length recombinant human sRAGE) was injected before middle cerebral artery occlusion (MCAO) induction and 4 h after MCAO. The β2-adrenoreceptor inhibitor ICI 118,551 (Sigma) was administered intraperitoneally at 4 mg/kg body weight before MCAO and at 4, 8, and 12 h after MCAO (Mracsko et al., 2014). Neutralization of circulating cytokines was achieved by intraperitoneal injection of 200 μg each of anti-IL-1β, anti-TNF-α, or anti-IL-6 antibodies (all from eBioscience, functional grade purified) in a total volume of 200 μl PBS intraperitoneally. Control mice received 300 μg of isotype control antibody. Organ sampling (brain, spleen, thymus, bone marrow, blood from retro-orbital sinus) for further analysis was performed in anesthesia with ketamin/xylazine. Rectal temperature and body weight were measured daily. Neurological deficits were assessed by a modified “Bederson score” (Bederson et al., 1986): 0, no deficit; 1, forelimb flexion;

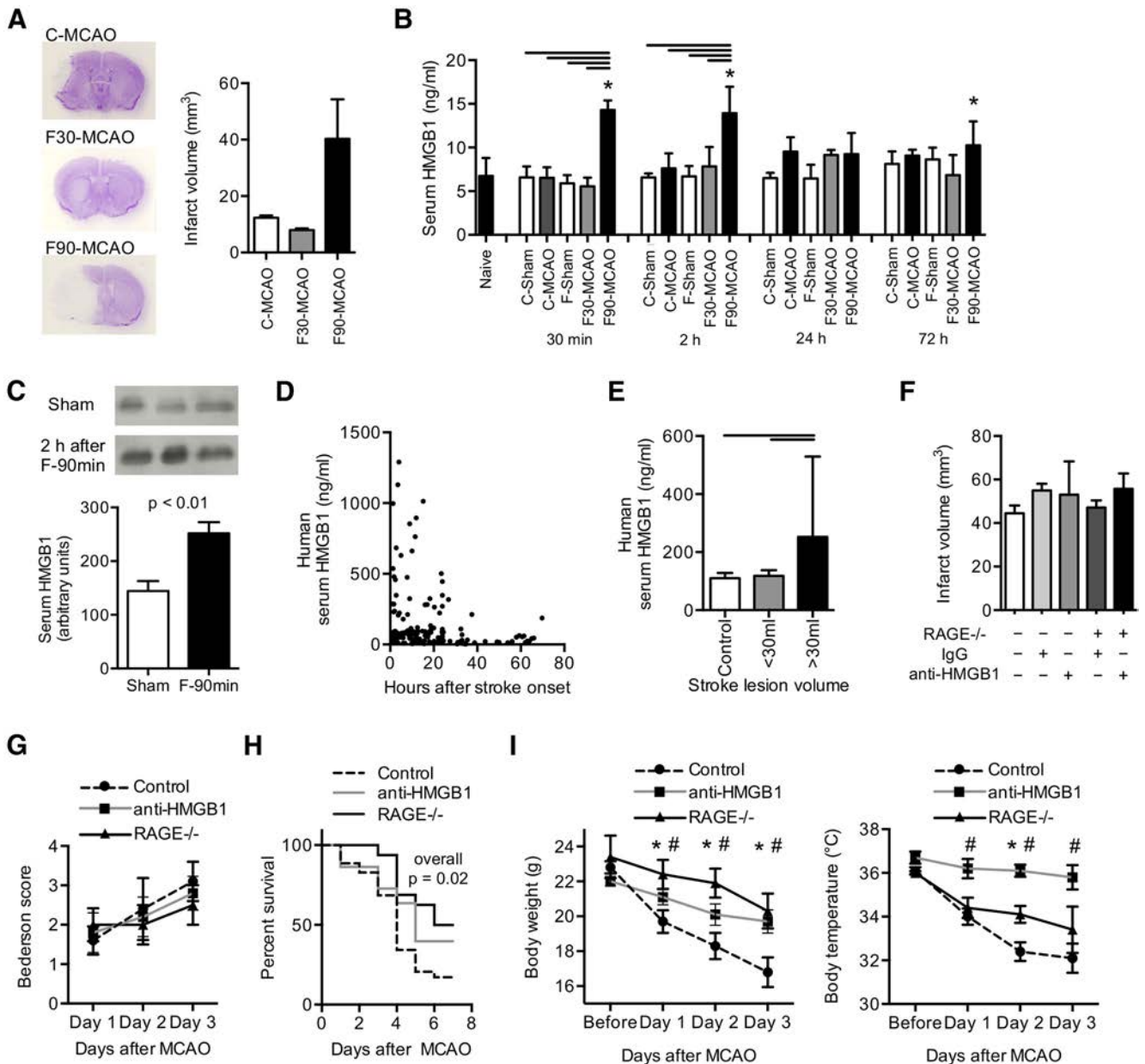


Figure 1. Inhibition of the HMGB1 pathway after stroke improves mortality. **A**, Representative cresyl-violet-stained brain sections (left) after permanent distal MCA occlusion (C-MCAO), 30 min or 90 min transient proximal filament-MCAO (F30-MCAO and F90-MCAO), and analysis of mean infarct volumes in the respective MCAO model (3 d after MCAO, $n = 12–15$ per model, C57BL/6J WT mice). **B**, Serum HMGB1 concentration was measured by ELISA in unoperated naive animals, in the three stroke models, and in respective sham-operated animals (C-sham and F-sham, respectively) at the indicated time points after MCAO ($n = 6$ per group). * $p < 0.05$, between naive and the indicated group. Bars represent $p < 0.05$ between marked groups within one time point. Data are representative for 3 individual experiments per time point. **C**, Increase of serum HMGB1 in the 90 min filament-occlusion model was verified by Western blot analysis at 2 h after MCAO compared with the sham-operated control mice ($n = 4$ per group). **D**, Dot plot analysis of HMGB1 serum concentrations of ischemic stroke patients up to 72 h after stroke onset ($n = 153$). **E**, Serum HMGB1 was measured in matched control patients without stroke ($n = 20$) and in stroke patients. For analysis of stroke patients ($n = 104$), only blood samples of individual patients (no repetitive measurements) up to 24 h after symptom onset were included and patient groups dichotomized into small/moderate (<30 ml) and severe (>30 ml) lesion volumes. **F**, Stroke lesion volume was analyzed 3 d after 90 min filament-occlusion MCAO (F-90 min) in control animals (C57BL/6J) and $RAGE^{-/-}$ animals receiving anti-HMGB1 or control (isotype IgG) treatment. Infarct volumes did not significantly differ among groups ($n = 18–34$ per group, 4 individual experiments, $p = 0.21$). **G**, The Bederson score reflecting poststroke motor deficits was not affected by anti-HMGB1 treatment or RAGE deficiency. **H**, Kaplan–Meier curves of poststroke survival within the first week after F-90 min MCAO in control, anti-HMGB1 treated, and $RAGE^{-/-}$ mice. Overall p value = 0.02; Mantel–Cox test; $n = 32$ (control), 17($RAGE^{-/-}$), 22(anti-HMGB1). p value ($RAGE^{-/-}$ vs control) = 0.008. **I**, Body weight (left) and rectal body temperature (right) were measured before surgery and on poststroke days 1–3 ($n = 15–18$ per group). * $p < 0.05$, control versus $RAGE^{-/-}$. # $p < 0.05$, control versus anti-HMGB1. **F–I**, Data are representative of 4 individual experiments.

2, decreased resistance to lateral push; 3, unidirectional circling; 4, longitudinal spinning; 5, no movement. Sensorimotor deficit was measured using the Rotarod test as previously described (Jones and Roberts, 1968; Liesz et al., 2013b). Briefly, mice were trained at first at constant 4 rpm, then three times at acceleration from 4 to 40 rpm in 210 s. Baseline assessment was performed as for training with acceleration and the mean calculated from three runs with a 10 min break in between. Time was

stopped if the mouse fell off the beam or passively rotated twice on the beam. Assessment 24 h after MCAO was performed similar to baseline measurement.

Experimental stroke models

Coagulation model. We used this stroke model for experiments shown in Figure 1A, B. Mice were anesthetized with 1.0%–2.0% halothane in O_2 /

N₂O. After making a 1 cm skin incision between the left eye and ear, we drilled a burr hole through the temporal skull. We removed the dura mater and occluded the MCA permanently using a bipolar electrocoagulation forceps (ERBOTOM, Erbe). During the operation, body temperature was kept at 37°C using a feedback controlled heating pad. We sutured the skin lesion and placed the mouse in a cage under an infrared heating lamp until recovery from anesthesia. Sham treatment was given according to the same surgical protocol as for MCAO but without coagulation of the MCA. The overall mortality in the coagulation model was <5% for the 3 d observation period.

Filament model. We used this model for all remaining experiments. Mice were anesthetized with 1.0%–2.0% halothane in O₂/N₂O-enriched air. We placed the laser Doppler probe over the cortical area supplied by the MCA. Baseline CBF was measured as relative perfusion units and defined as 100% flow. After neck dissection, we made an incision into the left external carotid artery between two ligations and advanced a silicon-covered 8-0 nylon monofilament through the internal carotid artery to occlude the MCA. MCA occlusion was documented as a decrease in relative perfusion values by laser Doppler to <20% of original flow, a less pronounced decrease in CBF was used as an exclusion criterion. We fixed the filament in this position by ligation, closed the neck, removed the Doppler probe, and placed the mouse in its cage. Then, 30 min (only for experiments in Fig. 1A, B) or 90 min, respectively, after filament insertion, the mouse was anesthetized again and the filament removed. After we closed the surgical wound, the mice were transferred to their cages with free access to water and food. During the operations body temperature was kept at 37°C with a feedback-controlled heating pad. We maintained normal body temperature of the mice between operations and until recovery after the procedure by an infrared heating lamp. Sham operation was performed in exactly the same manner as described above, including repeated anesthesia 30 or 90 min after sham surgery, except that the filament was only introduced briefly into the external carotid artery. The overall mortality in the 30 min occlusion model was <5% for the 3 d observation period; mortality for the 90 min occlusion model is reported in Figure 1H.

Assessment of infarct volume. We anesthetized the mice and perfused them transcardially with 20 ml normal saline. We removed the brains from the skull and froze them immediately in isopentane (–20°C). We cut 20- μ m-thick coronal cryosections every 400 μ m, stained the sections using a standard cresyl-violet staining protocol, scanned them at 600 dpi, and analyzed the infarct area on each section (ImageJ). The Swanson method was applied to indirectly measure the infarct area and to correct for cortical swelling (Swanson et al., 1990). The total infarct volume was determined by integrating measured areas and distances between sections.

Analysis of HMGB1 by electrospray ionization liquid chromatography mass spectrometry. All chemicals and solvents were of the highest available grade (Sigma). Samples were precleared with 50 μ l protein G-Sepharose beads for 1 h at 4°C. Supernatant HMGB1 was immunoprecipitated with 5 μ g rabbit anti-HMGB1 (Abcam; ab18256) for 16 h at 4°C as previously described (Antoine et al., 2009). Free thiol groups within HMGB1 were alkylated for 90 min with 10 mM iodoacetamide at 4°C. Cysteine residues in disulfide bonds were then reduced with 30 mM DTT at 4°C for 1 h followed by alkylation of newly exposed thiol groups with 90 mM NEM at 4°C for 10 min. Samples were subjected to trypsin (Promega) or GluC (New England Biolabs) digestion according to manufacturer's instructions and desalted using ZipTip C18 pipette tips (Millipore). Characterization of whole protein molecular weights, acetylated lysine residues, or redox modifications on cysteine residues within HMGB1 were determined as described previously by whole protein electrospray ionization or tandem mass spectrometry (Antoine et al., 2012; Nyström et al., 2013) using either an AB Sciex QTRAP 5500 or an AB Sciex TripleTOF 5600 (Sciex Inc.). Peptide analysis was determined using an AB Sciex QTRAP 5500 equipped with a NanoSpray II source by in-line liquid chromatography using a U3000 HPLC System (Dionex), connected to a 180 μ m \times 20 mm nanoAcquity UPLC C18 trap column and a 75 μ m \times 15 cm nanoAcquity UPLC BEH130 C18 column via reducing unions. A gradient from 0.05% TFA (v/v) to 50% ACN/0.08% TFA (v/v) in 40 min was applied at a flow rate of 200 nl/min. The ionspray potential

was set to 2200–3500 V, the nebulizer gas to 19, and the interface heater to 150°C.

ELISA. Human and mouse serum and cell culture supernatants were collected and immediately frozen at –80°C until analysis. Commercial ELISA kits were used for the quantitative analysis of HMGB1 (IBL) and cytokine expression of IL-1 β , TNF- α , IL-6, and IL-12p40 (all R&D Systems).

Homecage behavior analysis. Mice were held individually in 37 \times 16 \times 13 cm transparent plastic cages as homecages. Mice were recorded for 17–24 h for each day/night/d cycle before MCAO and at day 1 and/or day 3 after MCAO using CCD cameras and an infrared illumination system during the dark cycle. The camera angle was set up for recording of the long side of cages to observe horizontal as well as vertical activities, such as rearing and hanging. Ethovision (EthovisionXT, version 4.1, by Noldus Information Technologies) video tracking software was used to digitize the trials at a rate of 12.5 frames/s. Total distance moved, rearing time, and rearing frequency were determined using animal center point analysis according to areas indicated in Figure 2F.

Bacterial culture. For bacterial blood cultures, 30 μ l blood was drawn from each mouse and diluted in 270 μ l sterile PBS. For bacterial lung cultures, both lung lobes were homogenized in PBS in a total volume of 300 μ l; 50 μ l of each blood sample or 100 μ l of each lung homogenate was plated on Columbia agar with 5% sheep blood (BD Biosciences). Plates were incubated at 37°C in the presence of 5% CO₂ and colony forming units were evaluated after 24 h.

Determination of bacterial DNA in lung homogenates by quantitative PCR. Bacterial load in lung homogenates was determined applying a quantitative real-time PCR that amplifies 16S ribosomal DNA. Both lung lobes were homogenized, and DNA was extracted using the QIAmpDNA Mini kit (QIAGEN) according to the manufacturer's instructions with an eluate volume of 100 μ l. Samples were amplified with primers targeting conserved regions within the 16S rRNA gene (forward, 5'-TGG AGC ATG TGG TTT AAT TCG A-3'; reverse, 5'-TGC GGG ACT TAA CCC AAC A-3'). A defined plasmid standard (16S rRNA amplicon from *Escherichia coli*, cloned in pCR2.1, Invitrogen; plasmids quantified by spectrophotometry) was used as positive control for qPCR. Samples were assayed in triplicate in a 25 μ l reaction mixture containing 2 μ l of template DNA, 12.5 μ l of 2 \times Fast SYBR Green Master Mix (Applied Biosystems) and 12.5 pmol of forward primer and reverse primer (MWG). Cycling conditions were as follows: 95°C for 10 min, followed by 40 cycles at 95°C for 15 s and 60°C for 1 min each. For quantification, background levels of the nontemplate control were subtracted from the specific samples.

Western blotting. Proteins were isolated for HMGB1 and ARG1 Western blotting from samples using ice-cold RIPA buffer as previously reported (Liesz et al., 2013b). Lysates were electrophoresed, transferred to nitrocellulose membranes, and blocked with skim milk. Blocked membranes were probed with rabbit anti-HMGB1 (1:1000) or incubated with sheep anti-ARG1 (1:500; R&D Systems) in TBS-T plus 5% milk overnight at 4°C Peroxidase-conjugated goat anti-rabbit and donkey anti-sheep secondary antibodies were used, respectively, and blots developed by standard chemiluminescence protocols.

Stress mediator analysis. Serum cortisol and metanephrine/normetanephrine concentrations were measured in the central laboratory of the University Hospital Heidelberg by the same procedures used and validated for routine diagnostic analysis. Cortisol concentrations were measured by chemiluminescence immunoassays, and serum metanephrine/normetanephrine were detected by ELISA.

Magnetic cell sorting. MACS sorting using magnetic beads was used for isolation of CD11b-, CD11c-, and CD3-positive cells for *in vitro* studies. Single-cell suspensions were prepared from spleens of the respective naive donor animals or after experimental brain ischemia as indicated in the manuscript. Single-cell suspensions were then processed for further purification of the subpopulation according to the manufacturer's protocol using commercial MACS kits (Miltenyi Biotec) for the purification of the indicated population (total T cells, monocytes, dendritic cells, myeloid-derived suppressor cells).

Real-time PCR. RNA was isolated from spleens or isolated cells using the RNeasy kit (QIAGEN). Reverse transcription was performed with the

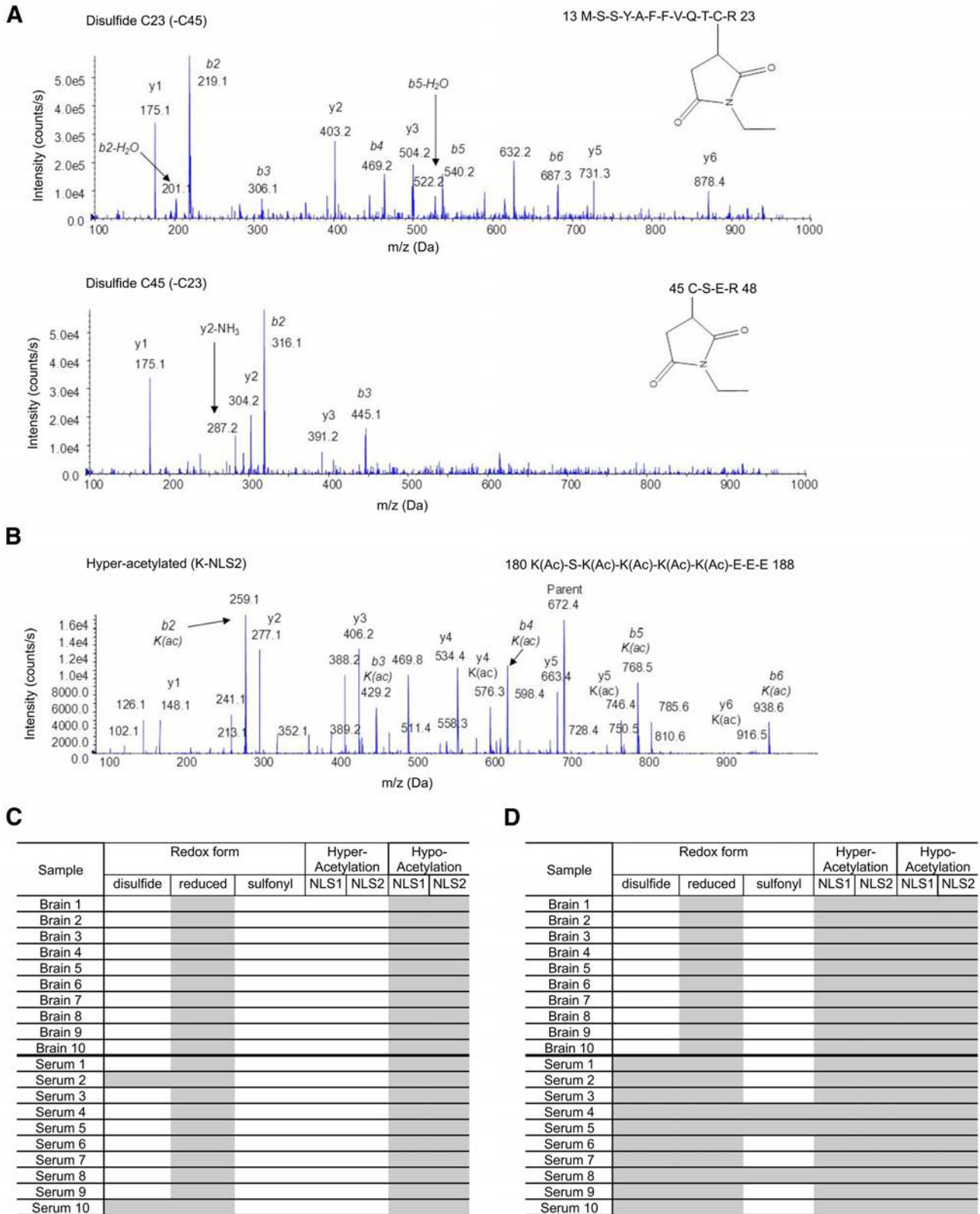


Figure 2. HMGB1 is released from necrotic brain tissue and matures to its cytokine-inducing form. **A**, Mass spectrometric characterization of the critical HMGB1 isoform with cytokine-inducing properties as categorized by the C23–C45 disulfide (NEM adduct) redox form. **B**, Representative spectrum of the tandem mass spectrometric characterization of a peptide (amino acids 180–188) covering the lysine (K) residues within nuclear localization sequence (NLS) 2 of HMGB1, depicting the hyperacetylated state of HMGB1-NLS2. Acetyl modifications are represented as (ac) on specific lysine residues (K181, K182, K183, and K184). **C, D**, Tabular overview of the detected isoforms of post-translationally modified HMGB1 in ipsilateral brain hemispheres and serum samples at 2 h (**C**) and 24 h (**D**) after F-90 min MCAO. Gray shading represents the presence of redox isoforms at cysteine residues and of the acetylation state at lysine residues within both nuclear localization signals (NLS) of HMGB1. C23–C45 disulfide isoforms mediate the cytokine-inducing HMGB1 activity. Hypoacetylation of the NLS regions indicates the nuclear localization and origin of HMGB1. Hyperacetylation of HMGB1’s NLS regions is involved in cytoplasmic shuttling of HMGB1.

High Capacity complementary DNA Archive Kit and real-time PCR with SYBR-Green assays on an ABI7500 real-time PCR system (Applied Biosystems). Primers were purchased as ready-to-use primer sets for each gene (Super Array). All assays were run in duplicate. Expression of each gene was quantified according to the relative standard curve method relative to the expression of the housekeeping gene encoding for β -actin.

In vitro assays

T-cell stimulation assay. For intracellular cytokine staining of isolated T cells, we plated single-cell suspensions of 300,000 mononuclear cells on 96-well plates (RPMI-1640, + 10% FCS, + glutamine, + HEPES, + penicillin/streptomycin, + mercaptoethanol). Each sample was processed in triplicate. We primed the cells for 48 h with plate-bound anti-mouse CD3e (clone 145-2C11, BD Biosciences) and 2 μ g/ml soluble anti-mouse CD28 (clone 37, clone 51, BD Biosciences), followed by re-stimulation with 500 ng calcimycin (Sigma-Aldrich), 5 ng/ml PMA (Sigma-Aldrich), and protein transport inhibitor (BD GolgiPlug, BD Biosciences) for 5 h.

Dendritic cell stimulation assay. CD11c⁺ splenic dendritic cells were isolated by MACS following the manufacturer's protocol (Miltenyi Biotec). CD11c⁺ cells were cultured at a concentration of 100,000 cells/well for 24 h. Fully phosphorothioate modified CpG-ODN 1668 (TIB Molbiol) was used at a concentration of 100 nM by adding the stimulus directly into the culture medium.

Marrow-derived suppressor cell (MDSC) suppression assay. CD11b⁺ Ly-6C_{high}⁺ cells were isolated by MACS and cocultured with CD3⁺ T cells (MACS-isolated) at the indicated ratio with a total cell count of 200,000 cells per well of a 96-well round-bottom plate. T cells were labeled with CFSE (CFSE cell proliferation kit, Invitrogen), and their proliferation was stimulated by plate-bound anti-CD3e (10 μ g/ml) and addition of concavalin A at 2 μ g/ml for a culture time of 42 h. Suppression of T-cell proliferation was assessed by measuring the CFSE dilutions and analyzed using Flowjo 4.2 software (TreeStar).

HMGB1 stimulation assay. For assessment of the cytokine-inducing activity of HMGB1, mixed splenocyte cultures (Fig. 2D) or cocultures of T cells with antigen-presenting cells (APCs) (Fig. 2E) were used. Erythrocyte-depleted primary cell suspensions of spleens from naive animals were used for mixed splenocyte cultures. For cocultures, T cells were isolated by MACS (T cell isolation kit I, Miltenyi) and APCs were isolated using the same kit. APCs were either irradiated or received sham treatment (placement in chamber with no irradiation). Cells were cultured in RPMI-1640 medium, "Cytokine HMGB1" (C23-C45 disulfide bond, purchased from HMGBiotech) was added to the culture medium at the indicated concentrations.

Flow cytometry. We collected organs (spleen, blood, mesenteric lymph nodes, and bone marrow) after transcardial perfusion with saline at various time points after MCAO for flow cytometric analysis. We stained single-cell suspensions for anti-mouse CD3 (clone 17A2), CD4 (clone RM 4–5), CD8 (clone 53–6.7), B220 (clone RA3–6B2), NK1.1 (clone PK136), Ly-6C (clone HK1.4), Ly-6G (Gr-1; clone RB6–8C5), CD80 (clone 16–10A1), CD86 (clone GL1), CD25 (clone PC61), CD69 (clone H1.2F3), CD11b (clone M1/70), MHC-II (M5/114.15.2), and CD11c (clone N418). Expression of IFN- γ (clone XMG1.2) and IL-4 (clone 11B11) was intracellularly detected after stimulation of T cells by the above published stimulation protocol.

Blood samples from stroke patients for FACS analysis were collected in EDTA tubes and immediately processed. Mononuclear cells were isolated by Ficoll gradient centrifugation and single-cell suspensions stained for anti-human CD11b (clone ICRF44), CD33 (clone P67.6), and HLA-DR (clone L243). We performed flow cytometry on a Becton Dickinson FACS Calibur and analyzed the data by CellQuest Pro software.

Statistical analysis. Sample size of the experiments was determined by *a priori* calculation presuming Type I error of 0.05, power of 0.8, and specific variance based on according preexperiments using *g** power statistical software. All values in bar graphs are expressed as mean \pm SD. We analyzed infarct volumes and functional outcome tests by two-tailed Student's *t* test after validating the normal distribution of these datasets (Kolmogorov–Smirnov test) or for >2 groups by ANOVA with Tukey *post hoc* analysis. For the remaining data without normal distribution, we

used two-tailed Wilcoxon rank-sum test for two groups or the Kruskal–Wallis test with Dunn's multiple comparison *post hoc* analysis test for more than two groups, using GraphPad Prism 5 software. *p* < 0.05 was considered statistically significant.

Results

HMGB1 is released from necrotic brain lesions

We analyzed HMGB1 serum concentrations by ELISA in different experimental stroke models varying by location and volume of the resulting infarct (Fig. 1A) and detected a significant increase only after large infarcts at early time points after stroke (Fig. 1B). This was verified by HMGB1 Western blotting at 2 h after stroke onset (Fig. 1C). We also found massively increased HMGB1 serum concentrations in stroke patients within the first hours after symptom onset (Fig. 1D). To verify HMGB1 release in human stroke, we further evaluated HMGB1 concentrations in blood samples from 104 patients (patient characteristics summarized in Table 1) within 24 h after symptom onset of small or large lesions (dichotomized by the median infarct volume, in this cohort 30 ml) and compared it with control patients (Fig. 1E). Because human and murine results showed a consistent pattern of early HMGB1 release into the circulation after extensive ischemic brain lesions, further experimental studies were performed exclusively in the 90 min transient MCAO model.

We analyzed the impact of blocking HMGB1 by neutralizing antibodies or by elimination of its receptor RAGE in knock-out mice on stroke outcome. Infarct volumes (Fig. 1F) and basic sensory-motor deficits measured by the Bederson score (Fig. 1G) did not differ significantly among anti-HMGB1 treated animals, *RAGE*^{-/-} mice, and controls in our experiments. Intriguingly, despite the lack of effect on infarct size and neurological deficit, 7 d mortality was substantially reduced in *RAGE*^{-/-} mice (*p* = 0.008, *n* = 22) and tended also to be lower in anti-HMGB1-treated mice (*p* = 0.07, *n* = 17) (Fig. 1H). Both HMGB1 neutralization and RAGE deficiency also attenuated loss of body weight and hypothermia after stroke (Fig. 1I). This dissociation between similar lesion size and differing mortality might indicate that HMGB1-RAGE blockade modified important systemic consequences of brain infarction rather than resulting in immediate structural neuroprotection.

HMGB1 matures in the circulation to its cytokine-inducing isoform

Because the biological activity of HMGB1 is critically dependent on the redox state of cysteine residues at C23, C45, and C106 (Yang et al., 2013), we analyzed post-translational HMGB1 modifications by tandem mass spectrometry (Fig. 2A,B). At 2 h after ischemia, the fully reduced isoforms with no cytokine-inducing but chemoattractant activity predominated in brain and serum samples as the disulphide form was not detected in any of the investigated brains and only in two often serum samples. Moreover, the exclusively hypoacetylated state confirmed the passive release of HMGB1 from necrotic cells (Fig. 2C, summary). In contrast, the cytokine-inducing C34-C45 disulphide HMGB1 isoform (Yang et al., 2010) was found as the prevalent isoform in serum samples at 24 h but could still not be detected in brain samples of the corresponding animals (Fig. 2D). These results indicate HMGB1 maturation in the blood circulation toward its cytokine-stimulating isoform after initial (passive) release from the necrotic brain tissue.

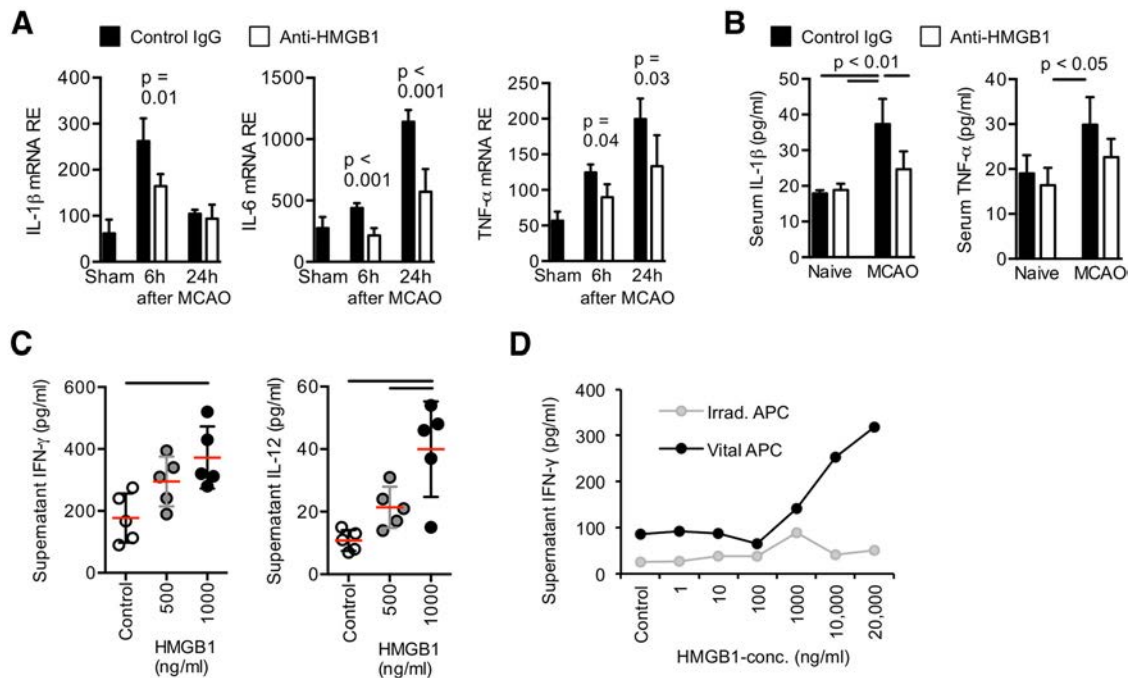


Figure 3. HMGB1 signaling induces early innate and adaptive immune activation. **A**, Cytokine mRNA expression was analyzed in spleens at the indicated time points after MCAO ($n = 7$ per group and time point). **B**, Expression levels of IL-1 β and TNF- α were verified on protein level in the serum of control mice (isotype IgG) and anti-HMGB1-treated mice without brain lesion (naive) and 24 h after F-90 min MCAO by ELISA ($n = 6$ per group). **A, B**, Data are representative of 2 individual experiments per time point. **C**, The cytokine-inducing function of HMGB1 was tested *in vitro*. Interferon- γ (left) and IL-12 (right) concentration was analyzed in supernatants of mixed splenocyte cultures stimulated with disulphide-HMGB1 at the indicated concentration and compared with unstimulated samples (control). Bars represent $p < 0.05$ between indicated groups. Each data point represents one individual experiment. **D**, Naive CD3 $^{+}$ T cells were cocultured with untreated (vital) or irradiated APCs and stimulated with HMGB1 at the indicated concentration for 24 h. Interferon- γ concentrations were measured in the supernatant by ELISA (data representative of 5 individual experiments). Vital APCs are required for stimulation of IFN- γ production by T cells.

The early phase after brain injury is characterized by massive systemic cytokine secretion mediating sickness behavior

To determine the contribution of HMGB1 signaling on sterile systemic inflammation, cytokine concentrations were determined within the acute phase after brain ischemia. Expression levels of the proinflammatory cytokines IL-1 β , TNF- α , and IL-6 were markedly increased in the acute phase after stroke onset (Fig. 3A). Antibody-mediated neutralization of HMGB1 significantly attenuated splenic expression and serum concentrations of these proinflammatory cytokines (Fig. 3A,B). Supporting the immune-stimulatory role of HMGB1, *in vitro* stimulation of splenocyte cultures with the cytokine-stimulating isoform of HMGB1 resulted in increased expression of T cell- (IFN- γ) and monocyte- (IL-12) derived cytokine secretion (Fig. 3C). Moreover, we detected a dose–response relation for HMGB1 concentration and IFN- γ secretion by isolated T cells, which depended on the presence of viable APCs (Fig. 3D).

Weight loss and hypothermia, as shown in Figure 1I, are considered as basal markers of sickness in models of immune-mediated diseases (Dantzer, 2006). We further investigated this phenomenon in a homecage behavior analysis setup, which enabled the automated analysis of circadian rhythm and complex mouse behavior (Jhuang et al., 2010; Spulber et al., 2012) (Fig. 4A). Although no behavioral difference was detected between RAGE $^{-/-}$ animals and WT controls at baseline before MCAO (data not shown), we detected a disturbance in circadian rhythm at day 1 after stroke. This was more pronounced in WT compared with RAGE $^{-/-}$ animals with respect to arousal after the start of the day cycle (6 A.M.) and disparity between overall night and day activity (Fig. 4B). Furthermore, mobility and exploratory behavior (total distance moved), targeted movements to reach the water bottle

(rearing time and frequency), and challenging physical activities (hanging time) were significantly less affected during the early phase after stroke induction in RAGE $^{-/-}$ compared with WT mice (Fig. 4C).

To investigate the role of the peripheral cytokine release in the acute phase after brain injury as the potential link between RAGE deficiency and improved behavior, we antagonized IL-1 β , TNF- α , and IL-6 by neutralizing antibodies and analyzed key features of sickness behavior as introduced above. Infarct volumetry revealed similar infarct volumes in control- and anti-cytokine-treated mice (Fig. 4D). Additionally, focal sensorimotor dysfunction analyzed by the Rotarod test did not differ between the treatment groups (Fig. 4E). This demonstrated that peripheral cytokine neutralization had no immediate impact on the primary brain lesion. In contrast, homecage behavior analysis revealed a similar treatment effect of cytokine antagonization as previously seen in RAGE-deficient mice. The cytokine neutralization improved the stroke-induced disturbances in circadian rhythm with reduced variation between light and dark periods (Fig. 4F). It also improved overall motility as depicted by analysis of total distance moved in the first 2 h of the light period (6 A.M. to 8 A.M.) (Fig. 4G).

RAGE signaling promotes MDSC expansion

Based on the finding that APC viability is critical for the impact of HMGB1 on lymphocyte function (Fig. 3D), we further analyzed the role of monocytes in this model. We found an expansion of a specific immature monocyte subpopulation in the spleen, characterized by the CD11b $^{+}$ Ly-6C $^{+}$ MHC-II $_{low}$ expression pattern after stroke (Fig. 5A), which was abrogated by anti-HMGB1 treatment (Fig. 5B). Further analysis of this population in spleen and bone marrow revealed both increased splenic proliferation (marker Ki-67) and a reduced proportion of this subpopulation

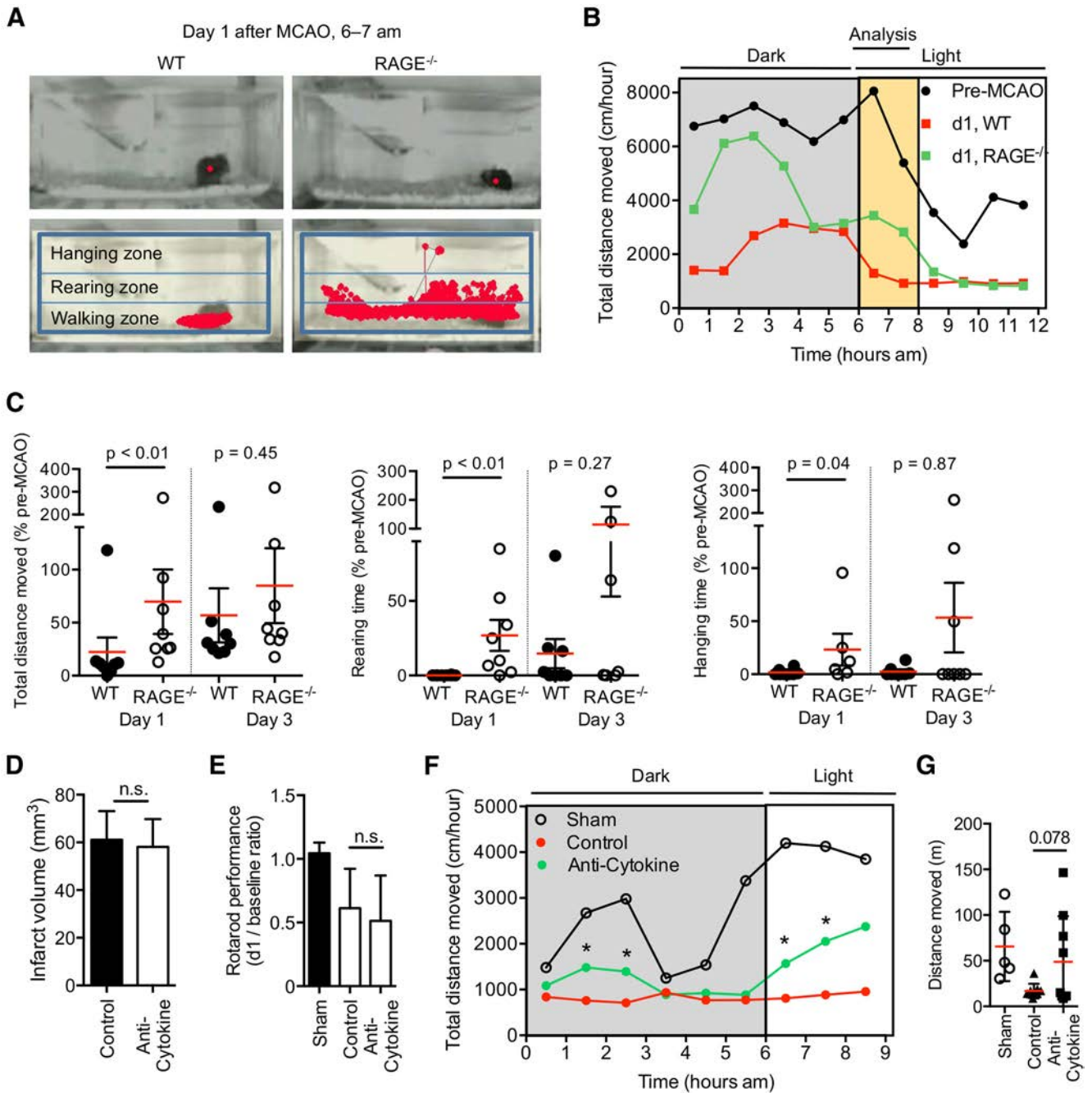
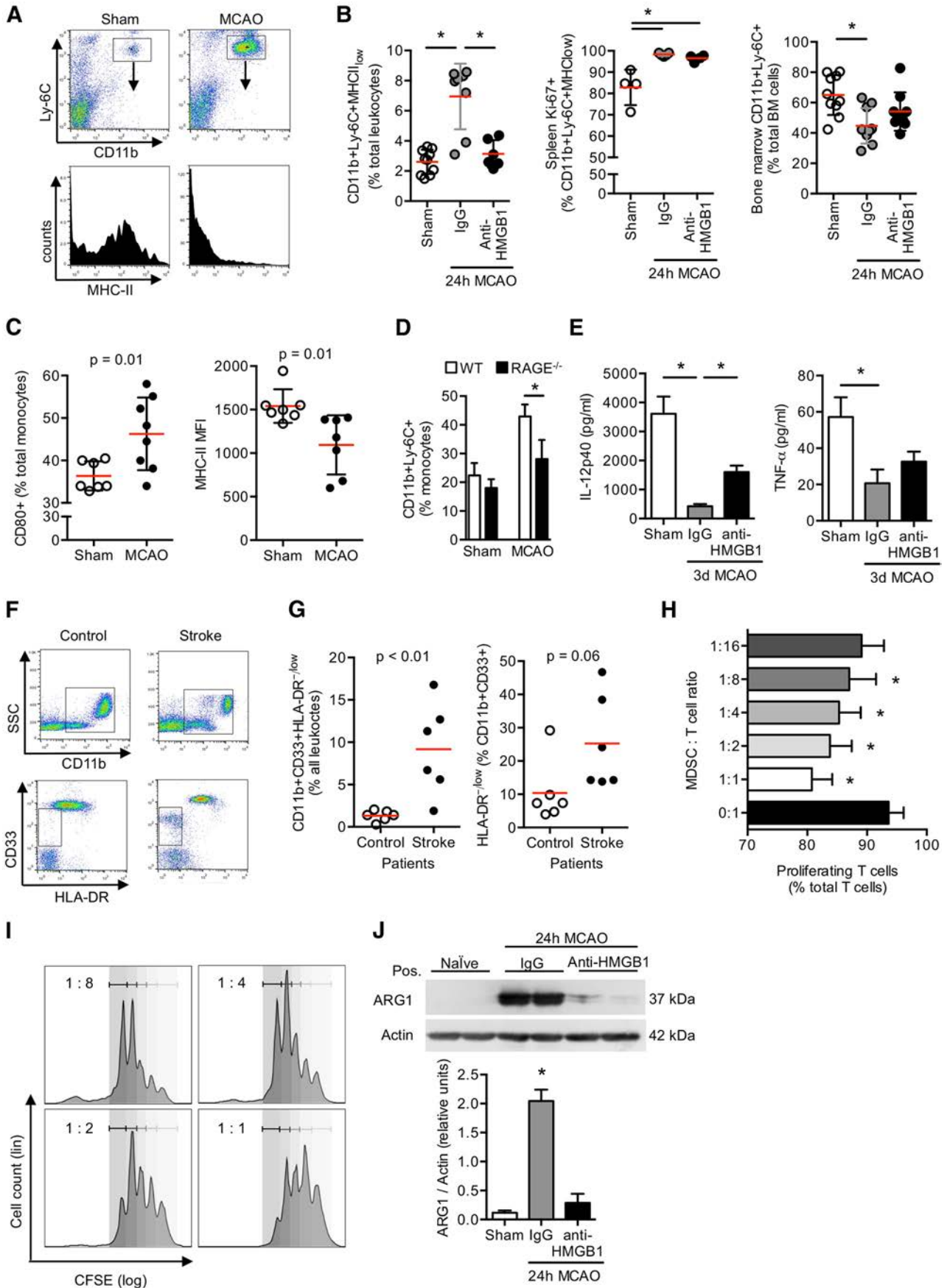


Figure 4. RAGE signaling mediates sickness-like behavior in the acute phase after stroke. **A**, Representative images of the unmodified tracking zones for continuous recording by the homecage behavior system (top). Analysis fields (hanging and rearing zones) and tracking (red lines) of mice in their home cages, indicated for 1 h recording (bottom). **B**, Brain ischemia by F-90 min MCAO induces a disturbed circadian rhythm with reduced activation response after a shift of night-day cycle at 6 A.M. Data are depicted for total distance moved per 1 h during the 12 h recording period (6 h dark and light cycle, each) and indicate a different degree of disturbed circadian rhythm between *RAGE*^{-/-} and WT mice at day 1 (d1) after MCAO. **C**, Results of the homecage behavior analyses for overall mobility (moving distance: left) or motivation to challenging physical activity (rearing time: middle; hanging time: right) shown as cumulative data during the 2 h period from 6 A.M. to 8 A.M. at day 1 and day 3 after MCAO in WT control and *RAGE*^{-/-} mice. Data were obtained in 3 individual experiments. **D**, Infarct volumetry 24 h after 90 min transient MCAO in mice receiving neutralizing antibodies against IL-1, TNF- α , and IL-6 (anti-cytokine) or isotype control IgG (control). **E**, Sensorimotor deficits were determined in the corresponding groups as in **D** and in a sham-operated group 24 h after F-90 min MCAO and normalized to baseline values. *n.s.*, Not significant. **F**, The disturbed circadian rhythm after MCAO compared with sham treatment is improved in the anti-cytokine treated group as depicted by the approximation of the activity pattern to one of mice with sham surgery. **G**, Analysis of the total distance moved within the first 2 h of the light period (6 A.M. to 8 A.M.). **D–G**, Data were obtained from 3 individual experiments; *n*(sham) = 9, *n*(control) = 9, *n*(anti-cytokine) = 9.

in the bone marrow (Fig. 5B). These findings are compatible with a combination of local splenic proliferation as well as bone marrow egress of immature monocytes. Moreover, stroke in WT mice resulted in an increase in CD80 expression and a reduction of MHC-II expression on monocytes (Fig. 5C). The stroke-induced rise of immature splenic monocytes compared with

sham-operated mice was significantly reduced in *RAGE*^{-/-} animals 3 d after MCAO, supporting the role of HMGB1-RAGE signaling on immature monocyte recruitment (Fig. 5D).

To assess functional capabilities of splenic monocytes after stroke that were independent of the RAGE signaling pathway, we performed stimulation assays with the TLR9-ligand CpG-ODN.



This revealed substantially reduced IL-12 and TNF- α secretion by monocytes 3 d after brain ischemia consistent with a reduced responsiveness of splenic monocytes resulting from functional exhaustion. *In vivo* anti-HMGB1 treatment partially attenuated monocytic hyporesponsiveness to *in vitro* stimulation as shown by increased IL-12 secretion in the anti-HMGB1-treated group compared with control mice, although it had no effect on TNF- α production (Fig. 5E). Next, we analyzed the frequency of immature monocytes, delineated by expression of CD11b⁺CD33⁺HLA⁻, in stroke patients with extensive brain lesions (>100 ml lesion volume) and matched control patients without neurological disease (Fig. 5F; Table 2). We detected a significant expansion of immature monocytes also after human stroke (Fig. 5G). We further analyzed the functional properties of the expanded CD11b⁺Ly-6C⁺ monocyte population to stimulate or inhibit T cells. Splenic CD11b⁺ monocytes isolated 3 d after stroke used as APCs in coculture with CD3⁺ T cells had a suppressive effect on T-cell proliferation (Fig. 5H,I). Additionally, arginase-1 (Arg1) expression, a marker of myeloid-derived suppressor cells (Rodríguez and Ochoa, 2008; Gabrilovich and Nagaraj, 2009), was massively increased in poststroke splenic monocytes, which was prevented by *in vivo* pretreatment with anti-HMGB1 (Fig. 5J).

Poststroke lymphocytopenia in the subacute phase is partially mediated by HMGB1 signaling

We investigated the role of the HMGB1-RAGE pathway on the previously documented decrease in immune cell cellularity in the subacute phase after stroke (Prass et al., 2003; Offner et al., 2006b; Liesz et al., 2009) (Fig. 6A–D). RAGE deficiency, but not anti-

HMGB1 treatment, reduced splenic lymphocyte apoptosis after brain ischemia (Fig. 6A,B). Similarly, the stroke-induced reduction of circulating blood T cells was prevented in RAGE-deficient mice (Fig. 6C). The postischemic effect on B-cell and granulocyte counts, however, was not influenced by either anti-HMGB1 treatment or by RAGE- or MyD88 deficiency, respectively (data not shown). Furthermore, we observed a relative increase of activated T cells (activation markers CD25 and CD69) in RAGE^{-/-} mice compared with WT mice after stroke (Fig. 6D). Because of the incomplete antagonization of the immunosuppressive phenotype by RAGE deficiency, we further investigated the impact of TLR-mediated pathways in stroke-induced immune disturbances using MyD88^{-/-} mice. We detected a similar pattern for T-cell counts in spleen and blood as for RAGE^{-/-} mice after stroke with partial abrogation of lymphopenia in MyD88^{-/-} mice without further augmentation by anti-HMGB1 treatment (Fig. 6E). In summary, these results indicate that the immunosuppressive and lymphotoxic effects of extensive brain ischemia are mediated at least in part by HMGB1 via the RAGE and the TLR-MyD88 pathways.

HMGB1-RAGE signaling is a distinct alternative signaling pathway after acute brain injury

To control for potential confounding factors known for the used stroke model of large brain lesion, we performed additional analyses to investigate alternative explanations for the observed effects independent of the HMGB1-RAGE pathway. Previous reports have demonstrated bacterial infections in this model, which could have interfered with the immunological and behavioral readout parameters investigated in this study. However, we did not detect bacteria in lung homogenates or blood of any mice (Fig. 7A). Furthermore, catecholamines released by activation of the sympathetic autonomous nervous system have been reported as mediators of poststroke immunosuppression (Prass et al., 2003; Meisel et al., 2005). Therefore, we measured serum concentrations of glucocorticoid and catecholamine stress mediators in WT control mice, anti-HMGB1 treated, and RAGE-deficient mice after stroke without detecting significant differences among groups (Fig. 7B). Next, we aimed to analyze the functional role of catecholamine signaling on critical parameters affected by the HMGB1-RAGE pathway in the previous experiments, such as cytokine release, spleen cellularity, and MDSC expansion. Therefore, we treated mice either with the β 2-adrenoreceptor blocker (b2-INH) ICI 118,551 (Mracsko et al., 2014), sRAGE, or the combination of both. We observed that the inhibition of the RAGE pathway by sRAGE-treatment, but not blockade of the adrenergic b2 receptor by b2-INH, abrogated the increased systemic IL-6 secretion after brain ischemia (Fig. 7C). Both sRAGE treatment and b2-INH injection prevented the expansion of the CD11b⁺Ly-6C⁺ monocyte fraction (compare with Fig. 5B). However, b2-INH injection also caused a significant reduction in this cell population compared with control-treated mice (Fig. 7D). On the other hand, the marked reduction of spleen cellularity (Fig. 7E) was not affected by b2-INH but significantly abrogated by sRAGE treatment. Interestingly, the combination of the RAGE as well as the catecholamine signaling had an additive effect on this parameter. These results indicate that the HMGB1-RAGE and the stress-mediator pathways might be largely independent but differentially involved in specific signaling cascades, such as acute cytokine release and immunosuppressive pathways.

←

Figure 5. Stroke induces immune exhaustion and expansion of immature monocytes via HMGB1-RAGE signaling in the subacute phase after stroke. **A**, Representative FACS plots for CD11b/Ly-6C expression of splenic mononuclear cells (CD45⁺ gated) 3 d after sham or F-90 min MCAO operation and the respective histogram for MHC-II expression of the double-positive cell population. **B**, Cell count of myeloid-derived progenitor cells (CD11⁺Ly-6C⁺MHC-II^{low}) and their proliferation (CD11⁺Ly-6C⁺Ki-67⁺) was analyzed in spleens at 24 h after sham operation or F90 min-MCAO with control (IgG) or anti-HMGB1 treatment (two left panels). Cell count of CD11b⁺Ly-6C⁺ cells in the bone marrow was determined in the same groups (right panel). Bars represent $p < 0.05$ between indicated groups. **C**, Splenic CD11c⁺ dendritic cells were analyzed for CD80 and MHC-II expression at 3 d after sham operation (control) or MCAO. **D**, Frequency of immature CD11⁺Ly-6C⁺ monocytes was compared between WT and RAGE^{-/-} mice 3 d after F90 min-MCAO or sham surgery ($n = 6$ per group). **E**, Splenic CD11c⁺ dendritic cells (1×10^5 cells) harvested from sham-operated animals and control antibody (IgG) or anti-HMGB1 treated animals 3 d after MCAO were stimulated with 1 μ M CpG-ODN overnight, and IL12p40 and TNF- α cytokine concentrations were measured in the cell culture supernatant ($n = 6$ per group). **B–E**, Results are representative of at least two individual experiments per set. **F**, Representative FACS dot plots for CD11b (top) and CD33/HLA-DR expression (gated for CD11b⁺, bottom) of total blood leukocytes (CD45⁺ gated) from control or stroke patients. **G**, Blood cell counts of immature CD11b⁺CD33⁺ monocytes (left) and their HLA-DR expression were analyzed in control patients with no neurological disease or in stroke patients at 24 h after extensive brain ischemia. **H**, Suppression assay analysis was performed to determine the suppressive function of splenic CD11b⁺Ly-6C⁺ monocytes harvested from donor animals 24 h after F90 min-MCAO (MDSC). T cells and MDSCs were cocultured at the indicated ratio and the proliferation of CFSE-labeled T cells analyzed by FACS (shown as percentage of total CD3⁺ T cells). CD11b⁺Ly-6C⁺ cells after MCAO are potent suppressors of T-cell proliferation. Data are representative of 5 individual experiments. **I**, Representative plots with fitted peaks for cell proliferation analysis by FlowJo software as used for MDSC suppression assay analysis shown before. Labeling in the plot indicates MDSC:T-cell ratio. **J**, Representative Western blot images (top) and analysis of ARG1 protein expression (bottom). ARG1 expression was measured in isolated splenic CD11b⁺ cells from sham-operated animals and control antibody (IgG) or anti-HMGB1 treated mice 24 h after F90 min-MCAO. Analysis is depicted as normalized ARG1 density values to actin expression. * $p < 0.05$ ($n = 5$ per group, 2 individual experiments).

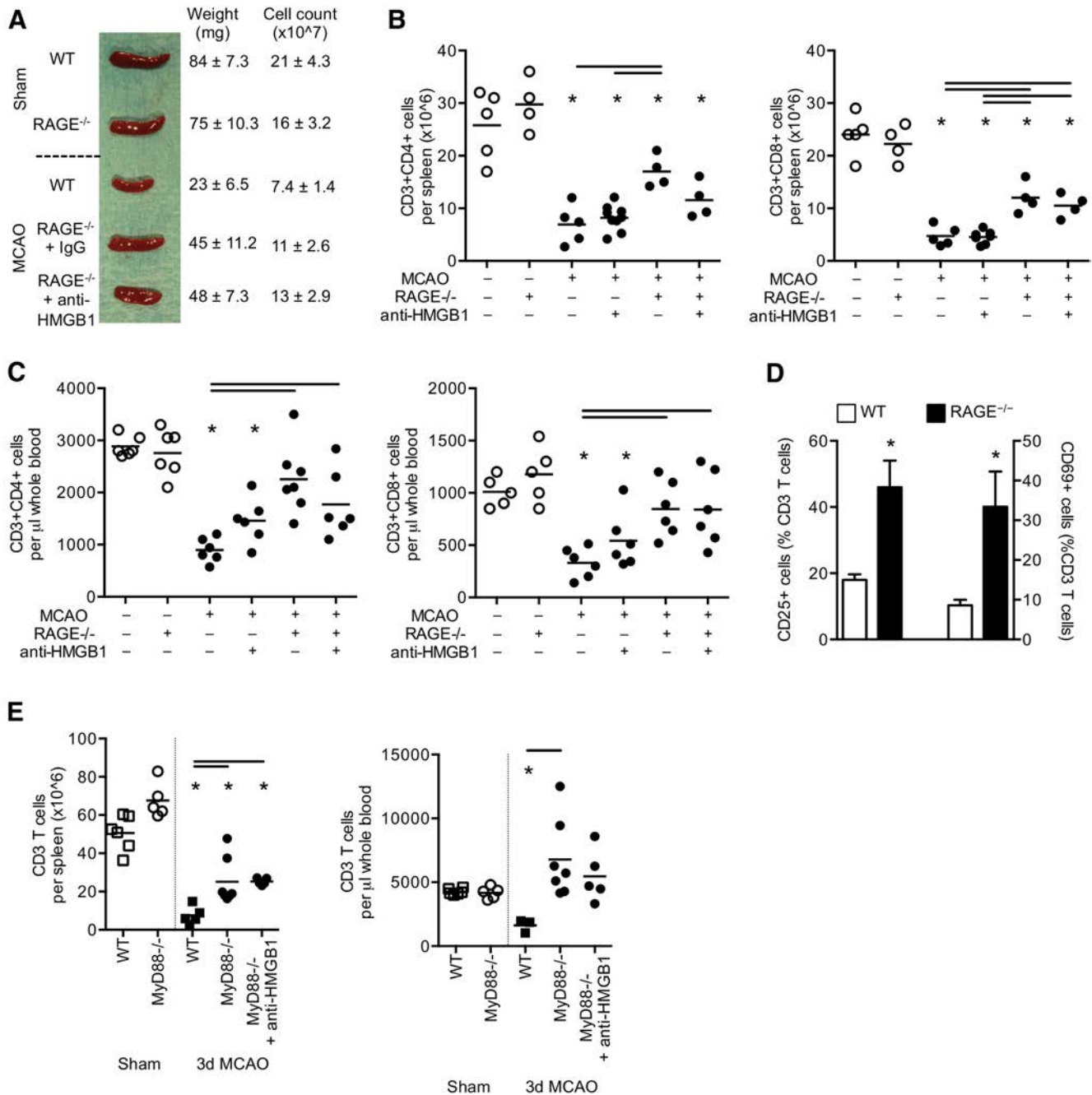


Figure 6. HMGB1-RAGE signaling induces profound compromise of the peripheral adaptive immune system in the subacute phase after stroke. **A**, Representative images, mean weight, and cellularity (\pm SD) of spleens 3 d after sham operation or F90 min-MCAO in WT mice and RAGE^{-/-} mice receiving control or anti-HMGB1 treatment ($n = 5-7$ per group). MCAO induces a profound reduction in spleen weight and cell count, which is significantly reversed in RAGE^{-/-} mice. **B**, Flow cytometric analysis of absolute cell counts of T_{helper} (CD3⁺CD4⁺) and T_{cytotoxic} (CD3⁺CD8⁺) cells per spleen and (**C**) per microliter of whole blood in sham-operated animals and 3 d after F90 min-MCAO in WT and RAGE^{-/-} mice receiving additional control IgG antibodies or anti-HMGB1 treatment. * $p < 0.05$, between control animals of the same mouse strain and the indicated group. Bars represent $p < 0.05$ between marked groups within the MCAO⁺ groups. **D**, T-cell activation was analyzed (CD69⁺ right y-axis and CD25⁺ left y-axis, respectively) in spleens of WT and RAGE^{-/-} mice 3 d after MCAO ($n = 6$ per group). **E**, The downstream signaling pathway of TLRs on CD3⁺ T cells was analyzed in MyD88^{-/-} mice. T-cell counts were measured per total spleen (left) and microliters of whole blood (right) in sham-operated animals and 3 d after F90 min-MCAO in WT and MyD88^{-/-} mice treated with control or anti-HMGB1 antibodies. * $p < 0.05$, between sham-operated animals of the same mouse strain and the indicated MCAO group. Bars represent $p < 0.05$ between marked groups within the MCAO groups.

Discussion

This study presents data supporting a novel concept of brain-immune interaction after acute brain lesions in which soluble danger signals from the brain mediate a complex immunomodulatory reaction in the peripheral immune system. Previous studies have focused on the role of HMGB1 and other DAMPs on immediate tissue injury within a defined organ, such as the heart

and the brain (Andrassy et al., 2008; Muhammad et al., 2008; Shichita et al., 2012). This is the first study uncovering suprasystemic cross signaling via RAGE largely by cytokine-inducing isoforms of the soluble mediator HMGB1 released from the necrotic brain. Our findings provide new insights into the peripheral immune alterations in response to brain injury and propose brain-released alarmins as important mediators of the systemic

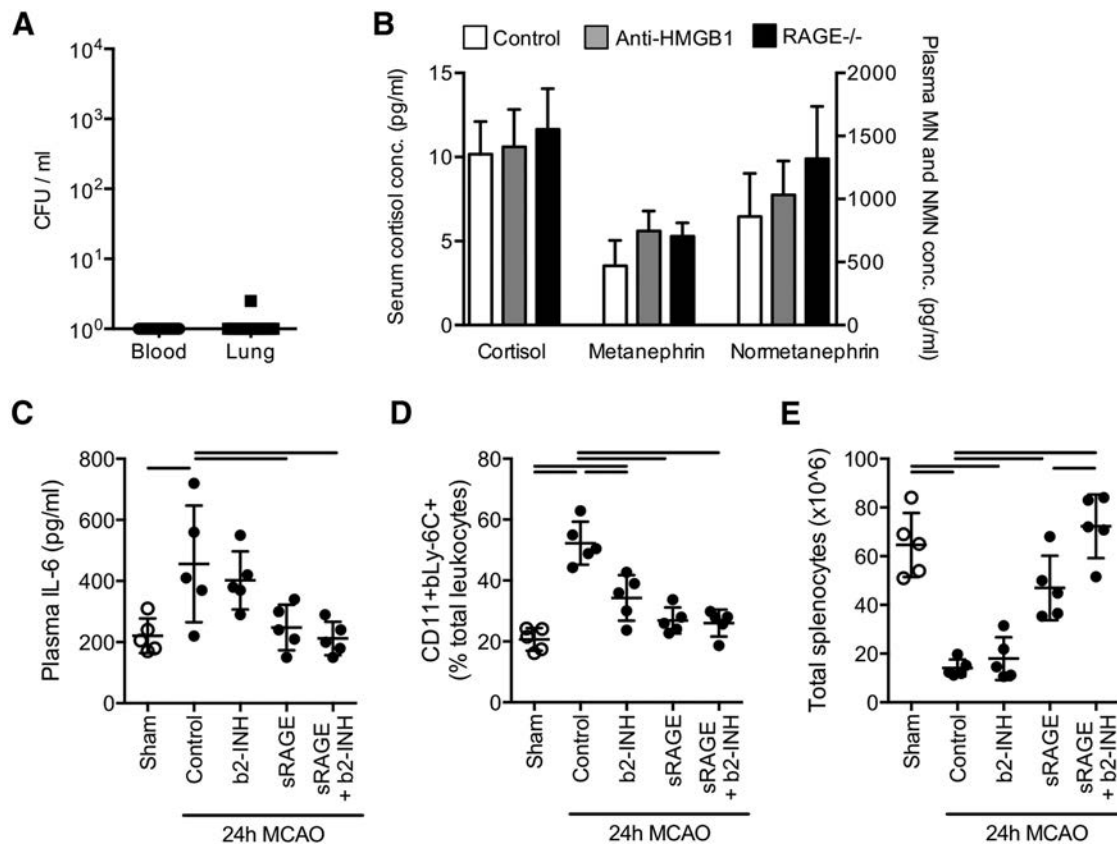


Figure 7. The HMGB1-RAGE pathway is distinct from infectious or catecholamine-mediated effects. **A**, Microbiological analysis of blood samples and lung homogenates 3 d after 90 min Filament-MCAO for presence of bacteria. No significant growth of colony forming units (CFU) was detected after 24 h of incubation time on blood agar plates in any sample ($n = 21$, 2 individual experiments). **B**, Serum concentrations of cortisol and the catecholamines metanephrine and normetanephrine were measured 24 h after stroke induction ($n = 7$ per group, 2 individual experiments). Mice were treated with the β_2 -adrenoreceptor inhibitor ICI 118,551 (b2-INH) and/or sRAGE as indicated in Materials and Methods. **C**, sRAGE treatment, but not b2-INH, significantly reduced plasma IL-6 concentrations 24 h after F90 min-MCAO. **D**, The expansion of CD11b⁺Ly-6C⁺ MDSCs at 24 h after F90 min-MCAO was significantly reduced by sRAGE and, to a lesser extent, by b2-INH and without a measurable additive effect. **E**, The reduction in spleen cellularity induced by MCAO was abrogated by b2-INH as well sRAGE treatment with an additive effect. **C–E**, Data were obtained in three individual experiments; $n = 5$ per group.

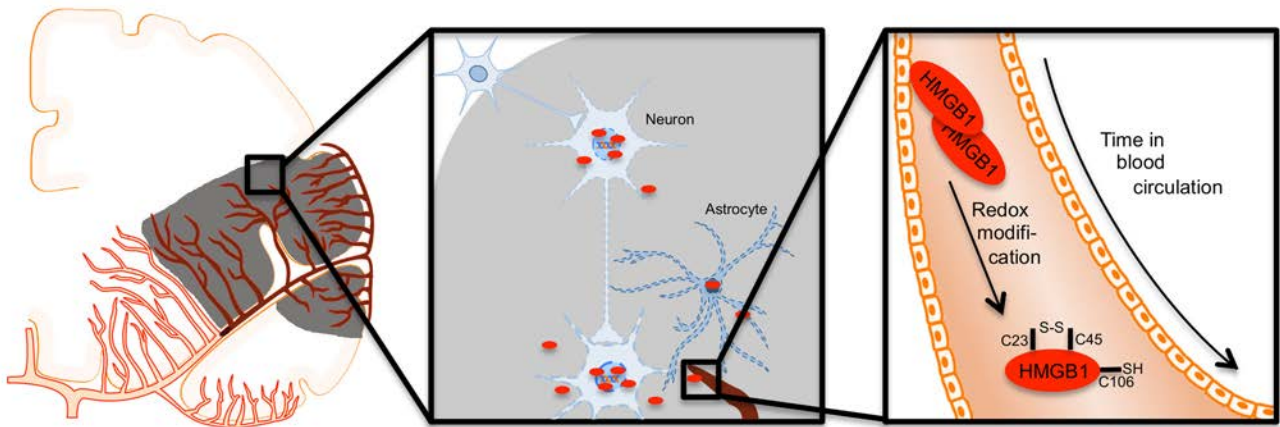
immune response leading to complex behavioral and metabolic sequelae.

Our results are of clinical relevance for patients presenting with severe acute brain injury because their prognosis is strongly influenced by secondary immune-mediated complications. In the early phase after clinical stroke and traumatic brain injury features of sickness behavior, including sleep disorders, fatigue, and depression, are common (Dantzer, 2006; Crosby et al., 2012), which affect secondary morbidity and physical recovery (Willey et al., 2010; Lerdal and Gay, 2013). The concept of proinflammatory cytokines as the cause of clinical sickness behavior and peripheral inflammation is well established, and IL-1 β , IL-6, and TNF- α are seen as the main mediators (Dantzer et al., 2008). These cytokines are also strongly upregulated in the periphery during the acute phase after brain ischemia as shown in the present and previous reports (Offner et al., 2006a; Chamorro et al., 2012), but the underlying signaling and the resulting pathophysiological implications were unknown. In this study, we identified the HMGB1-RAGE signaling pathway as the critical route inducing this overshooting immune reaction after brain injury. Inhibiting this signaling pathway improved the systemic metabolic and behavioral consequences of stroke and reduced mortality but did not affect the size of the brain lesions. Similarly, direct neutralization of the overshooting cytokine-release in the acute phase after MCAO improved similar behavioral parameters, such as

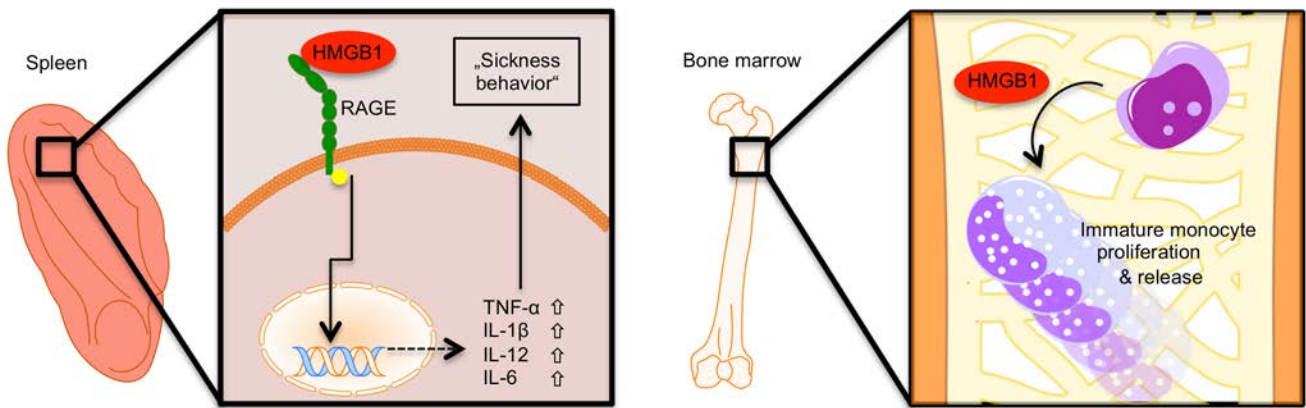
circadian rhythm and mobility as for inhibition of the HMGB1-RAGE pathway, supporting the concept of HMGB1-RAGE mediated cytokine-induced behavioral alterations. Because cytokine-induced sickness behavior is still not well established as a distinct syndrome in the clinical setting and also requires more comprehensive characterization in experimental models, future studies will have to further validate this concept. Additionally, we cannot exclude immediate modulatory effects of HMGB1-RAGE signaling on brain structures that are not primarily affected by the brain ischemia (e.g., hippocampus). Also, stress mediators, which are released after acute brain injury, might have a currently unknown direct impact on poststroke behavior mimicking cytokine-induced sickness behavior (see below).

Immunosuppression predisposes patients to bacterial infections, which contribute substantially to poststroke morbidity (Katzan et al., 2003). Based mainly on an experimental landmark study using the β blocker propranolol (Prass et al., 2003), catecholamines have been suggested as the key mediators of poststroke immune suppression and infectious complications (Dirnagl et al., 2007; Iadecola and Anrather, 2011). Furthermore, a previous study reported the modulation of hepatic iNKT cells by noradrenergic signals after experimental stroke (Wong et al., 2011). Indeed, most immune cells express catecholaminergic receptors and may undergo cell death after *in vitro* stimulation with metanephrines, but blockade of β adrenergic receptor *in vivo* and

A HMGB1 release



B Early phase



C Subacute phase

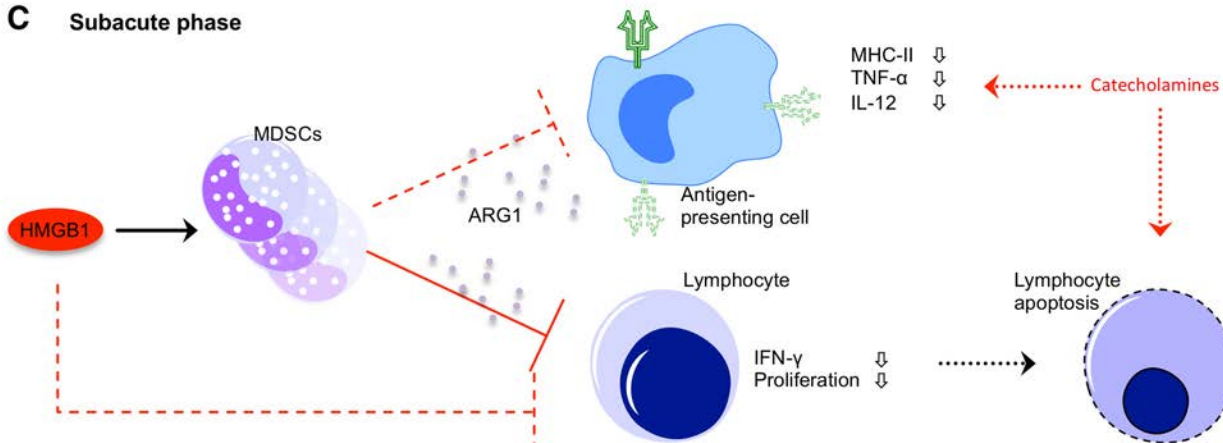


Figure 8. Schematic overview of the proposed mechanisms of HMGB1 release and its biological activity after acute stroke. **A**, After acute vessel occlusion, cells of the hypoperfused territory become necrotic and release HMGB1 (fully reduced, hypoacetylated) from its nuclear localization. Between 2 and 24 h after ischemia onset, the (C23–C45) disulphide “cytokine HMGB1” becomes the predominant HMGB1 isoform. **B**, Differential effects of HMGB1 in the spleen (left) and bone marrow (right) in the acute phase (<24 h) after stroke. Splenic monocytes are activated via a RAGE-dependent pathway, producing increased amounts of proinflammatory cytokines. In the bone marrow, HMGB1 induces proliferation of immature monocytes and their release to the circulation. **C**, The expanded population of (bone marrow-derived) immature monocytes has features of myeloid-derived suppressor cells, which inhibit lymphocyte activation via arginase (ARG1) secretion and might induce lymphocyte apoptosis. Splenic and circulating APCs have an “exhausted” phenotype characterized by reduced MHC-II expression and decreased cytokine production upon stimulation. Inadequate costimulatory signaling to lymphocyte induces T-cell dysfunction and might lead to apoptosis. Additionally, increased catecholamine levels in the subacute phase after stroke result in impaired monocyte function and lymphocyte reduction probably independent of HMGB1–RAGE signaling.

in vitro fails to prevent lymphocytopenia, the hallmark of immunodepression (Mracsko et al., 2014). Although increased catecholamine blood levels have been reported after experimental and clinical stroke (Chamorro et al., 2007; Urra et al., 2009b),

their correlation with lymphopenia, humoral immunosuppression or bacterial infections was not confirmed in a recent study in stroke patients (Liesz et al., 2013a). Moreover, the catecholaminergic concept of poststroke immune depression suggests the in-

involvement of structures of the autonomic nervous system (e.g., the insula) and a laterality of the observed effect (right vs left hemisphere). However, the evidence from clinical and experimental studies rather points to lesion size instead of lesion location as the primary determinant of immune depression (Gendron et al., 2002; Hug et al., 2009; Liesz et al., 2013a). Therefore, the link between acute ischemic brain injury and the impact on the peripheral immune system remained to be identified. Genetic or pharmacological blockage of pattern recognition receptor signaling via HMGB1 and RAGE in this study abrogated cellular immunosuppression and also restored the activation of lymphocytes in the subacute phase after stroke. We have performed experiments comparing the differential effects of inhibiting the RAGE signaling cascade and beta2-adrenergic signaling on key outcome parameters of the acute immunostimulatory phase (cytokine release) and the subsequent immunosuppressive state in the subacute phase (spleen cellularity and MDSC expansion). Our findings suggest that alarmin-mediated pathways and the poststroke stress-related catecholaminergic effects are largely independent. While brain-released alarmins are released early after brain injury and might cause peripheral immune activation and subsequent immune exhaustion, catecholamines might represent an additional signaling pathway in the subacute phase compromising poststroke immune function (Fig. 8).

The concept of “stroke-induced immunodepression” (Meisel et al., 2005; Dirnagl et al., 2007) has been perceived as an independent and isolated immunological phenomenon after acute brain injury. However, our results suggest that this immunosuppressive state in the subacute phase after stroke has to be integrated as only one feature of the complex systemic immunomodulation by disturbed brain-immune communication. We detected a marked release of HMGB1 from the ischemic brain in the hyperacute phase after the lesion. Mass spectrometric analysis revealed a “maturation” of the post-translationally unmodified, fully reduced isoform of HMGB1 toward the cytokine-inducing isoform within the acute phase (Fig. 8A). For the cytokine-stimulating function of HMGB1, its residues at C23 and C45 must form a disulfide bond, whereas the unpaired C106 within BoxB must be in the reduced thiol state (Yang et al., 2010). This isoform is a very strong stimulus for various types of immune cells comparable with the stimulatory function of bacterial antigens, such as LPS (Lotze and Tracey, 2005). In this study, we have identified the induction of an “exhausted phenotype” of mature splenic monocytes after the initial (over)activation of the peripheral immune cells by brain-released HMGB1 in the acute phase (Fig. 8B,C). The induction of reduced responsiveness of monocytes/macrophages to endotoxins or bacterial stimuli after a strong inflammatory reaction has been described in immunological conditions, such as sepsis or sterile inflammatory response (Randow et al., 1995; Haupt et al., 1998; Cavaillon et al., 2005). This hyporesponsive state of innate immune cells encompasses the reduced expression of MHC and costimulatory molecules as well as the impaired secretion of proinflammatory cytokines (TNF- α and IL-12). These features have also been reported after brain ischemia (Hug et al., 2009; Urra et al., 2009b; Vogelgesang et al., 2013). Inhibition of the initially overshooting immune activation in the hyperacute phase by neutralizing HMGB1 interaction with its receptors ameliorated also the secondary monocyte exhaustion, indicating a functional link between the distinct and opposing immunological phenotypes observed in the acute and subacute phase after brain lesion.

In addition to the exhaustion of mature monocytes, we de-

scribe here for the first time the HMGB1-induced expansion of a monocyte subpopulation after stroke. This subpopulation has features of MDSCs and contributes to the immunosuppressive state in the subacute phase. However, the source of this expanding population could not be determined with certainty. Our findings suggest that it might arise from bone marrow egress, result from peripheral expansion, or represent a mere phenotypical change in the monocyte population. The phenotype of MDSCs was previously identified in several disease models as CD11b⁺Gr-1⁺ cells, although distinct functional subsets have meanwhile been characterized in different immunological milieus and disease models (Gabilovich and Nagaraj, 2009). Although a relative expansion of monocytes after stroke was noted also in previous clinical and experimental studies (Vogelgesang et al., 2008; Liesz et al., 2009, 2013a), the phenotypical and functional characteristics of this expanding population had not been analyzed so far. We detected a strong suppressive function of the expanding CD11⁺Ly-6C⁺ population on lymphocytes. Additionally, the expression of Arg1 was strongly increased in the splenic monocyte population. Previous reports suggested a suppressive and even toxic function of MDSCs on lymphocytes by upregulation of Arg1, which induces apoptosis in activated lymphocytes by limiting the essential L-arginine concentration needed for lymphocyte viability (Bronte et al., 2003; Rodríguez and Ochoa, 2008). This novel finding of MDSC expansion and increased Arg1 expression might be one mechanism explaining the induction of lymphocytopenia after stroke, a key feature of poststroke immunosuppression syndrome (Meisel et al., 2005). Indeed, lymphocytopenia has been consistently described in this study and previously in patients and experimental models of extensive brain lesions (Vogelgesang et al., 2008; Klehmet et al., 2009; Urra et al., 2009a) and was found to be an independent predictor of poststroke infections in patients (Liesz et al., 2013a). The above-mentioned characteristics of lymphocyte-suppressing MDSCs after stroke and the necessity of APCs for the stimulation of T cells by HMGB1 demonstrated herein, suggest an interaction of monocytes/APCs with lymphocytes downstream of the HMGB1-mediated pathways. However, the exact molecular pathways underlying this potential monocyte/APC–lymphocyte interaction after brain ischemia require further investigation. Furthermore, also other immunosuppressive cell populations induced by the acute brain injury might be involved in the observed peripheral immune alterations.

In conclusion, our data strongly suggest that HMGB1 release from the ischemic brain and signaling through the pattern recognition receptor RAGE is a key mechanism of the intricate peripheral immune response after brain injury that has profound consequences on clinical outcome. Interfering with this pathway may provide a promising therapeutic target for prevention of immune-mediated complications of acute brain damage.

References

- Adachi O, Kawai T, Takeda K, Matsumoto M, Tsutsui H, Sakagami M, Nakanishi K, Akira S (1998) Targeted disruption of the MyD88 gene results in loss of IL-1- and IL-18-mediated function. *Immunity* 9:143–150. [CrossRef Medline](#)
- An C, Shi Y, Li P, Hu X, Gan Y, Stetler RA, Leak RK, Gao Y, Sun BL, Zheng P, Chen J (2014) Molecular dialogs between the ischemic brain and the peripheral immune system: dualistic roles in injury and repair. *Prog Neurobiol* 115:6–24. [CrossRef Medline](#)
- Andrassy M, Volz HC, Igwe JC, Funke B, Eichberger SN, Kaya Z, Buss S, Autschbach F, Pleger ST, Lukic IK, Bea F, Hardt SE, Humpert PM, Bianchi ME, Mairbäurl H, Nawroth PP, Remppis A, Katus HA, Bierhaus A (2008) High-mobility group box-1 in ischemia-reperfusion injury of the heart. *Circulation* 117:3216–3226. [CrossRef Medline](#)

- Antoine DJ, Williams DP, Kipar A, Jenkins RE, Regan SL, Sathish JG, Kittingham NR, Park BK (2009) High-mobility group box-1 protein and keratin-18, circulating serum proteins informative of acetaminophen-induced necrosis and apoptosis in vivo. *Toxicol Sci* 112:521–531. [CrossRef Medline](#)
- Antoine DJ, Jenkins RE, Dear JW, Williams DP, McGill MR, Sharpe MR, Craig DG, Simpson KJ, Jaeschke H, Park BK (2012) Molecular forms of HMGB1 and keratin-18 as mechanistic biomarkers for mode of cell death and prognosis during clinical acetaminophen hepatotoxicity. *J Hepatol* 56:1070–1079. [CrossRef Medline](#)
- Bederson JB, Pitts LH, Tsuji M, Nishimura MC, Davis RL, Bartkowski H (1986) Rat middle cerebral artery occlusion: evaluation of the model and development of a neurologic examination. *Stroke* 17:472–476. [CrossRef Medline](#)
- Bianchi ME (2009) HMGB1 loves company. *J Leukoc Biol* 86:573–576. [CrossRef Medline](#)
- Bronte V, Serafini P, Mazzoni A, Segal DM, Zanovello P (2003) L-arginine metabolism in myeloid cells controls T-lymphocyte functions. *Trends Immunol* 24:302–306. [CrossRef Medline](#)
- Cavaillon JM, Adrie C, Fitting C, Adib-Conquy M (2005) Reprogramming of circulatory cells in sepsis and SIRS. *J Endotoxin Res* 11:311–320. [CrossRef Medline](#)
- Chamorro A, Amaro S, Vargas M, Obach V, Cervera A, Gómez-Choco M, Torres F, Planas AM (2007) Catecholamines, infection, and death in acute ischemic stroke. *J Neurol Sci* 252:29–35. [CrossRef Medline](#)
- Chamorro Á, Meisel A, Planas AM, Urra X, van de Beek D, Veltkamp R (2012) The immunology of acute stroke. *Nat Rev Neurol* 8:401–410. [CrossRef Medline](#)
- Crosby GA, Munshi S, Karat AS, Worthington E, Lincoln NB (2012) Fatigue after stroke: frequency and effect on daily life. *Disabil Rehabil* 34:633–637. [CrossRef Medline](#)
- Dantzer R (2006) Cytokine, sickness behavior, and depression. *Neurol Clin* 24:441–460. [CrossRef Medline](#)
- Dantzer R, O'Connor JC, Freund GG, Johnson RW, Kelley KW (2008) From inflammation to sickness and depression: when the immune system subjugates the brain. *Nat Rev Neurosci* 9:46–56. [CrossRef Medline](#)
- Dirnagl U, Klehmet J, Braun JS, Harms H, Meisel C, Ziemssen T, Prass K, Meisel A (2007) Stroke-induced immunodepression: experimental evidence and clinical relevance. *Stroke* 38:770–773. [CrossRef Medline](#)
- Gabrilovich DI, Nagaraj S (2009) Myeloid-derived suppressor cells as regulators of the immune system. *Nat Rev Immunol* 9:162–174. [CrossRef Medline](#)
- Gendron A, Teitelbaum J, Cossette C, Nuara S, Dumont M, Geadah D, du Souich P, Kouassi E (2002) Temporal effects of left versus right middle cerebral artery occlusion on spleen lymphocyte subsets and mitogenic response in Wistar rats. *Brain Res* 955:85–97. [CrossRef Medline](#)
- Haupt W, Riese J, Mehler C, Weber K, Zowe M, Hohenberger W (1998) Monocyte function before and after surgical trauma. *Dig Surg* 15:102–104. [CrossRef Medline](#)
- Hug A, Dalpke A, Wiczorek N, Giese T, Lorenz A, Auffarth G, Liesz A, Veltkamp R (2009) Infarct volume is a major determiner of stroke immune cell function and susceptibility to infection. *Stroke* 40:3226–3232. [CrossRef Medline](#)
- Iadecola C, Anrather J (2011) The immunology of stroke: from mechanisms to translation. *Nat Med* 17:796–808. [CrossRef Medline](#)
- Jhuang H, Garrote E, Mutch J, Yu X, Khilnani V, Poggio T, Steele AD, Serre T (2010) Automated home-cage behavioural phenotyping of mice. *Nat Commun* 1:68. [CrossRef Medline](#)
- Jones BJ, Roberts DJ (1968) A rotarod suitable for quantitative measurements of motor incoordination in naive mice. *Naunyn Schmiedebergs Arch Exp Pathol Pharmacol* 259:211. [CrossRef Medline](#)
- Katzan IL, Cebul RD, Husak SH, Dawson NV, Baker DW (2003) The effect of pneumonia on mortality among patients hospitalized for acute stroke. *Neurology* 60:620–625. [CrossRef Medline](#)
- Kilkenny C, Browne WJ, Cuthill IC, Emerson M, Altman DG (2010) Improving bioscience research reporting: the ARRIVE guidelines for reporting animal research. *PLoS Biol* 8:e1000412. [CrossRef Medline](#)
- Klehmet J, Harms H, Richter M, Prass K, Volk HD, Dirnagl U, Meisel A, Meisel C (2009) Stroke-induced immunodepression and stroke infections: lessons from the preventive antibacterial therapy in stroke trial. *Neuroscience* 158:1184–1193. [CrossRef Medline](#)
- Lerdal A, Gay CL (2013) Fatigue in the acute phase after first stroke predicts poorer physical health 18 months later. *Neurology* 81:1581–1587. [CrossRef Medline](#)
- Liesz A, Hagemann S, Zschoche C, Adamek J, Zhou W, Sun L, Hug A, Zorn M, Dalpke A, Nawroth P, Veltkamp R (2009) The spectrum of systemic immune alterations after murine focal ischemia: immunodepression versus immunomodulation. *Stroke* 40:2849–2858. [CrossRef Medline](#)
- Liesz A, Rieger H, Purrucker J, Zorn M, Dalpke A, Möhlenbruch M, Englert S, Nawroth PP, Veltkamp R (2013a) Stress mediators and immune dysfunction in patients with acute cerebrovascular diseases. *PLoS One* 8:e74839. [CrossRef Medline](#)
- Liesz A, Zhou W, Na SY, Hämmerling GJ, Garbi N, Karcher S, Mracsko E, Backs J, Rivest S, Veltkamp R (2013b) Boosting regulatory T cells limits neuroinflammation in permanent cortical stroke. *J Neurosci* 33:17350–17362. [CrossRef Medline](#)
- Liliensiek B, Weigand MA, Bierhaus A, Nicklas W, Kasper M, Hofer S, Plachky J, Gröne HJ, Kurschus FC, Schmidt AM, Yan SD, Martin E, Schleicher E, Stern DM, Hämmerling GG, Nawroth PP, Arnold B (2004) Receptor for advanced glycation end products (RAGE) regulates sepsis but not the adaptive immune response. *J Clin Invest* 113:1641–1650. [CrossRef Medline](#)
- Lotze MT, Tracey KJ (2005) High-mobility group box 1 protein (HMGB1): nuclear weapon in the immune arsenal. *Nat Rev Immunol* 5:331–342. [CrossRef Medline](#)
- Meisel C, Schwab JM, Prass K, Meisel A, Dirnagl U (2005) Central nervous system injury-induced immune deficiency syndrome. *Nat Rev Neurosci* 6:775–786. [CrossRef Medline](#)
- Mracsko E, Liesz A, Karcher S, Zorn M, Bari F, Veltkamp R (2014) Differential effects of sympathetic nervous system and hypothalamic-pituitary-adrenal axis on systemic immune cells after severe experimental stroke. *Brain Behav Immun* 41:200–209. [CrossRef Medline](#)
- Muhammad S, Barakat W, Stoyanov S, Murikinati S, Yang H, Tracey KJ, Bendszus M, Rossetti G, Nawroth PP, Bierhaus A, Schwaninger M (2008) The HMGB1 receptor RAGE mediates ischemic brain damage. *J Neurosci* 28:12023–12031. [CrossRef Medline](#)
- Nyström S, Antoine DJ, Lundbäck P, Lock JG, Nita AF, Hogstrand K, Grandien A, Erlandsson-Harris H, Andersson U, Applequist SE (2013) TLR activation regulates damage-associated molecular pattern isoforms released during pyroptosis. *EMBO J* 32:86–99. [CrossRef Medline](#)
- Offner H, Subramanian S, Parker SM, Afentoulis ME, Vandenbark AA, Hurn PD (2006a) Experimental stroke induces massive, rapid activation of the peripheral immune system. *J Cereb Blood Flow Metab* 26:654–665. [CrossRef Medline](#)
- Offner H, Subramanian S, Parker SM, Wang C, Afentoulis ME, Lewis A, Vandenbark AA, Hurn PD (2006b) Splenic atrophy in experimental stroke is accompanied by increased regulatory T cells and circulating macrophages. *J Immunol* 176:6523–6531. [CrossRef Medline](#)
- Prass K, Meisel C, Höflich C, Braun J, Halle E, Wolf T, Ruscher K, Victorov IV, Priller J, Dirnagl U, Volk HD, Meisel A (2003) Stroke-induced immunodeficiency promotes spontaneous bacterial infections and is mediated by sympathetic activation reversal by poststroke T helper cell type 1-like immunostimulation. *J Exp Med* 198:725–736. [CrossRef Medline](#)
- Qin S, Wang H, Yuan R, Li H, Ochani M, Ochani K, Rosas-Ballina M, Czura CJ, Huston JM, Miller E, Lin X, Sherry B, Kumar A, Larosa G, Newman W, Tracey KJ, Yang H (2006) Role of HMGB1 in apoptosis-mediated sepsis lethality. *J Exp Med* 203:1637–1642. [CrossRef Medline](#)
- Random F, Syrbe U, Meisel C, Krausch D, Zuckermann H, Platzer C, Volk HD (1995) Mechanism of endotoxin desensitization: involvement of interleukin 10 and transforming growth factor beta. *J Exp Med* 181:1887–1892. [CrossRef Medline](#)
- Rodríguez PC, Ochoa AC (2008) Arginine regulation by myeloid derived suppressor cells and tolerance in cancer: mechanisms and therapeutic perspectives. *Immunol Rev* 222:180–191. [CrossRef Medline](#)
- Shichita T, Hasegawa E, Kimura A, Morita R, Sakaguchi R, Takada I, Sekiya T, Ooboshi H, Kitazono T, Yanagawa T, Ishii T, Takahashi H, Mori S, Nishibori M, Kuroda K, Akira S, Miyake K, Yoshimura A (2012) Peroxiredoxin family proteins are key initiators of post-ischemic inflammation in the brain. *Nat Med* 18:911–917. [CrossRef Medline](#)
- Spulber S, Edoff K, Hong L, Morisawa S, Shirahata S, Ceccatelli S (2012) Molecular hydrogen reduces LPS-induced neuroinflammation and promotes recovery from sickness behaviour in mice. *PLoS One* 7:e42078. [CrossRef Medline](#)

- Swanson RA, Morton MT, Tsao-Wu G, Savalos RA, Davidson C, Sharp FR (1990) A semiautomated method for measuring brain infarct volume. *J Cereb Blood Flow Metab* 10:290–293. [CrossRef Medline](#)
- Urta X, Cervera A, Villamor N, Planas AM, Chamorro A (2009a) Harms and benefits of lymphocyte subpopulations in patients with acute stroke. *Neuroscience* 158:1174–1183. [CrossRef Medline](#)
- Urta X, Cervera A, Obach V, Climent N, Planas AM, Chamorro A (2009b) Monocytes are major players in the prognosis and risk of infection after acute stroke. *Stroke* 40:1262–1268. [CrossRef Medline](#)
- Vogelgesang A, Grunwald U, Langner S, Jack R, Bröker BM, Kessler C, Dressel A (2008) Analysis of lymphocyte subsets in patients with stroke and their influence on infection after stroke. *Stroke* 39:237–241. [CrossRef Medline](#)
- Vogelgesang A, Becker KJ, Dressel A (2013) Immunological consequences of ischemic stroke. *Acta Neurol Scand* 129:1–12. [CrossRef Medline](#)
- Willey JZ, Disla N, Moon YP, Paik MC, Sacco RL, Boden-Albala B, Elkind MS, Wright CB (2010) Early depressed mood after stroke predicts long-term disability: the Northern Manhattan Stroke Study (NOMASS). *Stroke* 41:1896–1900. [CrossRef Medline](#)
- Wong CH, Jenne CN, Lee WY, Léger C, Kubes P (2011) Functional innervation of hepatic iNKT cells is immunosuppressive following stroke. *Science* 334:101–105. [CrossRef Medline](#)
- Yang H, Hreggvidsdottir HS, Palmblad K, Wang H, Ochani M, Li J, Lu B, Chavan S, Rosas-Ballina M, Al-Abed Y, Akira S, Bierhaus A, Erlandsson-Harris H, Andersson U, Tracey KJ (2010) A critical cysteine is required for HMGB1 binding to Toll-like receptor 4 and activation of macrophage cytokine release. *Proc Natl Acad Sci U S A* 107:11942–11947. [CrossRef Medline](#)
- Yang H, Antoine DJ, Andersson U, Tracey KJ (2013) The many faces of HMGB1: molecular structure-functional activity in inflammation, apoptosis, and chemotaxis. *J Leukoc Biol* 93:865–873. [CrossRef Medline](#)

4.2 Brain-released alarmins and stress response synergize in accelerating atherosclerosis progression after stroke.

The risk for recurrent stroke is approximately 13 % in the first year after stroke and increases up to 30 % within 5 years after the first ischemic event. Large-artery atherosclerosis (LAA) is the main cause for a first stroke and is also associated with the highest recurrence rate.

Stroke induces a multiphasic, systemic immunomodulation in response to the acute brain injury. While the subacute immunosuppression after stroke has been well described to be a risk factor for secondary infections, the consequences of immune activation in the acute and chronic phase after stroke are barely investigated. The hypothesis was that systemic immune activation after stroke could impact inflammatory comorbidities of stroke patients such as atherosclerosis. We observed that stroke exacerbates atheroprogession via alarmin-mediated propagation of vascular inflammation. Activation of RAGE-signaling cascades by brain-derived alarmins such as high mobility group box 1 (HMGB1) induced monocyte and endothelial activation. Increase in vascular inflammation resulted in increased plaque load and plaque vulnerability after stroke. *De novo* recruitment of activated monocytes via the CCL2-CCR2 chemokine pathway to atherosclerotic lesions was a key event in stroke-induced vascular inflammation. Neutralization of circulating alarmins or a knockdown of RAGE ameliorated the post-stroke atheroprogession. Pro-inflammatory mechanisms driven by brain-released alarmins synergized in their atherogenic effect with the stress-mediated, adrenergic mobilization of monocytes from the bone marrow after stroke. Blockage of β 3-adrenoreceptors decreased the egress of myeloid monocytes after stroke, but only the neutralization of circulating alarmins reduced systemic monocyte activation and aortic invasion of activated monocytes.

These findings identify the RAGE-signaling pathway as a critical mechanism leading to exacerbation of atheroprogession after stroke. Finally, these findings suggest the alarmin-RAGE pathway as a novel therapeutic target to prevent immunological comorbidities in stroke patients.

Author contribution: Design of the experiments, performing the experiments, analyses of the experiments, interpretation of the results and writing the manuscript

(Copyright permission under the “license to publish” of the American Association for the Advancement of Science (AAAS))

STROKE

Brain-released alarmins and stress response synergize in accelerating atherosclerosis progression after stroke

Stefan Roth,^{1,2} Vikramjeet Singh,^{1,2} Steffen Tiedt,^{1,2} Lisa Schindler,^{1,2} Georg Huber,³ Arie Geerlof,³ Daniel J. Antoine,⁴ Antoine Anfray,⁵ Cyrille Orset,⁵ Maxime Gauberti,⁵ Antoine Fournier,⁵ Lesca M. Holdt,⁶ Helena Erlandsson Harris,⁷ Britta Engelhardt,⁸ Marco E. Bianchi,⁹ Denis Vivien,⁵ Christof Haffner,¹ Jürgen Bernhagen,^{1,2} Martin Dichgans,^{1,2} Arthur Liesz^{1,2*}

Copyright © 2018
The Authors, some
rights reserved;
exclusive licensee
American Association
for the Advancement
of Science. No claim
to original U.S.
Government Works

Stroke induces a multiphasic systemic immune response, but the consequences of this response on atherosclerosis—a major source of recurrent vascular events—have not been thoroughly investigated. We show that stroke exacerbates atheroprotection via alarmin-mediated propagation of vascular inflammation. The prototypic brain-released alarmin high-mobility group box 1 protein induced monocyte and endothelial activation via the receptor for advanced glycation end products (RAGE)–signaling cascade and increased plaque load and vulnerability. Recruitment of activated monocytes via the CC-chemokine ligand 2–CC-chemokine receptor type 2 pathway was critical in stroke-induced vascular inflammation. Neutralization of circulating alarmins or knockdown of RAGE attenuated atheroprotection. Blockage of β 3-adrenoreceptors attenuated the egress of myeloid monocytes after stroke, whereas neutralization of circulating alarmins was required to reduce systemic monocyte activation and aortic invasion. Our findings identify a synergistic effect of the sympathetic stress response and alarmin-driven inflammation via RAGE as a critical mechanism of exacerbated atheroprotection after stroke.

INTRODUCTION

The risk of recurrent vascular events after stroke is high and remains elevated even years after first stroke (1, 2). The enhanced risk of secondary events encompasses large artery stroke and myocardial infarction, both manifestations of atherosclerosis (3, 4). Atherosclerosis is a chronic inflammatory condition of the arterial vessel wall, characterized by an imbalance in lipid metabolism and recruitment of immune cells leading to a chronic inflammatory milieu (5, 6). Key steps further include infiltration by monocytes, secretion of proteolytic enzymes, fibrous cap thinning, and plaque rupture, eventually causing end-organ damage due to ischemia. Previous work in experimental myocardial infarction has demonstrated an accelerating effect of this event on atheroprotection (7, 8), which has recently been linked to a stress-mediated mobilization of monocytes from bone marrow niches via adrenergic signaling (7). The same study further provided initial evidence for accelerated atheroprotection after experimental stroke (7). However, the mechanisms underlying enhanced atheroprotection after stroke have so far not been investigated.

Stroke promotes a multiphasic immunomodulation in the systemic immune compartment with an early sterile inflammatory response within hours and a chronic inflammatory response that is observed both in mice and in stroke patients (9–11). We previously demonstrated that this systemic immunomodulation is triggered by alarmins

released from necrotic brain tissue (12). This specifically involves the prototypic alarmin high-mobility group box 1 (HMGB1). Alarmins can have chemoattractant as well as cytokine-inducing properties and interact with pattern recognition receptors such as toll-like receptors and the receptor for advanced glycation end products (RAGE) on various immune and nonimmune cell populations (13).

In light of these observations, we hypothesized that stroke might promote vascular inflammation and atheroprotection via an alarmin-driven systemic immune response. Here, we confirm exacerbation of atheroprotection after stroke and specifically identify a key role of the alarmin–RAGE pathway acting in synergy with the sympathetic stress response for de novo recruitment of activated monocytes to atherosclerotic lesions.

RESULTS

Stroke exacerbates atheroprotection via increased vascular monocyte recruitment

To determine the effect of stroke on exacerbation of atheroprotection, we fed 8-week-old apolipoprotein E-deficient (*ApoE*^{−/−}) mice (14), a well-established mouse model for atherosclerosis, a high-cholesterol diet (HCD) for 8 weeks before the induction of experimental stroke and assessed plaque load after an additional 4 weeks of HCD (Fig. 1A and fig. S1). Overall plaque load in whole aorta was significantly ($P = 0.002$) increased in mice undergoing stroke surgery compared to sham surgery as assessed by en face staining (Fig. 1B). Likewise, significantly ($P < 0.0001$) increased plaque load was observed throughout the aortic valve (Fig. 1, C to E). Similar results were also obtained in female animals (fig. S2). To evaluate whether stroke-induced plaque formation was accompanied by vascular inflammation, we next performed flow cytometric analysis of whole-aorta cell suspensions. In contrast to other immune cell populations (fig. S3), monocyte cell counts and, more specifically, the number of proinflammatory CD11b⁺ Ly6C^{high} monocytes per aorta were increased after stroke compared to sham (Fig. 1, F and G). We further found an increase in the enzymatic

¹Institute for Stroke and Dementia Research, Klinikum der Universität München, 81377 Munich, Germany. ²Munich Cluster for System Neurology (SyNergy), 80336 Munich, Germany. ³Institute of Structural Biology, Helmholtz Centre Munich, 85764 Munich, Germany. ⁴Medical Research Council Center for Drug Safety Science, Department for Molecular and Clinical Pharmacology, University of Liverpool, L69 3GE Liverpool, UK. ⁵INSERM, Université de Caen-Normandie, CHU de Caen, INSERM UMR-S U1237, Physiopathology and Imaging of Neurological Disorders, GIP Cyceron, 14074 Caen, France. ⁶Institute of Laboratory Medicine, Klinikum der Universität München, 81377 Munich, Germany. ⁷Department of Medicine, Karolinska University Hospital, SE-171 76 Stockholm, Sweden. ⁸Theodor Kocher Institute, University of Bern, Freiestrasse 1, 3012 Bern, Switzerland. ⁹Faculty of Medicine, San Raffaele University, 20132, Milan, Italy.

*Corresponding author. Email: arthur.liesz@med.uni-muenchen.de

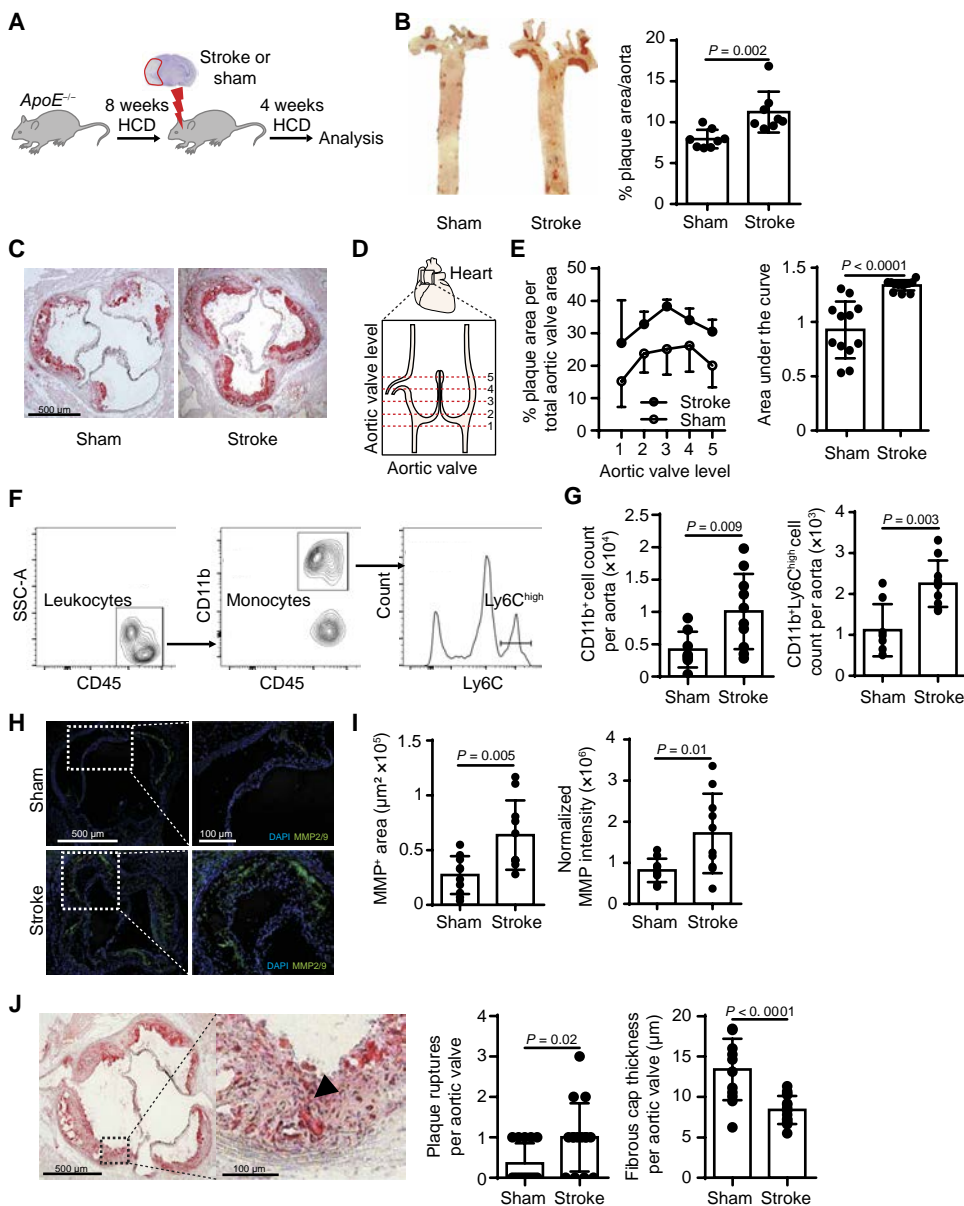


Fig. 1. Stroke exacerbates atheroprogession. (A) Experimental design: Apolipoprotein E-deficient mice fed a high-cholesterol diet (HCD-fed *ApoE*^{-/-}) underwent stroke or sham surgery and were sacrificed 1 month after surgical procedure. (B) Representative whole-aorta en face Oil Red O staining in sham and stroked mice (left) and quantification of the plaque load 1 month after stroke in sham and stroked animals (right, *U* test, *n* = 8 per group). (C) Representative images of Oil Red O–stained aortic valve sections 1 month after stroke or sham surgery. (D) Schematic representation of aortic valve. Red lines indicate the location of the sections analyzed in the study. (E) Quantification of aortic valve plaque load shown as percentage of plaque area per aortic valve in each section shown in (D) (left) and the area under the curve (right, *U* test, *n* = 12 per group). (F) Representative gating strategy for flow cytometric analysis of aortic monocytes. SSC-A, side scatter area. (G) Flow cytometric analysis of whole-aorta lysates showing total monocytes (CD11b⁺; left) and the proinflammatory subset (Ly6C^{high}; right) cell counts after stroke induction compared to sham (*U* test, *n* = 9 to 10 per group). (H) Representative images of aortic valve in situ zymography for 4',6-diamidino-2-phenylindole (DAPI) (nuclear marker, blue) and matrix metalloproteinase 2/9 (MMP2/9) (representing enzymatically active areas, green) 1 month after surgery. (I) Quantification of MMP2/9 activity shown as enzymatically active area and normalized intensity (*U* test, *n* = 12 per group). (J) Representative images of Oil Red O–stained aortic valve sections 1 month after stroke (left) and quantification of number of plaque ruptures and cap thickness in aortic valve sections 1 month after sham or stroke surgery (*U* test, *n* = 14 to 15 per group). The arrowhead in the high-magnification image indicates a buried fibrous cap in lesion.

activity of matrix metalloproteinase 2 (MMP2) and MMP9 as detected by in situ zymography (Fig. 1, H and I). Because increased MMP activity is associated with plaque instability (15), we further investigated morphological markers of vulnerable plaques using previously established protocols (16). Cap thickness was reduced, and the number of highly unstable plaques increased in mice undergoing stroke surgery compared to sham surgery, suggesting a more vulnerable plaque morphology after stroke (Fig. 1J). Moreover, we analyzed plaques at the carotid bifurcation area, a predilected site for stenosis and plaque rupture in stroke patients, observing also in this area a trend toward increased plaque load after stroke (fig. S4). To determine whether the increased vascular inflammation was due to local proliferation or de novo recruitment of proinflammatory monocytes, we next implanted osmotic pumps releasing bromodeoxyuridine (BrdU) for detection of cell proliferation. In addition, we intraperitoneally (ip) administered 1×10^7 CCR2^{RFP/+} reporter monocytes, expressing red fluorescent protein (RFP) under the CC-chemokine receptor type 2 (CCR2) promoter, for detection of proinflammatory monocyte recruitment in HCD-fed *ApoE*^{-/-} mice after stroke or sham surgery (Fig. 2A). Although we found no difference in the proliferation rate of aortic monocytes/macrophages as assessed by BrdU incorporation (Fig. 2B and fig. S5), the recruitment of ip injected proinflammatory CCR2^{RFP/+} reporter cells into the aorta was substantially increased in stroke compared to sham group (Fig. 2, C and D, and fig. S6).

Stroke induces chemoattractant expression and endothelial activation

Next, we investigated the mechanisms underlying active aortic monocyte recruitment after stroke and explored the possibility that stroke treatment may elicit a specific chemokine/cytokine profile in the atherogenic aorta. To investigate the aortic chemokine profile, we performed a polymerase chain reaction (PCR) array for 86 chemokines and chemoattractant receptors using lysates of whole aortas obtained 3 days after stroke or sham surgery (table S1). We found that the transcription of 12 chemokines and chemoattractant receptors was up-regulated after stroke compared to sham (Fig. 2E). Notably, the

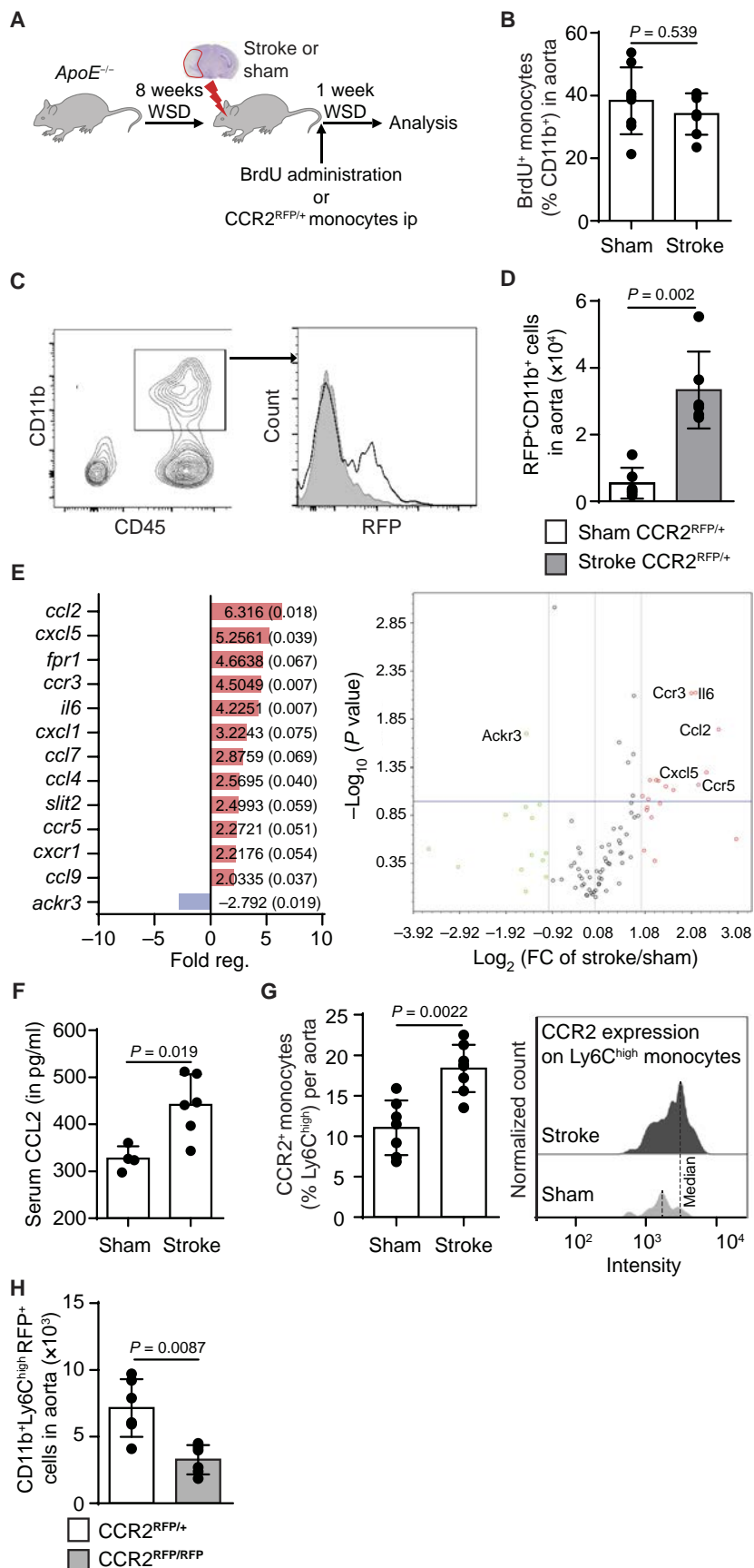
Downloaded from <http://stm.sciencemag.org/> by guest on March 14, 2018

Fig. 2. Stroke increases vascular inflammation via recruitment of inflammatory monocytes to atherosclerotic plaques.

(A) Schematic illustration of experimental design for data shown in (B) to (D): HCD-fed *ApoE*^{-/-} mice underwent sham or stroke surgery and received either continuous bromdeoxyuridine (BrdU) administration or CCR2^{RFP/+} bone marrow-derived cells intraperitoneally (ip). After 1 week, mice were sacrificed, and aortas and lymphoid organs were analyzed. **(B)** Analysis of BrdU⁺CD11b⁺ monocytes from aortas after stroke or sham surgery (*U* test, *n* = 5 to 7 per group). **(C)** Gating strategy and representative histogram plots (right) for invading red fluorescent protein–positive (RFP⁺) monocytes in aortas (white, sham; gray, stroke) and **(D)** corresponding quantification of RFP⁺CD11b⁺ monocytes in aorta (*U* test, *n* = 5 to 6 per group). **(E)** Fold change (FC) and adjusted *P* values (in parentheses) of chemokine and chemokine receptor transcription in aorta lysates 3 days after stroke compared to sham surgery (left; *n* = 3 per group, *P* < 0.1) and corresponding volcano plot for transcriptional regulation determined by real-time polymerase chain reaction arrays (right panel; *x* axis = fold change; *y* axis = *P* value, cutoff at <0.1). **(F)** Serum levels of CC-chemokine ligand 2 (CCL2) 1 week after stroke compared to sham surgery (*U* test, *n* = 4 to 6 per group). **(G)** Flow cytometric analysis of aortic CCR2⁺Ly6C^{high} monocytes (left) and CC-chemokine receptor type 2–positive (CCR2⁺) surface expression on inflammatory Ly6C^{high} monocytes (right) in aortas 3 days after stroke or sham surgery (*U* test, *n* = 7 per group). **(H)** Quantification of aortic invasion of adoptively transferred RFP-reporter cells from either CCR2-deficient (CCR2^{RFP/RFP}) or CCR2⁺ RFP⁺ donor mice (CCR2^{RFP/+}) (*U* test, *n* = 5 to 6 per group).

most up-regulated chemokine was CC-chemokine ligand 2 (CCL2), with a more than sixfold increase after stroke induction (fold change, 6.316; *P* = 0.018). CCL2 is secreted by foam cells in arterial lesions (17) and by activated endothelium (18) and attracts proinflammatory CCR2-expressing cells (19–21). Hence, we analyzed serum of mice after stroke and found increased CCL2 concentrations compared to sham-operated mice 1 week after sham surgery (Fig. 2F). In addition, we measured monocytic CCR2 expression by flow cytometry in aortas after stroke versus sham surgery, and we observed an increase in CCR2⁺ cell counts as well as CCR2 surface expression on inflammatory monocytes (Fig. 2G). One week after stroke induction, we detected fewer CD11b⁺Ly6C^{high} RFP⁺ monocytes in the aortas of mice injected ip with homozygous CCR2^{RFP/RFP} (CCR2-deficient) compared to heterozygous CCR2^{RFP/+} (CCR2-expressing) cells after stroke induction (Fig. 2H), indicating a critical role of the CCL2-CCR2 pathway in attraction of proinflammatory monocytes to the aorta after stroke.

Atherogenic monocyte recruitment is mediated by an orchestrated interplay of chemokine/chemokine receptor and integrin/adhesion molecule interactions with a pivotal role for endothelial activation. We found an increase mRNA expression of *Icam1* and *Vcam1*, key adhesion molecules in atherogenic monocyte recruitment, in aortas 3 days after stroke (Fig. 3A). In vivo molecular magnetic resonance imaging (MRI) using microsized particles of iron oxide–labeled vascular cell



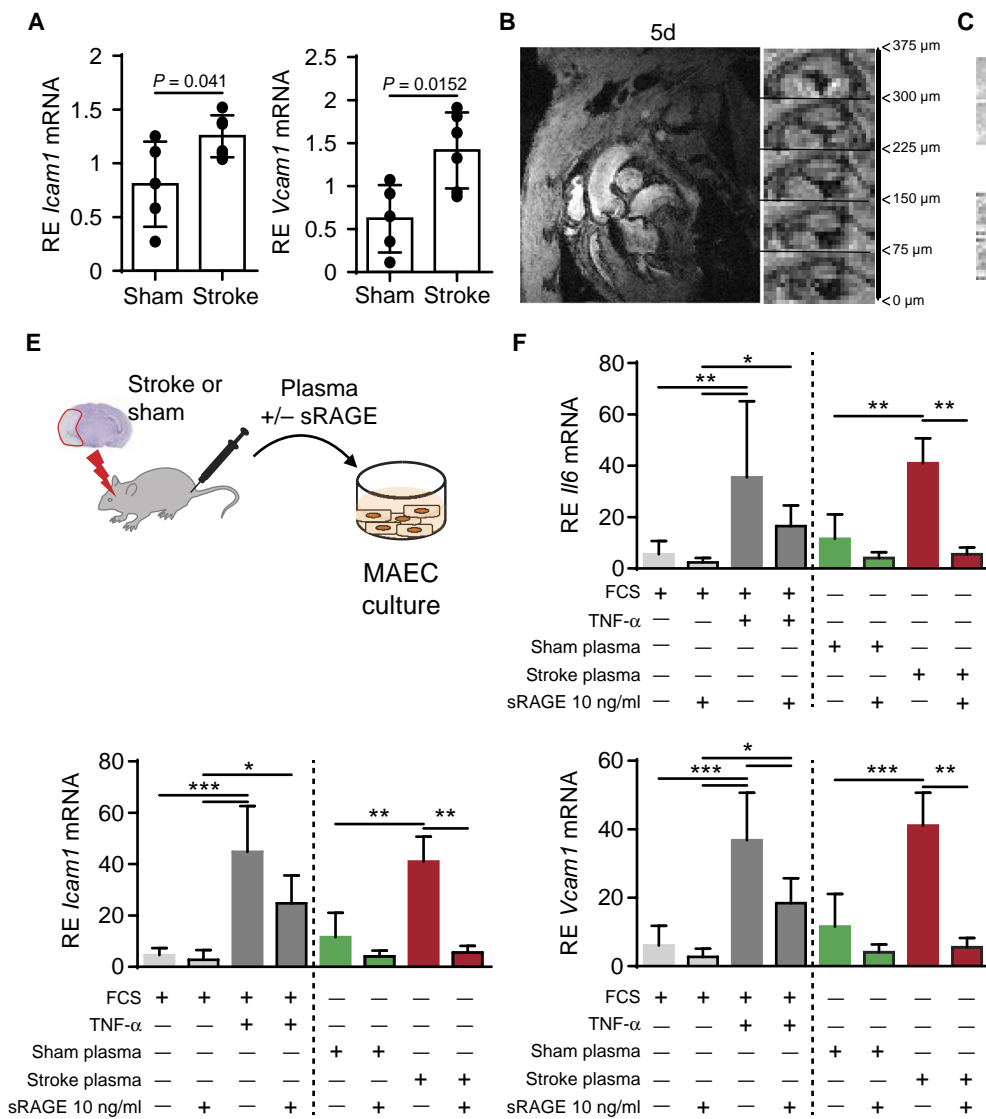


Fig. 3. Stroke induces inflammatory activation of the aortic endothelium. (A) Relative expression (RE) of *Icam1* and *Vcam1* transcription in whole-aorta lysates 3 days after sham or stroke (*U* test, *n* = 5 per group). (B) Vascular cell adhesion molecule-1 (VCAM-1)-targeted iron particles were used for molecular magnetic resonance imaging (MRI) of endothelial activation *in vivo* before and after stroke. Representative longitudinal and sagittal MRI images of aortic root area 5 days (5d) after stroke. (C) Representative comparison of the VCAM-1 signal volume of the same aortic valve before and 5 days after stroke surgery. (D) Quantification of VCAM-1 signal volume 5 days after stroke compared to baseline (*U* test, *n* = 5 per group). (E) Schematic illustration of experiments shown in (F). Wild-type (WT) mice received either stroke or sham surgery; 4 hours later, plasma was collected and used for conditioning media in murine aortic endothelial cell (MAEC) cultures. (F) RE of *Icam1*, *Vcam1*, and *Il6* mRNA in MAECs after being incubated with stroke or sham plasma and treated with soluble form of receptor for advanced glycation end products (sRAGE) (10 ng/ml) or vehicle (*H* test, *n* = 6 to 8 per group). For control conditions, fetal calf serum (FCS)-supplemented media without cytokine stimulus or with recombinant tumor necrosis factor- α (TNF- α ; 20 ng/ml) were used. **P* < 0.05, ***P* < 0.01, ****P* < 0.001.

adhesion molecule-1 (VCAM-1)-specific antibodies (22) revealed an increase in VCAM-1 signal volume at 5 days after stroke in aortic valves compared to baseline values before stroke induction (Fig. 3, B to D). These experiments provided strong support for the activation of the aortic endothelium after stroke. We hypothesized that the observed endothelial activation was likely mediated by soluble, proinflammatory mediators released from the ischemic brain as previously described by our group (12). To test this hypothesis, we used an *in vitro* endothelial culture system, subjecting murine aortic endothelial cells (MAECs) to stroke- or sham-conditioned plasma; control conditions included normal fetal calf serum-supplemented media with or without tumor necrosis factor- α (TNF- α) stimulation (Fig. 3E). We found that mRNA expression of *Vcam1*, *Icam1*, and *Il6* increased after conditioning with stroke plasma compared to sham plasma, with expression similar to stimulation of MAECs by TNF- α (Fig. 3F). Moreover, we found that addition of the soluble form of RAGE (sRAGE; 10 ng/ml) decreased the expression of *Vcam1*, *Icam1*, and *Il6* after stimulating the MAECs with stroke plasma. These results support

the concept of poststroke endothelial activation by soluble plasma mediators such as cytokines and alarmins—druggable by decoy receptors such as sRAGE—with an ensuing active recruitment of monocytes via CCR2-dependent pathways.

Poststroke alarmin release induces immune activation via the RAGE signaling pathway

Acute stroke leads to massive release of proinflammatory alarmins such as the prototypic alarmin HMGB1 from hypoxia-stressed and necrotic tissue (12). We confirmed the increase of plasma HMGB1 concentrations acutely (24 hours) after experimental stroke and expanded this observation to the chronic phase (30 days) when HMGB1 plasma levels were still more than threefold elevated after stroke compared to sham (Fig. 4A). We next reduced systemic alarmins *in vivo* using sRAGE as a decoy receptor for circulating alarmins (23). We treated mice 30 min before surgery and 4 hours after surgery with an intraperitoneal bolus (4 mg/kg) of sRAGE or vehicle and compared monocytic activation and cytokine expression in whole-spleen

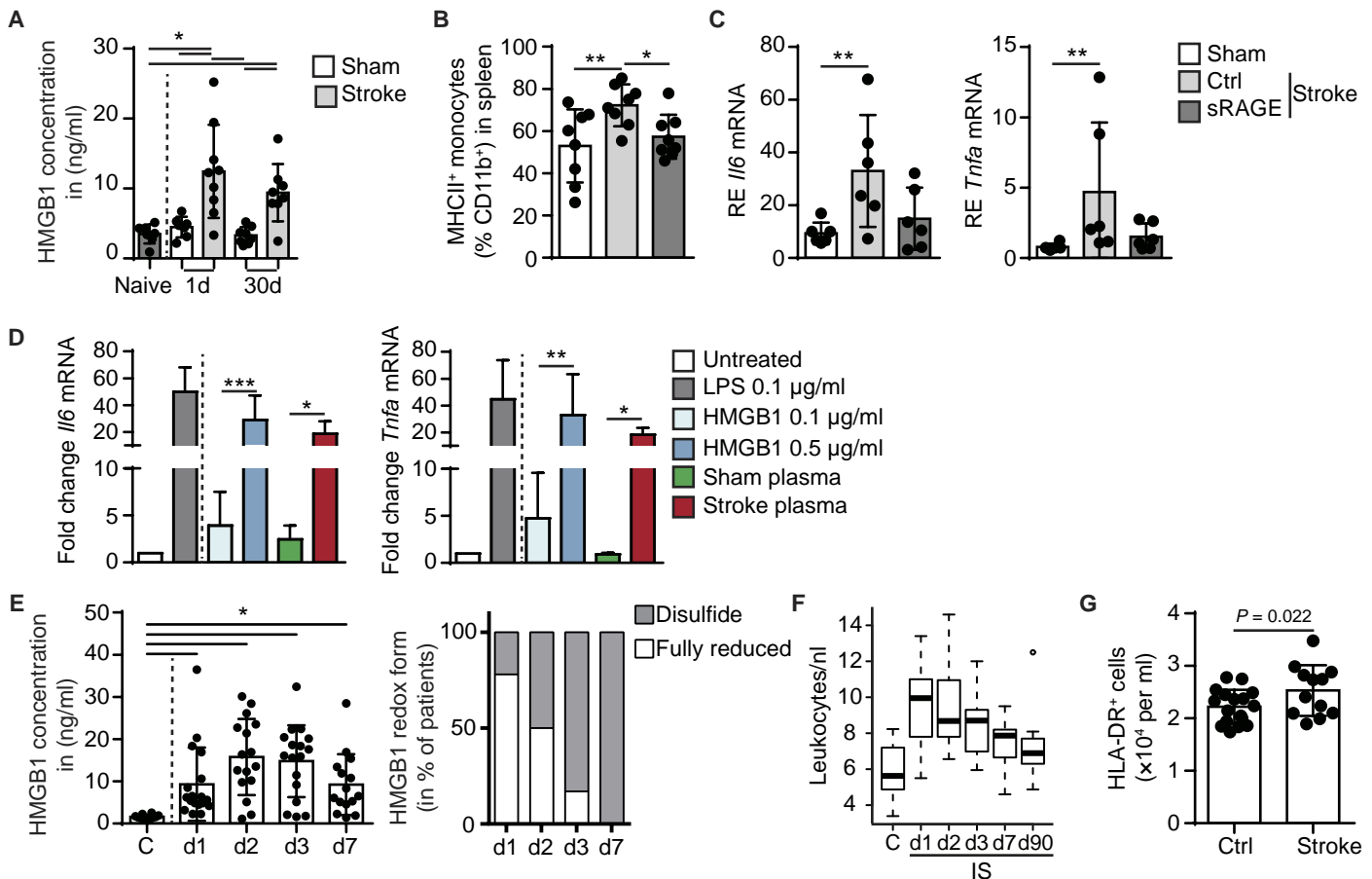


Fig. 4. HMGB1 induces systemic innate immune activation after stroke. (A) Plasma high-mobility group box 1 (HMGB1) concentrations were measured by enzyme-linked immunosorbent assay in naïve, sham, and stroke HCD-fed *ApoE*^{-/-} mice 1 and 30 days after surgery [one-way analysis of variance (ANOVA), $n = 7$ to 9 per group]. (B) Flow cytometric analysis of major histocompatibility complex class II–positive (MHCII⁺) expression of splenic myeloid cells from HCD-fed *ApoE*^{-/-} mice 3 days after stroke with vehicle or sRAGE treatment (one-way ANOVA, $n = 8$ per group). (C) RE of *Il6* and *Tnfa* mRNA in spleen of sham-operated and stroked vehicle-treated or sRAGE-treated WT mice 3 days after surgical procedure (H test, $n = 6$ per group). (D) RE of *Il6* and *Tnfa* mRNA of isolated murine splenic monocytes from WT mice, which were stimulated with recombinant HMGB1 (0.1 and 0.5 $\mu\text{g/ml}$), murine sham and stroke plasma (50%), and lipopolysaccharide (LPS) (0.1 $\mu\text{g/ml}$) in vitro (H test, $n = 5$ to 8 per group). (E) Plasma concentration of HMGB1 acquired by quantitative mass spectrometry analysis at different time points (days 1 to 7) in stroke patients and age-matched controls (C; left; $n = 15$ to 18 per group, one-way ANOVA). Changes in the distribution of HMGB1 reduction/oxidation (redox) state from fully reduced to disulfide state over the first week after stroke (right; $n = 15$ to 18 per group). (F) Quantification of blood leukocyte counts in ischemic stroke (IS) and control patients ($n = 15$ to 18 per group). (G) Flow cytometric analysis of human patient blood samples for human leukocyte antigen (HLA-DR⁺) cell count as an indication of monocyte activation at up to 60 days after large IS compared to age-matched controls (t test, $n = 12$ to 17 per group). * $P < 0.05$, ** $P < 0.01$, *** $P < 0.001$.

lysates 3 days after stroke. Compared to sham-operated mice, mice undergoing stroke surgery showed an increase of major histocompatibility complex class II (MHCII) expression as a monocytic activation marker (Fig. 4B) and elevated *Il6* and *Tnfa* mRNA expression (Fig. 4C). In contrast, sRAGE treatment abrogated the increase in MHCII expression and cytokine mRNA expression after stroke (Fig. 4, B and C). To investigate the role of soluble plasma mediators in monocyte activation more specifically, we treated primary monocyte cultures with recombinant HMGB1 or conditioned medium with plasma from sham-operated or stroked mice. Analysis of the mRNA expression revealed a dose-dependent increase in *Il6* and *Tnfa* expression after treatment with recombinant endotoxin-free HMGB1 as well as plasma from stroked animals, confirming a key role for soluble mediators such as HMGB1 in the activation of monocytes (Fig. 4D). Accordingly, we also detected substantially increased serum HMGB1 concentrations in human stroke patients both in the acute (within

first 48 hours) and subacute phase (72 hours and 7 days) (Fig. 4E and table S2). Analysis of the different human HMGB1 reduction/oxidation (redox) forms by mass spectrometry identified the functionally relevant cytokine-inducing disulfide HMGB1 isoform as the predominant modification after 3 days after stroke (Fig. 4E). This finding is in accordance with our previous observations on HMGB1 redox modifications in experimental stroke in mice showing that disulfide HMGB1 is the key mediator resulting in activation and expansion of the systemic monocyte population after stroke (12, 24, 25). The increase of proinflammatory HMGB1 was reflected in the pattern of transient leukocytosis during the time course after stroke (Fig. 4F). Moreover, C-reactive protein blood levels and neutrophil counts were increased after stroke, reflecting the alarmin-driven sterile inflammatory response (fig. S7). Accordingly, we also detected an increase in the frequency of activated human leukocyte antigen (HLA-DR⁺) cells 2 months after human stroke (Fig. 4G).

In light of the effective abrogation of the poststroke systemic immune response in the presence of sRAGE, we aimed to test the effect of sRAGE treatment on stroke-induced atheroprotection. Atherosclerotic animals were treated before and after surgery with an intraperitoneal bolus (4 mg/kg) of sRAGE, and aortic plaque load was analyzed after sham or stroke surgery (Fig. 5A). We found reduced plaque loads in aortas of mice receiving sRAGE compared to control-treated mice after stroke, whereas no difference was detected for the sham-operated groups between control and sRAGE treatment (Fig. 5B). Correspondingly, the overall survival rate and normalization of post-stroke weight loss were improved in sRAGE-treated animals (fig. S8), and the same pattern of treatment efficacy was observed for the plaque load in aortic valves (fig. S9). In addition, flow cytometric analysis revealed that sRAGE abrogated poststroke increase in total CD45⁺ CD11b⁺ as well as CD11b⁺Ly6C^{high} proinflammatory monocyte cell counts in aortas 4 weeks after stroke induction (Fig. 5C). Assessment of the lipid profiles of HCD-fed *ApoE*^{-/-} mice revealed no differences after stroke induction and sRAGE treatment, except for the nonatherogenic (26) triglyceride levels (fig. S10).

Given the potent effect of sRAGE on neutralizing the effects of poststroke alarmins on vascular inflammation and atheroprotection, we aimed to more specifically investigate the contribution of the RAGE-dependent pathway. To down-regulate RAGE in vivo, we administered RAGE-specific small interfering RNA (siRNA) in HCD-fed *ApoE*^{-/-} mice and found a knockdown of aortic RAGE mRNA and protein expression 3 days after hydrodynamic intravenous siRNA injection of 10 nmol of RAGE-silencing or negative control siRNA (Fig. 5, D and E). siRNA-induced RAGE knockdown reduced aortic total and proinflammatory monocyte counts 7 days after stroke induction compared to control treatment with nonspecific siRNA (Fig. 5F). As RAGE also engages ligands other than HMGB1, we next aimed to test the specific contribution of HMGB1 as a potential mediator leading to RAGE-mediated atheroprotection. Neutralizing circulating HMGB1 by intraperitoneal injection of HMGB1-specific monoclonal antibodies (4 mg/kg) immediately after experimental ischemia attenuated the increase in cellular vascular inflammation after stroke induction (Fig. 5G). However, neither infarct volume nor behavioral deficits were affected by the sRAGE or HMGB1-specific antibody treatment compared to control treatment 1 week after experimental stroke. Moreover, using HMGB1-specific antibodies in wild-type (WT) mice reduced monocyte expansion and activation in blood and increased cell number in spleen 24 hours after stroke (fig. S11). To further elaborate on the role of HMGB1 as a proinflammatory mediator of atheroprotection, we administered recombinant HMGB1 to HCD-fed *ApoE*^{-/-} mice without any surgical intervention. We found increased monocyte counts in whole-aorta lysates (Fig. 5H) and exacerbated plaque loads in aortic valves 7 days after HMGB1 injection (Fig. 5, I and J). In addition, we detected an up-regulation of *Il6*, *Icam1*, and *Vcam1* mRNA expression in whole-aorta lysates (fig. S12), resembling the proinflammatory expression pattern found in aortas of mice undergoing stroke (compared to Fig. 3A). Together, these results indicate that HMGB1—and potentially other alarmins released from the necrotic brain tissue—induces a sterile, systemic immune response via vascular RAGE, which in turn results in exacerbation of vascular inflammation after stroke.

Alarmin release and sympathetic stress response synergize in poststroke atheroprotection

We aimed to further dissect the differential contribution of the sympathetic innervation versus alarmin-driven cascades on the observed

effects of systemic immune activation and vascular inflammation after stroke. In accord with earlier findings (27), we observed a decrease in overall myeloid cell count of the femur bone marrow at 24 hours after stroke (Fig. 6A). This was associated with an increase in tyrosine hydroxylase expression along sympathetic fibers in the femur bone marrow (Fig. 6, B and C). These results indicated a potential release of monocytes from the bone marrow after sympathetic innervation due to a stroke-induced stress response. We and others previously observed a splenic expansion of myeloid cells after stroke induction (12, 28). Hence, we tested the possibility of myeloid cell trafficking from the bone marrow to the spleen after stroke using an in vivo cell-tracking approach. After in vivo labeling of the bone marrow by quantum dot (Qdot) nanocrystals—nanometer-scaled fluorophores incorporated in the cytoplasm of living cells—we found an increased number of Qdot⁺ monocytes in spleen after stroke compared to sham surgery (Fig. 6, D and E), whereas the Qdot⁺ cell count in bone marrow decreased after stroke (fig. S13). To further investigate the contribution of the splenic immune compartment to poststroke vascular inflammation, we performed splenectomy versus sham surgery in HCD-fed *ApoE*^{-/-} mice before stroke induction in both groups. Seven days after stroke, we found reduced aortic monocyte counts in splenectomized animals and a decreased plaque load in aortic valves compared to the nonsplenectomized but stroked control group (Fig. 6, F and G); however, splenectomy had no effect on infarct severity or bone marrow monocyte count (fig. S14). Together, these findings suggest a role for sympathetic innervation in mobilization of myeloid cells from the bone marrow niche as well as maturation/activation of monocytes in the splenic immune compartment, thus contributing to stroke-induced atheroprotection.

To further test this hypothesis, we analyzed the differential contribution of the alarmin signaling cascade and sympathetic innervation on monocyte cellularity and activation using sRAGE decoy receptors and the β 3-adrenoreceptor inhibitor SR59230A (7, 29). Blocking β 3-adrenoreceptors but not sRAGE treatment suppressed the egress of CD11b⁺CD45⁺ monocytes from the bone marrow, whereas both treatment regimens increased overall spleen cellularity (Fig. 6, H and I). Notably, β 3-adrenoreceptor blockage did not alter HMGB1 plasma concentrations after stroke (fig. S15). sRAGE treatment abrogated monocyte activation in the spleen after stroke, whereas adrenoreceptor blockage affected MHCII up-regulation only when applied in combination with sRAGE (Fig. 6J). In blood, we observed similar treatment effects with only the combination of adrenoreceptor and sRAGE blockage being effective in decreasing monocyte activation (fig. S16). We further investigated synergistic effects of neutralizing sympathetic activation and alarmin neutralization on exacerbation of vascular inflammation after stroke. Although both treatments attenuated the increase in aortic monocyte counts after stroke, blocking of alarmin signaling using sRAGE was required to attenuate the increase in activated MHCII⁺ monocytes in atherosclerotic lesions after stroke (Fig. 6K). We additionally analyzed the impact of adrenoreceptor and sRAGE blockage on aortic valve plaque load. In accordance with the synergistic effects of adrenoreceptor and sRAGE blockage on inflammatory markers of vascular inflammation, only the combined treatment was effective in reducing aortic plaque load compared to the control treatment (Fig. 6L). These results suggest that sympathetic activation during the acute stress response after stroke drives bone marrow egress of monocytic cells, whereas brain-released alarmins are required for monocyte activation (fig. S17).

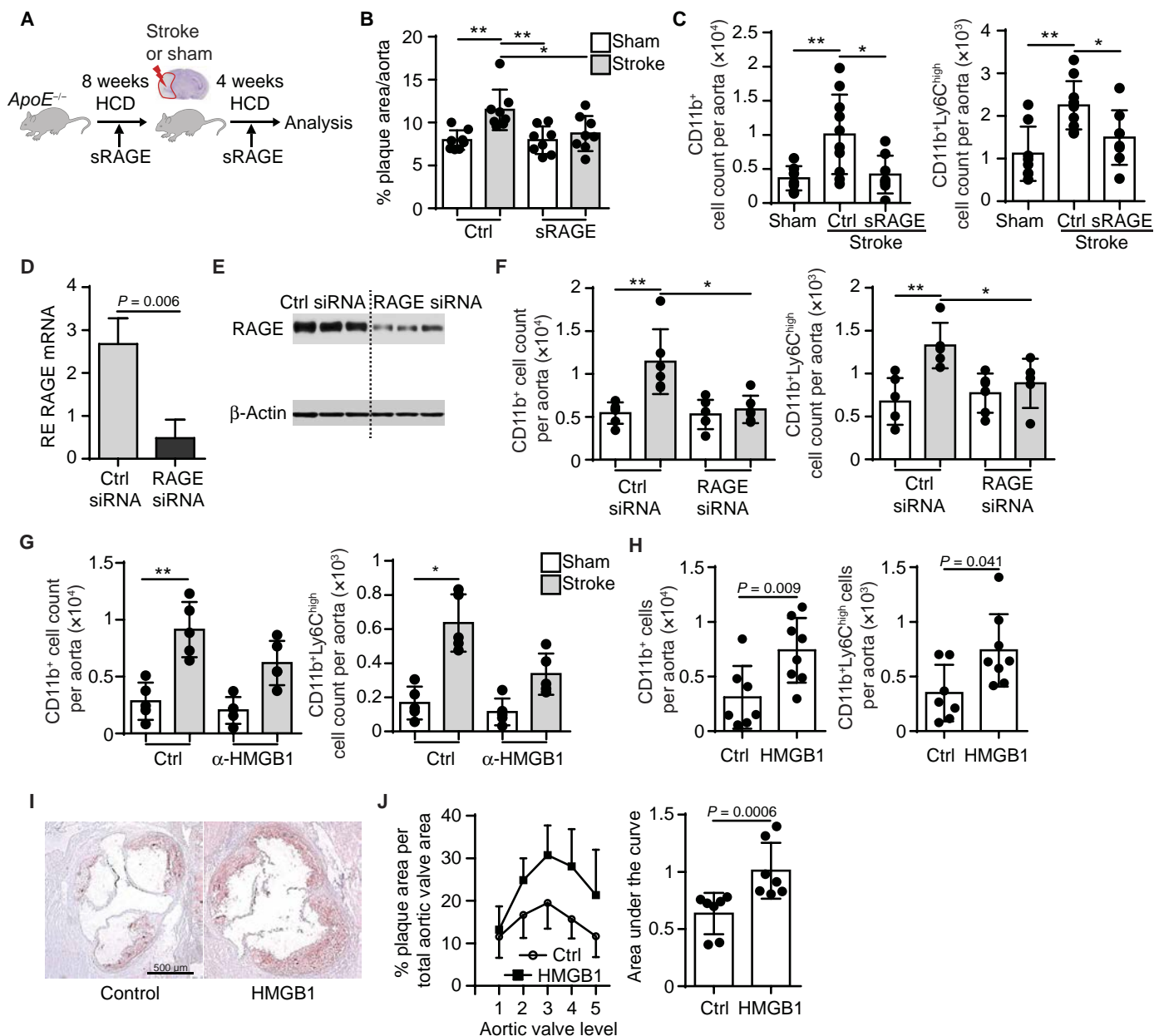


Fig. 5. Stroke induces atheroprotection via the RAGE-signaling pathway. (A) Schematic illustration of experimental design for data shown in (B) to (D): HCD-fed *ApoE*^{-/-} mice received either an intraperitoneal injection of sRAGE or vehicle treatment 30 min before and 4 hours after the respective surgery and were sacrificed 1 month later. (B) Quantification of the overall plaque area per aorta 1 month after surgery in stroke or sham mice treated with sRAGE or vehicle (ANOVA, *n* = 8 per group). (C) Flow cytometric analysis of whole aorta for CD11b⁺ and CD11b⁺Ly6C^{high} monocyte counts after stroke with sRAGE or vehicle treatment compared to sham-operated mice 1 month after surgery (*H* test, *n* = 7 to 8 per group). (D) RAGE mRNA expression 3 days after hydrodynamic intravenous injection of RAGE-specific small interfering RNA (siRNA) or control siRNA (Ctrl; *U* test, *n* = 5 per group). (E) RAGE protein expression 3 days after RAGE-specific or control siRNA injection (*n* = 3 per group). (F) HCD-fed *ApoE*^{-/-} mice received stroke or sham surgery 3 days after hydrodynamic RAGE-specific or control siRNA injection and were sacrificed 7 days later for flow cytometric analysis of whole aortas for CD11b⁺ and CD11b⁺Ly6C^{high} monocyte counts (*H* test, *n* = 5 to 6 per group). (G) Mice received HMGB1-specific or control immunoglobulin G antibodies immediately after surgery (sham or stroke), and CD11b⁺ and CD11b⁺Ly6C^{high} monocyte counts were analyzed with flow cytometry 7 days later (*H* test, *n* = 5 to 6 per group). (H) Flow cytometric analysis for CD11b⁺ and CD11b⁺Ly6C^{high} monocyte counts of whole aortas 7 days after an intraperitoneal injection of vehicle or rHMGB1 to HCD-fed *ApoE*^{-/-} mice (*U* test, *n* = 7 to 8 per group). (I) Representative images of Oil Red O stained aortic valve sections 7 days after rHMGB1 administration. (J) Comparison of Oil Red O⁺ area on five consecutive sections in aortic valves (left). Area under the curve analysis of the individual aortic valves (right) after HMGB1 administration compared to control-treated naïve *ApoE*^{-/-} mice (*U* test, *n* = 7 per group). **P* < 0.05, ***P* < 0.01.

DISCUSSION

Large-artery atherosclerosis is a major cause of stroke that is also associated with an unexpectedly high recurrence rate (1, 2). We have

shown that experimental stroke induces exacerbation of atheroprotection. Enhanced vascular inflammation after stroke depended on a synergistic effect of sympathetic recruitment of monocytes from the

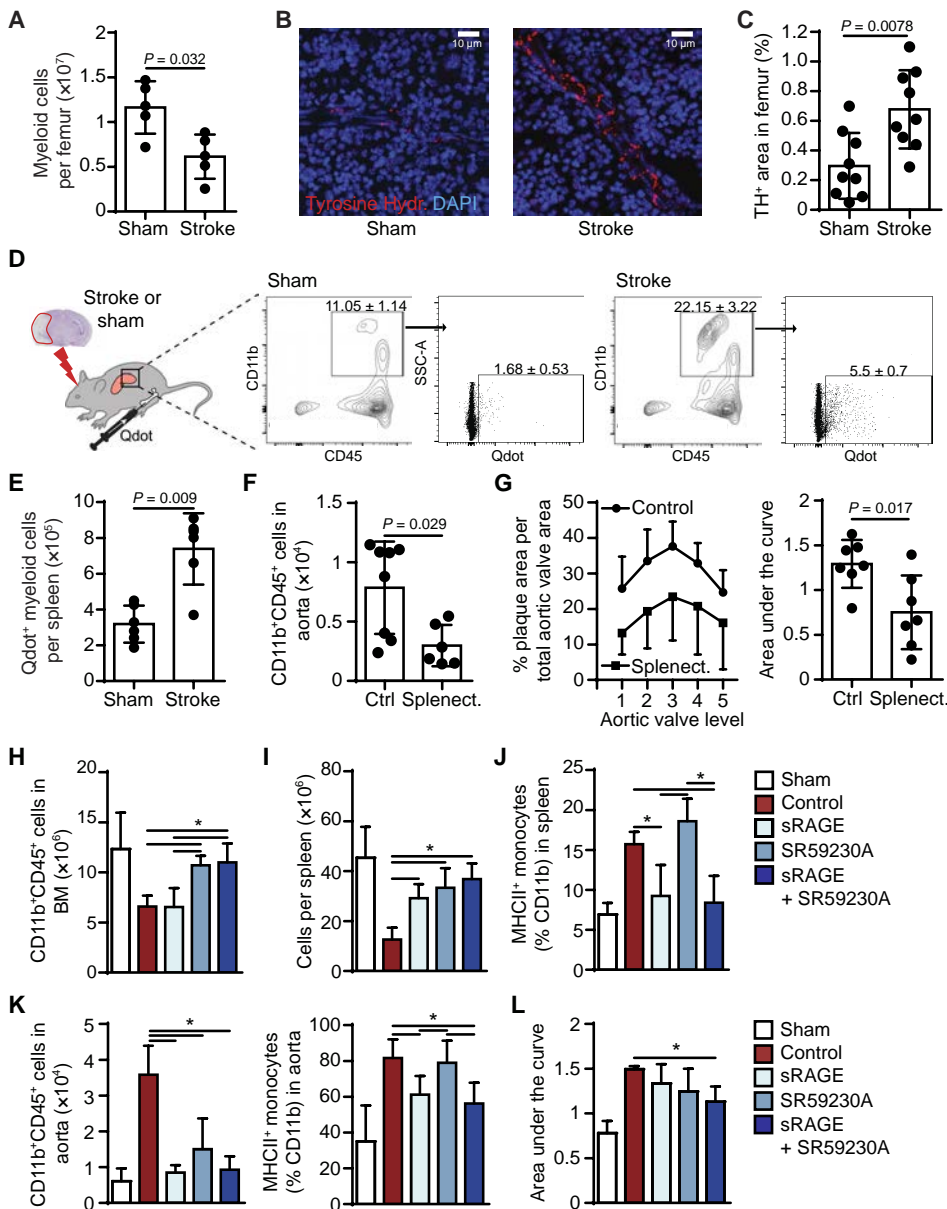


Fig. 6. Alarmin release and sympathetic stress response synergize in poststroke atheroprotection. (A) Flow cytometric analysis of myeloid cellularity in femur bone marrow 24 hours after stroke compared to sham surgery. (B) Representative images of immunofluorescence staining for tyrosine hydroxylase (TH) in femoral bone marrow 24 hours after stroke and sham surgery. (C) Quantification of TH⁺ area after stroke compared to sham on femoral sections (*U* test, *n* = 7 per group). (D) WT mice received quantum dot (Qdot) nanocrystal injections in the femoral bone marrow 2 hours before stroke or sham surgery and were sacrificed 24 hours later (*U* test, *n* = 6 per group). Representative gating strategy for CD45⁺CD11b⁺ monocytes and Qdot⁺ myeloid cells in spleen after stroke or sham surgery. (E) Quantification of total Qdot⁺ myeloid cells in spleens after stroke compared to sham surgery (*U* test, *n* = 5 per group). (F) HCD-fed *ApoE*^{-/-} mice were splenectomized (Splenect.) before stroke or sham surgery and analyzed 7 days after stroke for total monocyte cell counts and proinflammatory Ly6C^{high} frequency in aortas 1 week after stroke. (G) Quantification of overall plaque area in aortic valves of splenectomized mice after stroke induction (*U* test, *n* = 6 to 8 per group). (H to J) WT mice received either sRAGE, β3-blocker SR59230, both combined, or vehicle treatment immediately after stroke, and bone marrow (BM) (H) and spleen (I and J) were analyzed by flow cytometry 24 hours later for the total myeloid (CD45⁺CD11b⁺) cell count and monocyte activation (percentage of MHCII⁺ monocytes; *H* test, *n* = 6 to 8 per group). (K) HCD-fed *ApoE*^{-/-} mice received sRAGE, SR59230, combination therapy, or control treatment immediately after stroke. Bar graphs represent the flow cytometric analysis of CD45⁺CD11b⁺ monocyte cell count, the percentage of MHCII⁺ monocytes, and Ly6C^{high} monocytes in aortas 1 week after stroke (*H* test, *n* = 7 to 8 per group). (L) Area under the curve analyzing plaque load in five consecutive sections of aortic valve for HCD-fed *ApoE*^{-/-} mice (*H* test, *n* = 5 to 6 per group). **P* < 0.05, ***P* < 0.01.

bone marrow niche and subsequent activation of innate immune and endothelial cells by circulating alarmins, attracting inflammatory monocytes to atherosclerotic lesions. We further identified the HMGB1-RAGE pathway as a critical signaling mechanism eliciting the sterile inflammatory response after stroke.

We observed a rapid translocation of bone marrow monocytes to the spleen after stroke. Myeloid monocyte mobilization has previously been shown to be critically mediated by sympathetic signaling via β3-adrenoreceptors in myocardial infarction models (27). Accordingly, we showed an important role of β3-adrenoreceptors in stroke-induced monocyte mobilization using specific inhibitors. However, although blocking sympathetic innervation attenuated monocyte evasion from the bone marrow, it did not affect monocyte activation, vascular inflammation, or plaque growth. Notably, previous studies in experimental and clinical stroke have associated the sympathetic stress response with subacute immunosuppression but not monocyte activation or vascular inflammation (30). Hence, our results strengthen the concept of a second mechanism promoting the inflammatory response after stroke, independent of sympathetic activation.

Aside from eliciting a local immune response with microglial activation, the release of HMGB1 and other alarmins from necrotic brain tissue induces a systemic response with cellular activation and massive cytokine secretion in peripheral immune organs (10, 12). Systemic immune activation involves a rapid sterile immune response acutely after stroke, followed by an immunosuppression during the subacute phase (days 2 to 7) after stroke. In addition, previous clinical studies have demonstrated a third phase characterized by a delayed chronic immune activation (from day 7 on) with elevated inflammatory markers for more than 1 year after stroke in patients (9, 31). The biological activity of HMGB1 depends critically on its redox state (32, 33). Fully reduced HMGB1 has chemoattractant properties, whereas disulfide HMGB1 has cytokine-inducing properties and the terminally oxidized sulfonil HMGB1 is anti-inflammatory (11). We observed that HMGB1 levels in stroke patients not only remained substantially increased during the first week after stroke but that the

proinflammatory disulfide HMGB1 species became the predominant isoform over this time course.

Monocytes/macrophages play a critical role in the development and propagation of atherosclerotic lesions. Monocyte invasion into atherogenic lesions has been shown to be instrumental in the initiation of atherosclerosis. In this phase, the chemokine-ligand receptor interaction plays a pivotal role. Studies have shown that CCR2 expression on monocytes is essential for recruitment into the adventitial space and for further plaque development (34, 35). In contrast, proliferation of macrophages has been demonstrated to be the key driver for lesion growth in established atherosclerosis (36). Surprisingly, we observed that poststroke exacerbation of established atherosclerotic lesions was associated with enhanced de novo recruitment of circulating monocytes to the vessel rather than increased local proliferation. A possible explanation for this phenomenon is that as a consequence of the strong inflammatory response after stroke, monocyte chemoattraction via the CCL2-CCR2 axis regains a predominant role for monocyte recruitment comparable to the initiation of the vascular inflammatory milieu (37). Aside from chemoattraction, endothelial expression of adhesion molecules is pivotal for monocyte recruitment. Intercellular adhesion molecule-1 (ICAM-1) and VCAM-1 are known to be essential for the arrest and extravasation of monocytes into the arterial wall (38). Our data unequivocally demonstrate the up-regulation of these critical adhesion molecules on aortic endothelial cells in mice by PCR, in vivo imaging, and in vitro cultures. In accord with our results, it was previously shown that HMGB1 can activate endothelial cells, leading to changes in the nuclear factors Sp-1 and nuclear factor κ B, with subsequent up-regulation of adhesion molecules and proinflammatory cytokines (18).

We observed a highly consistent effect of poststroke exacerbation of atherosclerosis pathology both in female and male mice, in aortas and aortic valves, and verified this phenomenon by in vivo MRI. However, a limitation of this study is that we were not able to fully investigate the link between poststroke atheroprotection and enhanced plaque rupture as a cause of recurrent stroke in the mouse atherosclerosis model. Atherosclerotic lesions of aorta and large arteries in animal models, including the *ApoE*-deficient model used here, rarely develop spontaneous destabilization and rupture with occlusive vascular thrombosis. We observed several surrogate markers of increased plaque vulnerability; however, increased incidence of plaque rupture and secondary ischemic brain lesions will have to be tested in more specific models that mimic human plaque rupture and ultimately in prospective clinical studies.

In conclusion, our data identify stroke-induced alarmin release from the ischemic brain as a critical mechanism activating inflammatory pathways and acting in synergy with an acute stress response after stroke to exacerbate atherosclerosis. Interfering with this sterile immune response by neutralizing brain-released alarmins may provide a therapeutic approach for stroke patients.

MATERIAL AND METHODS

Study design

The goal of this study was to investigate atheroprotection after stroke and describe the underlying mechanisms in an experimental model of ischemic stroke in *ApoE*^{-/-} mice. Sample sizes were calculated using GPower 3.1. On the basis of a previous report (7), we used a monocyte increase rate of 40% with an SD of 25%. Using an α error of 0.05 and power of 0.8, we calculated a group size of 8 (*t* test, two groups, unpaired).

Data were excluded from all mice that died during surgery. Detailed exclusion criteria for the experimental models were (i) insufficient middle cerebral artery (MCA) occlusion (blood flow reduction less than 80%), (ii) death during surgery, and (iii) lack of brain ischemia as quantified by histology (see table S3 for included/excluded animals per experiment). Animals were randomized to treatment groups, and all analyses were performed by investigators blinded to group allocation. Unblinding was performed after completion of statistical analysis. All animal experiments were performed and reported in accordance with the Animal Research: Reporting of In Vivo Experiments (ARRIVE) guidelines (39).

Experimental animals

All animal experiments were performed in accordance with the guidelines for the use of experimental animals and were approved by the government committee of Upper Bavaria (Regierungspraesidium Oberbayern, #175-2013). We used age-matched, male C57BL6/J mice (8 to 10 weeks, 22 to 24 g body weight; Charles River Laboratories). *ApoE*^{-/-} (the Jackson Laboratory) mice were fed an HCD (#88137, ssniff). Transient filament occlusion was performed in all *ApoE*^{-/-} after 8 weeks of HCD. CCR2-RFP knock-in mice were bred with CX3CR1-green fluorescent protein (GFP) mice (40).

Clinical stroke patient study population

Ischemic stroke patients were recruited within 24 hours of symptom onset. All patients had a final diagnosis of ischemic stroke as defined by an acute focal neurological deficit in combination with a diffusion-weighted imaging-positive lesion on MRI or a new lesion on a delayed computed tomography scan. Age- and comorbidity-matched patients without neurological disease were used as controls. The study was approved by the local ethics committee and was conducted in accordance with the Declaration of Helsinki and institutional guidelines. Written and informed consent was obtained from all subjects.

Statistical analysis

Data were analyzed using GraphPad Prism version 6.0. All summary data are expressed as means \pm SD. All data sets were tested for normality using the Shapiro-Wilk normality test. The groups containing normally distributed data were tested using a two-way Student's *t* test (for two groups) or analysis of variance (ANOVA) (for more than two groups). The remaining data were analyzed using the Mann-Whitney *U* test (for two groups) or *H* test (for more than two groups). Similar variance was assured for all groups, which were statistically compared. Differences with a *P* < 0.05 were considered to be statistically significant. *P* values were adjusted for comparison of multiple comparisons using Bonferroni correction.

SUPPLEMENTARY MATERIALS

www.sciencetranslationalmedicine.org/cgi/content/full/10/432/eaao1313/DC1
Materials and Methods

Fig. S1. Characterization of the 60-min filament MCA occlusion (fMCAo) model.

Fig. S2. Exacerbation of atherosclerotic lesions in aortic valves of male and female HCD-fed *ApoE*^{-/-} mice 1 month after fMCAo surgery.

Fig. S3. Immune cell counts in aorta of HCD-fed *ApoE*^{-/-} mice 1 month after experimental stroke.

Fig. S4. Analysis of atherosclerotic plaque load at the common carotid artery bifurcation in HCD-fed *ApoE*^{-/-} mice.

Fig. S5. Comparison of BrdU incorporation in aorta, blood, and spleen 1 week after experimental stroke surgery.

Fig. S6. RFP⁺CD11b⁺ cell counts in blood after experimental stroke surgery.

Fig. S7. Immunological data of stroke patients.

Fig. S8. Body weight and mortality in sRAGE treatment mice after stroke.

Fig. S9. Atherosclerotic lesions in aortic valves of male and female HCD-fed ApoE^{-/-} mice 1 month after experimental stroke and sRAGE treatment.

Fig. S10. Lipid profile of plasma samples 1 month after experimental stroke surgery and sRAGE treatment.

Fig. S11. Flow cytometric analysis of spleen and blood 24 hours after experimental stroke with anti-HMGB1 treatment.

Fig. S12. Recombinant HMGB1 in vivo administration exacerbates atherosclerosis.

Fig. S13. Quantification of in vivo Qdot labeling of femoral bone marrow 24 hours after experimental stroke.

Fig. S14. Myeloid cell count in femoral bone marrow and brain infarct volumetry after splenectomy.

Fig. S15. Impact of β 3-adrenoreceptor blockage on HMGB1 plasma levels after experimental stroke.

Fig. S16. Impact of β 3-adrenoreceptor blockage (SR59230A), alarmin blockage (sRAGE), and combined treatment on blood immune cells in WT mice.

Fig. S17. Schematic overview of proposed mechanism of atheroprotection after stroke.

Table S1. Primer list for quantitative PCR array (mouse chemokines and receptors).

Table S2. Demographic and clinical characteristics of the study population.

Table S3. Number of (excluded/included) animals in accomplished experiments.

References (41–49)

REFERENCES AND NOTES

- A. J. Grau, C. Weimar, F. Bugge, A. Heinrich, M. Goertler, S. Neumaier, J. Glahn, T. Brandt, W. Hacke, H.-C. Diener, Risk factors, outcome, and treatment in subtypes of ischemic stroke: The German stroke data bank. *Stroke* **32**, 2559–2566 (2001).
- J. Putaala, E. Haapaniemi, A. J. Metso, T. M. Metso, V. Arto, M. Kaste, T. Tatlisumak, Recurrent ischemic events in young adults after first-ever ischemic stroke. *Ann. Neurol.* **68**, 661–671 (2010).
- J. K. Lovett, A. J. Coull, P. M. Rothwell, Early risk of recurrence by subtype of ischemic stroke in population-based incidence studies. *Neurology* **62**, 569–573 (2004).
- W. B. Kannel, P. Sorlie, P. M. McNamara, Prognosis after initial myocardial infarction: The Framingham study. *Am. J. Cardiol.* **44**, 53–59 (1979).
- P. Libby, Inflammation in atherosclerosis. *Nature* **420**, 868–874 (2002).
- C. Weber, H. Noels, Atherosclerosis: Current pathogenesis and therapeutic options. *Nat. Med.* **17**, 1410–1422 (2011).
- P. Dutta, G. Courties, Y. Wei, F. Leuschner, R. Gorbatov, C. S. Robbins, Y. Iwamoto, B. Thompson, A. L. Carlson, T. Heidt, M. D. Majumdar, F. Lasitschka, M. Etzrodt, P. Waterman, M. T. Waring, A. T. Chicoine, A. M. van der Laan, H. W. M. Niessen, J. J. Piek, B. B. Rubin, J. Butany, J. R. Stone, H. A. Katus, S. A. Murphy, D. A. Morrow, M. S. Sabatine, C. Vinegoni, M. A. Moskowitz, M. J. Pittet, P. Libby, C. P. Lin, F. K. Swirski, R. Weissleder, M. Nahrendorf, Myocardial infarction accelerates atherosclerosis. *Nature* **487**, 325–329 (2012).
- A. P. Wright, M. K. Öhman, T. Hayasaki, W. Luo, H. M. Russo, C. Guo, D. T. Eitzman, Atherosclerosis and leukocyte–endothelial adhesive interactions are increased following acute myocardial infarction in apolipoprotein E deficient mice. *Atherosclerosis* **212**, 414–417 (2010).
- J. Schulze, D. Zierath, P. Tanzi, K. Cain, D. Shibata, A. Dressel, K. Becker, Severe stroke induces long-lasting alterations of high-mobility group box 1. *Stroke* **44**, 246–248 (2013).
- H. Offner, S. Subramanian, S. M. Parker, M. E. Afentoulis, A. A. Vandenbark, P. D. Hurn, Experimental stroke induces massive, rapid activation of the peripheral immune system. *J. Cereb. Blood Flow Metab.* **26**, 654–665 (2006).
- V. Singh, S. Roth, R. Veltkamp, A. Liesz, HMGB1 as a key mediator of immune mechanisms in ischemic stroke. *Antioxid. Redox Signal.* **24**, 635–651 (2016).
- A. Liesz, A. Dalpke, E. Mracsko, D. J. Antoine, S. Roth, W. Zhou, H. Yang, S.-Y. Na, M. Akhilaroglu, T. Fleming, T. Eigenbrod, P. P. Nawroth, K. J. Tracey, R. Veltkamp, DAMP signaling is a key pathway inducing immune modulation after brain injury. *J. Neurosci.* **35**, 583–598 (2015).
- J. Li, R. Kokkola, S. Tabibzadeh, R. Yang, M. Ochani, X. Qiang, H. E. Harris, C. J. Czura, H. Wang, L. Ulloa, H. Wang, H. S. Warren, L. L. Moldawer, M. P. Fink, U. Andersson, K. J. Tracey, H. Yang, Structural basis for the proinflammatory cytokine activity of high mobility group box 1. *Mol. Med.* **9**, 37–45 (2003).
- A. S. Plump, J. D. Smith, T. Hayek, K. Aalto-Setälä, A. Walsh, J. G. Verstuyft, E. M. Rubin, J. L. Breslow, Severe hypercholesterolemia and atherosclerosis in apolipoprotein E-deficient mice created by homologous recombination in ES cells. *Cell* **71**, 343–353 (1992).
- J. L. Johnson, A. H. Baker, K. Oka, L. Chan, A. C. Newby, C. L. Jackson, S. J. George, Suppression of atherosclerotic plaque progression and instability by tissue inhibitor of metalloproteinase-2: Involvement of macrophage migration and apoptosis. *Circulation* **113**, 2435–2444 (2006).
- J. Johnson, K. Carson, H. Williams, S. Karanam, A. Newby, G. Angelini, S. George, C. Jackson, Plaque rupture after short periods of fat feeding in the apolipoprotein E-knockout mouse: Model characterization and effects of pravastatin treatment. *Circulation* **111**, 1422–1430 (2005).
- K. J. Moore, F. J. Sheedy, E. A. Fisher, Macrophages in atherosclerosis: A dynamic balance. *Nat. Rev. Immunol.* **13**, 709–721 (2013).
- C. Fiuzza, M. Bustin, S. Talwar, M. Tropea, E. Gerstenberger, J. H. Shelhamer, A. F. Suffredini, Inflammation-promoting activity of HMGB1 on human microvascular endothelial cells. *Blood* **101**, 2652–2660 (2003).
- C.-L. Tsou, W. Peters, Y. Si, S. Slaymaker, A. M. Aslanian, S. P. Weisberg, M. Mack, I. F. Charo, Critical roles for CCR2 and MCP-3 in monocyte mobilization from bone marrow and recruitment to inflammatory sites. *J. Clin. Invest.* **117**, 902–909 (2007).
- C. Shi, E. G. Pamer, Monocyte recruitment during infection and inflammation. *Nat. Rev. Immunol.* **11**, 762–774 (2011).
- P. Dutta, H. B. Sager, K. R. Stengel, K. Naxerova, G. Courties, B. Saez, L. Silberstein, T. Heidt, M. Sebas, Y. Sun, G. Wojtkiewicz, P. F. Feruglio, K. King, J. N. Baker, A. M. van der Laan, A. Borodovsky, K. Fitzgerald, M. Hulsmans, F. Hoyer, Y. Iwamoto, C. Vinegoni, D. Brown, M. Di Carli, P. Libby, S. W. Hiebert, D. T. Scadden, F. K. Swirski, R. Weissleder, M. Nahrendorf, Myocardial infarction activates CCR2⁺ hematopoietic stem and progenitor cells. *Cell Stem Cell* **16**, 477–487 (2015).
- M. Gauberti, A. Montagne, O. A. Marcos-Contreras, A. Le Béhot, E. Maubert, D. Vivien, Ultra-sensitive molecular MRI of vascular cell adhesion molecule-1 reveals a dynamic inflammatory penumbra after strokes. *Stroke* **44**, 1988–1996 (2013).
- L. Park, K. G. Raman, K. J. Lee, Y. Lu, L. J. Ferran Jr., W. S. Chow, D. Stern, A. M. Schmidt, Suppression of accelerated diabetic atherosclerosis by the soluble receptor for advanced glycation endproducts. *Nat. Med.* **4**, 1025–1031 (1998).
- H. Offner, S. Subramanian, S. M. Parker, C. Wang, M. E. Afentoulis, A. Lewis, A. A. Vandenbark, P. D. Hurn, Splenic atrophy in experimental stroke is accompanied by increased regulatory T cells and circulating macrophages. *J. Immunol.* **176**, 6523–6531 (2006).
- A. Hug, A. Dalpke, N. Wiczorek, T. Giese, A. Lorenz, G. Auffarth, A. Liesz, R. Veltkamp, Infarct volume is a major determinant of post-stroke immune cell function and susceptibility to infection. *Stroke* **40**, 3226–3232 (2009).
- B. G. Talayero, F. M. Sacks, The role of triglycerides in atherosclerosis. *Curr. Cardiol. Rep.* **13**, 544–552 (2011).
- G. Courties, F. Herisson, H. B. Sager, T. Heidt, Y. Ye, Y. Wei, Y. Sun, N. Severe, P. Dutta, J. Scharff, D. T. Scadden, R. Weissleder, F. K. Swirski, M. A. Moskowitz, M. Nahrendorf, Ischemic stroke activates hematopoietic bone marrow stem cells. *Circ. Res.* **116**, 407–417 (2015).
- M. Nahrendorf, M. J. Pittet, F. K. Swirski, Monocytes: Protagonists of infarct inflammation and repair after myocardial infarction. *Circulation* **121**, 2437–2445 (2010).
- Y. Katayama, M. Battista, W.-M. Kao, A. Hidalgo, A. J. Peired, S. A. Thomas, P. S. Frenette, Signals from the sympathetic nervous system regulate hematopoietic stem cell egress from bone marrow. *Cell* **124**, 407–421 (2006).
- Á. Chamorro, A. Meisel, A. M. Planas, X. Urra, D. van de Beek, R. Veltkamp, The immunology of acute stroke. *Nat. Rev. Neurol.* **8**, 401–410 (2012).
- A. Liesz, H. Rieger, J. Purrucker, M. Zorn, A. Dalpke, M. Möhlenbruch, S. Englert, P. P. Nawroth, R. Veltkamp, Stress mediators and immune dysfunction in patients with acute cerebrovascular diseases. *PLOS ONE* **8**, e74839 (2013).
- D. J. Antoine, H. E. Harris, U. Andersson, K. J. Tracey, M. E. Bianchi, A systematic nomenclature for the redox states of high mobility group box (HMGB) proteins. *Mol. Med.* **20**, 135–137 (2014).
- E. Venereau, M. Casagrandi, M. Schiraldi, D. J. Antoine, A. Cattaneo, F. De Marchis, J. Liu, A. Antonelli, A. Preti, L. Raeli, S. S. Shams, H. Yang, L. Varani, U. Andersson, K. J. Tracey, A. Bachi, M. Uguccioni, M. E. Bianchi, Mutually exclusive redox forms of HMGB1 promote cell recruitment or proinflammatory cytokine release. *J. Exp. Med.* **209**, 1519–1528 (2012).
- L. Boring, J. Gosling, M. Cleary, I. F. Charo, Decreased lesion formation in CCR2^{-/-} mice reveals a role for chemokines in the initiation of atherosclerosis. *Nature* **394**, 894–897 (1998).
- J. Guo, M. Van Eck, J. Twisk, N. Maeda, G. M. Benson, P. H. E. Groot, T. J. C. Van Berkel, Transplantation of monocyte CC-chemokine receptor 2-deficient bone marrow into ApoE3-Leiden mice inhibits atherogenesis. *Arterioscler. Thromb. Vasc. Biol.* **23**, 447–453 (2003).
- C. S. Robbins, I. Hilgendorf, G. F. Weber, I. Theurl, Y. Iwamoto, J.-L. Figueiredo, R. Gorbatov, G. K. Sukhova, L. M. S. Gerhardt, D. Smyth, C. C. J. Zavitz, E. A. Shikani, M. Parsons, N. van Rooijen, H. Y. Lin, M. Husain, P. Libby, M. Nahrendorf, R. Weissleder, F. K. Swirski, Local proliferation dominates lesional macrophage accumulation in atherosclerosis. *Nat. Med.* **19**, 1166–1172 (2013).
- B. Coll, C. Alonso-Villaverde, J. Joven, Monocyte chemoattractant protein-1 and atherosclerosis: Is there room for an additional biomarker? *Clin. Chim. Acta.* **383**, 21–29 (2007).

38. J. Cros, N. Cagnard, K. Woollard, N. Patey, S.-Y. Zhang, B. Senechal, A. Puel, S. K. Biswas, D. Moshous, C. Picard, J.-P. Jais, D. D'Cruz, J.-L. Casanova, C. Trouillet, F. Geissmann, Human CD14^{dim} monocytes patrol and sense nucleic acids and viruses via TLR7 and TLR8 receptors. *Immunity* **33**, 375–386 (2010).
39. C. Kilkenny, W. J. Browne, I. C. Cuthill, M. Emerson, D. G. Altman, Improving bioscience research reporting: The ARRIVE guidelines for reporting animal research. *PLOS Biol.* **8**, e1000412 (2010).
40. N. Saederup, A. E. Cardona, K. Croft, M. Mizutani, A. C. Coteleur, C.-L. Tsou, R. M. Ransohoff, I. F. Charo, Selective chemokine receptor usage by central nervous system myeloid cells in CCR2-red fluorescent protein knock-in mice. *PLOS ONE* **5**, e13693 (2010).
41. J. B. Bederson, L. H. Pitts, M. Tsuji, M. C. Nishimura, R. L. Davis, H. Bartkowski, Rat middle cerebral artery occlusion: Evaluation of the model and development of a neurologic examination. *Stroke* **17**, 472–476 (1986).
42. H. R. Lo, Y. C. Chao, Rapid titer determination of baculovirus by quantitative real-time polymerase chain reaction. *Biotechnol. Prog.* **20**, 354–360 (2004).
43. S. Qin, H. Wang, R. Yuan, H. Li, M. Ochani, K. Ochani, M. Rosas-Ballina, C. J. Czura, J. M. Huston, E. Miller, X. Lin, B. Sherry, A. Kumar, G. Larosa, W. Newman, K. J. Tracey, H. Yang, Role of HMGB1 in apoptosis-mediated sepsis lethality. *J. Exp. Med.* **203**, 1637–1642 (2006).
44. M. J. Butcher, M. Herre, K. Ley, E. Galkina, Flow cytometry analysis of immune cells within murine aortas. *J. Vis. Exp.* **53**, 2848 (2011).
45. E. Maganto-Garcia, M. Tarrío, A. H. Lichtman, Mouse models of atherosclerosis. *Curr. Protoc. Immunol.* **Chapter 15**, 11–23 (2012).
46. T. A. Seimon, Y. Wang, S. Han, T. Senokuchi, D. M. Schrijvers, G. Kuriakose, A. R. Tall, I. A. Tabas, Macrophage deficiency of p38 α MAPK promotes apoptosis and plaque necrosis in advanced atherosclerotic lesions in mice. *J. Clin. Invest.* **119**, 886–898 (2009).
47. D. J. Antoine, D. P. Williams, A. Kipar, R. E. Jenkins, S. L. Regan, J. G. Sathish, N. R. Kitteringham, B. K. Park, High-mobility group box-1 protein and keratin-18, circulating serum proteins informative of acetaminophen-induced necrosis and apoptosis in vivo. *Toxicol. Sci.* **112**, 521–531 (2009).
48. S. Nyström, D. J. Antoine, P. Lundbäck, J. G. Lock, A. F. Nita, K. Högstrand, A. Grandien, H. Erlandsson-Harris, U. Andersson, S. E. Applequist, TLR activation regulates damage-associated molecular pattern isoforms released during pyroptosis. *EMBO J.* **32**, 86–99 (2013).
49. X. Ge, D. J. Antoine, Y. Lu, E. Arriazu, T.-M. Leung, A. L. Klepper, A. D. Branch, M. I. Fiel, N. Nieto, High mobility group box-1 (HMGB1) participates in the pathogenesis of alcoholic liver disease (ALD). *J. Biol. Chem.* **289**, 22672–22691 (2014).

Acknowledgments: We thank K. Thuß-Silczak for excellent technical assistance and U. Deutsch for maintaining transgenic mouse colonies at the University of Bern. CCR2^{RFP/RFP}CX3CR1^{GFP/+} mice were donated by I. F. Charo (University of California, San Francisco, USA) and R. Ransohoff (Biogen Idec, Boston, USA). sRAGE baculovirus was a donation by A.-M. Schmidt (New York University Langone Medical Center, New York City, USA). **Funding:** This study was funded by the excellence cluster of the German research foundation Munich Cluster for Systems Neurology (SyNergy) (EXC1010 to M.D., A.L., and J.B.) and the German Research Foundation (DFG) (LI-2534/2-1 to A.L., SFB1123-A03 to J.B., and SFB1123-B01 to L.M.H.). **Author contributions:** S.R. performed most of the experiments, analyzed the data, and wrote the manuscript. V.S. performed the fluorescence-activated cell sorting experiments and monocyte stimulation assays. S.T. acquired and analyzed the patient cohort. L.S. performed the MAEC stimulation experiments. G.H. and A.G. produced sRAGE. D.J.A. performed and analyzed the HMGB1 mass spectrometry. A.A., C.O., M.G., A.F., and D.V. performed in vivo MRI experiments and analyzed the imaging data. L.M.H. performed the blood biochemistry. D.V., H.E.H., B.E., and M.E.B. contributed the critical material and techniques for this study. C.H., J.B., and M.D. contributed the critical input to study design and manuscript writing. A.L. initiated and coordinated the study, analyzed the data, and wrote the manuscript. **Competing interests:** The authors declare that they have no competing interests. **Data and materials availability:** All primary data, detailed protocols, and noncommercially available materials can be requested from the corresponding author. The sRAGE vector was obtained under a material transfer agreement from A.-M. Schmidt (New York University School of Medicine, New York City, NY, USA).

Submitted 16 June 2017
 Accepted 14 February 2018
 Published 14 March 2018
 10.1126/scitranslmed.aao1313

Citation: S. Roth, V. Singh, S. Tiedt, L. Schindler, G. Huber, A. Geerloff, D. J. Antoine, A. Anfray, C. Orset, M. Gauberti, A. Fournier, L. M. Holdt, H. E. Harris, B. Engelhardt, M. E. Bianchi, D. Vivien, C. Haffner, J. Bernhagen, M. Dichgans, A. Liesz, Brain-released alarmins and stress response synergize in accelerating atherosclerosis progression after stroke. *Sci. Transl. Med.* **10**, eaao1313 (2018).

Brain-released alarmins and stress response synergize in accelerating atherosclerosis progression after stroke

Stefan Roth, Vikramjeet Singh, Steffen Tiedt, Lisa Schindler, Georg Huber, Arie Geerlof, Daniel J. Antoine, Antoine Anfray, Cyrille Orset, Maxime Gauberti, Antoine Fournier, Lesca M. Holdt, Helena Erlandsson Harris, Britta Engelhardt, Marco E. Bianchi, Denis Vivien, Christof Haffner, Jürgen Bernhagen, Martin Dichgans and Arthur Liesz

Sci Transl Med **10**, eaao1313.
DOI: 10.1126/scitranslmed.aao1313

An alarmin(g) consequence of stroke

Patients surviving a stroke are at an increased risk for subsequent cardiovascular events. Preclinical models have shown accelerated atherosclerosis after stroke; however, the mechanisms underlying this enhanced plaque formation and inflammation in arteries have not been investigated. Now, Roth *et al.* have discovered that stroke-induced alarmin high-mobility group box 1 (HMGB1) release and sympathetic stress response activation exert a synergistic effect, resulting in exacerbation of atherosclerotic plaques in mice. The authors suggest that interfering with these processes after stroke might reduce the risk of secondary cardiovascular events.

ARTICLE TOOLS	http://stm.sciencemag.org/content/10/432/eaao1313
SUPPLEMENTARY MATERIALS	http://stm.sciencemag.org/content/suppl/2018/03/09/10.432.eaao1313.DC1
RELATED CONTENT	http://stm.sciencemag.org/content/scitransmed/8/333/333ra50.full http://stm.sciencemag.org/content/scitransmed/10/426/eaag1328.full http://stm.sciencemag.org/content/scitransmed/7/299/299ra121.full http://stm.sciencemag.org/content/scitransmed/6/239/239sr1.full
REFERENCES	This article cites 49 articles, 17 of which you can access for free http://stm.sciencemag.org/content/10/432/eaao1313#BIBL
PERMISSIONS	http://www.sciencemag.org/help/reprints-and-permissions

Use of this article is subject to the [Terms of Service](#)

Supplementary Materials for

Brain-released alarmins and stress response synergize in accelerating atherosclerosis progression after stroke

Stefan Roth, Vikramjeet Singh, Steffen Tiedt, Lisa Schindler, Georg Huber, Arie Geerlof, Daniel J. Antoine, Antoine Anfray, Cyrille Orset, Maxime Gauberti, Antoine Fournier, Lesca M. Holdt, Helena Erlandsson Harris, Britta Engelhardt, Marco E. Bianchi, Denis Vivien, Christof Haffner, Jürgen Bernhagen, Martin Dichgans, Arthur Liesz*

*Corresponding author. Email: arthur.liesz@med.uni-muenchen.de

Published 14 March 2018, *Sci. Transl. Med.* **10**, eaao1313 (2018)
DOI: 10.1126/scitranslmed.aao1313

The PDF file includes:

Materials and Methods

Fig. S1. Characterization of the 60-min filament MCA occlusion (fMCAo) model.

Fig. S2. Exacerbation of atherosclerotic lesions in aortic valves of male and female HCD-fed *ApoE*^{-/-} mice 1 month after fMCAo surgery.

Fig. S3. Immune cell counts in aorta of HCD-fed *ApoE*^{-/-} mice 1 month after experimental stroke.

Fig. S4. Analysis of atherosclerotic plaque load at the common carotid artery bifurcation in HCD-fed *ApoE*^{-/-} mice.

Fig. S5. Comparison of BrdU incorporation in aorta, blood, and spleen 1 week after experimental stroke surgery.

Fig. S6. RFP⁺CD11b⁺ cell counts in blood after experimental stroke surgery.

Fig. S7. Immunological data of stroke patients.

Fig. S8. Body weight and mortality in sRAGE treatment mice after stroke.

Fig. S9. Atherosclerotic lesions in aortic valves of male and female HCD-fed *ApoE*^{-/-} mice 1 month after experimental stroke and sRAGE treatment.

Fig. S10. Lipid profile of plasma samples 1 month after experimental stroke surgery and sRAGE treatment.

Fig. S11. Flow cytometric analysis of spleen and blood 24 hours after experimental stroke with anti-HMGB1 treatment.

Fig. S12. Recombinant HMGB1 in vivo administration exacerbates atherosclerosis.

Fig. S13. Quantification of in vivo Qdot labeling of femoral bone marrow 24 hours after experimental stroke.

Fig. S14. Myeloid cell count in femoral bone marrow and brain infarct volumetry after splenectomy.

Fig. S15. Impact of β 3-adrenoreceptor blockage on HMGB1 plasma levels after experimental stroke.

Fig. S16. Impact of β 3-adrenoreceptor blockage (SR59230A), alarmin blockage (sRAGE), and combined treatment on blood immune cells in WT mice.

Fig. S17. Schematic overview of proposed mechanism of atheroprogession after stroke.

Table S1. Primer list for quantitative PCR array (mouse chemokines and receptors).

Table S2. Demographic and clinical characteristics of the study population.

Table S3. Number of (excluded/included) animals in accomplished experiments.

References (41–49)

Materials and Methods

Transient ischemia-reperfusion stroke model. Mice were anaesthetized with isoflurane delivered in a mixture of 30% O₂ and 70% N₂O. An incision was made between the ear and the eye in order to expose the temporal bone. A laser doppler probe was affixed to the skull above the middle cerebral artery (MCA) territory, and the mice were placed in supine position. A midline neck incision was made and the common carotid artery and left external carotid artery were isolated and ligated; a 2-mm silicon-coated filament (Doccol) was introduced via a small incision in the common carotid artery and inserted into the internal carotid artery, finally occluding the MCA which was confirmed by a corresponding decrease in blood flow (decrease in the laser doppler flow signal <20% of baseline value). After 60 minutes of occlusion, the animals were re-anesthetized, and the filament was removed. After recovery, the mice were kept in their home cage with facilitated access to water and food. Sham-operated mice received the same surgical procedure, except the filament was inserted and immediately removed, after 60 minutes mice were re-anesthetized. Body temperature was maintained at 37°C throughout surgery using a feedback-controlled heating pad. The overall mortality rate in this group (excluding the Sham-operated animals) was approximately 20 %. Exclusion criteria: 1. Insufficient MCA occlusion (a reduction in blood flow to >20% of the baseline value). 2. Death during the surgery. 3. Lack of brain ischemia as quantified post-mortem by histological analysis. A stroke assessment score was acquired 1 hour after reperfusion. For scoring the animal after surgical procedure a score from 0 (no stroke) to 5 (very severe stroke) based on general activity and body asymmetry was used (“modified Bederson Score”) (41).

Splenectomy. Mice were anaesthetized with isoflurane delivered in a mixture of 30% O₂ and 70% N₂O. A dorsal incision was made lateral to the spine and the abdominal cavity was entered. Blood vessels were ligated and spleen was removed by transecting the vessels distal to the ligature. Body temperature was maintained at 37°C throughout surgery using a

feedback-controlled heating pad. Mice were kept under controlled conditions until they were fully recovered from anesthesia.

Soluble mouse RAGE production. Soluble RAGE recombinant baculovirus was a kind gift from Dr. Ann-Marie Schmidt (New York University Langone Medical Center, USA). sRAGE recombinant virus was propagated in Sf21-cells and supernatant was kept at 4°C for further analysis and protein production. Low passage viral titer was determined by quantitative PCR (42). For protein production, Sf21 cells were seeded one day prior to infection with 1x10⁶ cells/mL. Cells were infected and incubated at 27°C. Three days later, supernatant (SN) was harvest, filtered and buffer exchanged to 0.1 PBS pH 6.9/50mM NaCl. sRAGE was captured by ion-exchange chromatography using a CptoS-5mL prepacked column (GE Healthcare) and eluted with 0.1xPBS, pH 6.9/600mM NaCl. Positive fractions were pooled, diluted 15-fold in 0.1PBS pH6.9/50mM NaCl and purified by ion-exchange chromatography using a ResourceS-1mL prepacked column (GE Healthcare). Positive fractions were pooled, dialyzed against PBS, pH 7.2, 10% glycerol at 4°C and stored at -80°C.

Drug & dye administration.

sRAGE: Mice received intraperitoneally three injections of sRAGE (Helmholtz), 30 min before, 24 h and 2 weeks after surgery. sRAGE was injected i.p. at a dose of 3.5 mg kg⁻¹ body weight in a final volume of 100 µl.

HMGB1: Mice received one bolus (100µg) of either anti-HMGB1 or isotype control IgG immediately after ischemia induction. The anti-HMGB1 antibody (m2G7, IgG2b) does not recognize HMGB2 and binds to the amino acids 53-63 within the box A domain of rodent and human HMGB1 (43) and was purified from hybridoma supernatant by protein G affinity chromatography. The absence of endotoxin contamination was verified by Limulus assay. Recombinant HMGB1 (rHMGB1) in fully-reduced and disulfide redox-state (HMGBiotech) was injected intraperitoneally (one bolus: 5 µg of each redox form (in total 10 µg) in a final volume of 100 µl PBS).

Bromodeoxyuridine (BrdU): BrdU (BD Pharmingen) was administered using osmotic mini-pumps implanted subcutaneously (Alzet model 1002) at a dose of 50µg/d for one week. Osmotic pumps were implanted immediately after stroke or sham surgery.

Qtracker 655: Qtracker 655 (Life technologies) was injected with a 10 µl microsyringe (Hamilton) directly into the femoral bone marrow at the corpus femoris 2 h before stroke or sham surgery at a total volume of 2 µl. Administration of sterile PBS was used as a control.

Adoptive myeloid cell transfer. Donor animals (CCR2^{RFP/+} or CCR2^{RFP/RFP}) were sacrificed and hind limbs were collected in Dulbecco's Modified Eagle Medium (DMEM). The muscle tissue was removed with 70 % ethanol in a petri dish. The bone marrow was flushed out of femur and tibia with DMEM using a syringe and the cell suspension was filtered through 40 µm cell strainers. After cells were washed and counted they were intraperitoneally injected in *ApoE*^{-/-} recipient mice (10⁷ cells per mouse) in a total volume of 200µl in saline.

Molecular MRI imaging with VCAM-1-targeted micron-sized iron oxide particles (MPIOs). MRI Experiments were carried out on a Pharmascan 7 T/12 cm system using surface coils (Bruker, Germany). Before imaging, the mice received an intravenous injection of 1 mg/kg of VCAM-1 targeted MPIOs through a tail vein catheter, as previously described (22). Thirty minutes thereafter, 3D T2*-weighted gradient echo imaging with flow compensation (GEFC, spatial resolution of 93µm x 70µm x 70µm interpolated to an isotropic resolution of 70 µm) using respiratory and cardiac gating (images were acquired during the end diastole), with TE/TR 6.2ms/~200ms and a flip angle (FA) of 20° was performed to visualize MPIOs bound to the aortic valve (acquisition time=8-15 min). During MRI, the mice were maintained under anesthesia with 2% isoflurane in 100% O₂. For image analysis, the first step was to crop the initial MRI in a 70x70 pixels picture, including the aortic valve and the surrounding blood. Then, 3D Otsu automated threshold was applied using ImageJ software and the signal void volume was computed in mm³.

Organ and tissue processing. Mice were deeply anaesthetized with ketamine (120 mg/kg) and xylazine (16 mg/kg) and venous blood was drawn via cardiac puncture of the right ventricle in 50mM EDTA (Sigma-Aldrich); the plasma was isolated by centrifugation at 3000 relative centrifugal force (rcf) for 10min and stored at -80 °C until further use. The blood pellet was resuspended in DMEM and erythrocytes were lysed using isotonic ammonium chloride buffer. Mice were then transcardially perfused with normal saline and aorta, heart, femurs and spleen were dissected. Spleen and femurs were transferred to Hank's balanced salt solution, homogenized and filtered through 40 µm cell strainers. Erythrocytes in spleens were lysed using isotonic ammonium chloride buffer.

To isolate mononuclear cells from aorta, the whole aorta was minced into small pieces and incubated in Roswell Park Memorial Institute (RPMI) medium containing 125 U/ml collagenase XI, 60 U/ml hyaluronidase I, 60 U/ml DNase I and 450 U/ml collagenase I (Sigma Aldrich) for 30min at 37 °C (44). The cell suspensions were then mechanically homogenized, filtered and washed prior to flow cytometry.

Infarct volumetry. Mice were sacrificed by over dose of ketamine-xylazine and perfused intracardially with 10 mL saline solution. Brains were removed and immediately frozen in powdered dry ice. Afterwards, brains were fixed in optimum cutting temperature compound (O.C.T., Tissue-tek) solution and 20µm coronal sections were cut on every 400µm. Sections were stained with cresyl violet and scanned at 600 dpi. Infarct area on each section was analyzed by ImageJ software (NIH). The Swanson method was applied to indirectly measure the infarct area and to correct for cortical swelling: [ischemic area] = [area of the contralateral hemisphere] - [nonischemic area of the ipsilateral hemisphere]. The total infarct volume was determined by integrating measured areas and distances between sections.

Monocyte activation assay. Splenic monocytes were isolated using CD11b⁺ magnetic-activated cell sorting (CD11b Micro beads, Miltenyi) and cultured (DMEM, 10 % FCS, 1 % Penicilin/Streptavidin) in 12-well flat-bottom plates (5x10⁵ cells per well). Purity of monocyte

Magnetic-activated cell sorting isolation was verified by flow cytometric analysis to be ≥ 95 %. Treatment with rHMGB1 (0.1 and 0.5 $\mu\text{g/ml}$), murine stroke or sham plasma (50 % in DMEM) was given in each well individually and 4 h later cells were harvested and prepared for further analysis.

In vitro murine aortic endothelium stimulation assay. Murine aortic endothelial cells (Innoprot, Ref: P10427) were seeded in fibronectin-coated 12-well flat-bottom plates (5×10^5 cells per well, Basal medium, 5 % FCS and 1 % Penicillin/Streptavidin, 1 % endothelial cell growth supplement) overnight. Cells were starved for 4 h (basal medium, 1 % Penicillin/Streptavidin) and before they received treatment (recombinant TNF- α : 20 ng/ml, plasma: 50 % in DMEM, recombinant HMGB1: 0.5 $\mu\text{g/ml}$). The plasma used to stimulate MAECs was collected from stroke- or sham-operated mice 4 h post-lesion. After a 4 h stimulation interval, cells were trypsinized, harvested, washed in PBS and stored at -20°C until further analysis.

Flow cytometry analysis. The following anti-mouse antibodies were used for cell stainings: anti-CD3 (clone: 17A2, eBioscience), anti-CD4 (clone: RM4-5, eBioscience), anti-CD45 (clone: 30-F11, eBioscience), anti-CD11b (clone: M1/70, eBioscience), anti-CD11c (clone: HL3, eBioscience), anti-Ly6C (clone: HK1.4, eBioscience), anti-Ly6G (clone: RB6-8C5, eBioscience), anti-MHC class II (clone: NIMR-4, eBioscience), anti-CCR2 (clone: FAB5538A, R&D systems), BrdU (clone: MOPC-21, BD Biosciences). Stainings were performed according to the manufacturer's protocols. Flow cytometric data was acquired on a BD FACSverse flow cytometer (BD Biosciences) and analyzed using FlowJo software (Treestar).

Oil Red O lipid staining. For whole aorta en face stainings, aortas were carefully dissected and adventitial fat was thoroughly trimmed away. Aortas then were cut open, unfolded, and pinned out on a silicon-elastomer for fixation in 4% paraformaldehyde (PFA) at 4°C overnight. The aortas then were washed for 4 h in PBS, afterwards placed in 100 % propylene

glycol for 2 min at 25 °C and finally transferred to 0.5 % Oil Red O for 3 h at 25 °C. Then aortas were washed in 85 % propylene glycol and stored in PBS until image acquisition (45). For lipid stainings of aortic valve sections, the ventricles were removed horizontally from dissected hearts, embedded in O.C.T compound (Tissue Tek) and consecutively cryosectioned. Sections were dried, post-fixed in 4 % PFA and stained after dehydration for 1 h in 0.5 % Oil Red O solution at 37 °C. Finally, sections were counterstained for nuclei with Mayer's Hematoxylin, air dried and mounted with pre-warmed gelatin (45). For lipid staining of the common carotid artery branches, the carotid bifurcation area was dissected and embedded in OCT. compound. After consecutive sectioning, lipid depositions were stained with the same Oil Red O staining protocol as stated above.

Quantification of cap thickness and plaque rupture. Aortic valve sections stained with Oil Red O and Hematoxylin were microphotographed and cap thickness was assessed. Three to five measurements representing the thinnest part of the cap were averaged for each plaque (46). Acute plaque rupture was accepted when a visible defect in the cap was accompanied by intrusion of erythrocytes in the plaque. In some animals, 1 or more buried fibrous caps were seen within the body of plaque which were also counted as a plaque rupture (16).

MMP 2 and 9 *in situ* zymography of aortic valve sections. DQ-gelatin (D12054, Invitrogen) was dissolved in reaction buffer (50 mM Tris-HCl, 150 mM NaCl, 5 mM CaCl₂, 200 mM sodium azide, pH 7.6). Cryosections were incubated for 3 h at 37 °C with the gelatin-containing reaction buffer. Negative control sections were pre-incubated for 1 h with the MMP-inhibitor 1,10-Phenathroline (Sigma). Nuclei were stained with DAPI. MMP activity was detected on an Axio Observer Z1 microscope with 10x magnification and a Fluorescein isothiocyanate (FITC) filter (Carl Zeiss). Data were expressed as MMP+ area(μm²) and normalized MMP intensity (Normalized MMP intensity = Integrated Density – (Selected valve Area x Background mean fluorescence)).

Tyrosine hydroxylase (TH) stainings. Dissected femurs (see above) were decalcified in 0,4 M ethylenediaminetetraacetic acid (EDTA, pH 7.4) for 72 hours. Femurs then were embedded in OCT compound (Tissue Tek) and consecutively sectioned. Sections were blocked with 10 % goat serum and 1 % bovine serum albumin (BSA) for 2 h. After washing with 0,025 % Triton X-100 in TBS, sections were incubated with an antibody against TH (rabbit, abcam) overnight at 4 °C. After washing, sections were then incubated with secondary antibody against rabbit (alexa-647, goat, DAKO) for 90 min at room temperature. Nuclei were stained with DAPI. Pictures were acquired with a confocal microscope at 40x magnification (LSM 880 Carl Zeiss).

Enzyme linked immunosorbent assay. HMGB1 levels were measured from diluted plasma samples (1:10) using a commercial assay kit according to the manufacturer's instructions (IBL international, Hamburg). For CCL-2 levels diluted samples (1:10) were measured using an ELISA kit according to a standard protocol (eBioscience).

Quantitative real time PCR (RT-PCR). Total RNA was purified from aorta, spleen, murine aortic endothelial cells (MAECs) and isolated monocytes using a RNeasy Mini Kit (Qiagen). Equal amount of RNA from each sample was used for cDNA synthesis using High Capacity cDNA Reverse Transcription Kit (Applied Biosystems). The quantitative expression of different cytokines was measured by quantitative real-time PCR with the LightCycler 480 II (Roche) and RT² qPCR Primer Assays and SYBR Green ROX qPCR Mastermix (Qiagen).

Primer sequences:

IL-1 β : forward '5-ACAGATGAAGTGCTCCTTCCA-3', reverse '5-GTCGGAGATTCGTAGCTGGAT-3'

IL-6: forward '5-CAGTTGCCTTCTTGGGACTGA-3', reverse '5-GGGAGTGGTATCCTCTGTGAAGTCT-3'

TNF- α : forward 5'-CAT CTT CTC AAA ATT CGA GTG ACA A-3', reverse 5'-TGG GAG TAG ACA AGG TAC AAC CC-3'

IFN- γ : forward 5'-TGGCATAGATGTGGAAGAAAAGAG-3', reverse 5'-
TGCAGGATTTTCATGTCACCAT-3'

ICAM-1: forward 5'-CAATTTCTCATGCCGCACAG-3', reverse 5'-
AGCTGGAAGATCGAAAGTCCG-3'

VCAM-1: forward 5'-TGAACCCAAACAGAGGCAGAGT-3', reverse 5'-
GGTATCCCATCACTTGAGCAGG-3'

RAGE: forward 5'-GGACCCTTAGCTGGCACTTAGA-3', reverse 5'-
GAGTCCCGTCTCAGGGTGTCT-3'

PPIA: forward '5'-ACGCCACTGTCGCTTTTC-3', reverse '5'-
ACCCGACCTCGAAGGAGA-3'

GAPDH: forward 5'-TGACGTGCCGCCTGGAGAAA-3', reverse 5'-
AGTGTAGCCCAAGATGCCCTTCAG-3'

RT-PCR array. The RT² PreAMP cDNA synthesis Kit (Qiagen) was used for the cDNA synthesis and RT² Profiler PCR Array for chemokines and chemokine receptors (PAMM-022Z, Qiagen) was measured in a Roche LightCycler 480. Finally, data was analyzed with RT² Profiler PCR Array Data analysis software (version3.5) from SABiosciences.

Quantification of patient infarct volumes. Infarct volumes were quantified on images from diagnostic scans, either computed tomography or magnetic resonance imaging (diffusion-weighted, T2 or fluid-attenuated inversion recovery). The modality and image with the largest infarct size was used for volumetry. Trained raters segmented infarcts manually slice-by-slice. The inter-rater reliability for this procedure showed an intraclass correlation coefficient of 0.993.

Analysis of HMGB1 isoforms by electrospray ionization liquid chromatography tandem mass spectrometry (ESI-LC-MS/MS). Samples were pre-cleared with 50 μ l protein G-Sepharose beads for 1h at 4°C and HMGB1 present was immunoprecipitated with 5 μ g of rabbit anti-HMGB1 (ab18256) for 16 h at 4°C as previously described (47). For the analysis

of HMGB1 post translational modifications, free thiol groups within HMGB1 were alkylated for 90 min with 10 mM iodoacetamide at 4°C. Cysteine residues in disulfide bonds were then reduced with 30 mM dithiothreitol at 4°C for 1 h followed by alkylation of newly exposed thiol groups with 90 mM NEM at 4°C for 10 min as previously described (33, 48). Samples were subjected to trypsin (Promega) or GluC (New England Biolabs) digestion according to manufacturer's instructions and de-salted using C18 zip-tips (Millipore). Characterization of post translational modifications within HMGB1 were determined as described previously using an AB Sciex QTRAP 5500 (Sciex Inc.) equipped with a NanoSpray II source by in-line liquid chromatography using a U3000 HPLC System (Dionex), connected to a 180 µm x 20 mm nanoAcquity UPLC C18 trap column and a 75 µm x 15 cm nanoAcquity UPLC BEH130 C18 column (Waters) via reducing unions. A gradient from 0.05% TFA (v/v) to 50% ACN/0.08% TFA (v/v) in 40 min was applied at a flow rate of 200 nL/min (49). The ion spray potential was set to 2,200-3,500 V, the nebulizer gas to 19 L/min and the interface heater to 150°C. Accurate mass and whole protein electrospray ionisation (ESI) mass spectrometry is determine as previously described using a AB Sciex TripleToF 5600+ system (49).

Figure S2

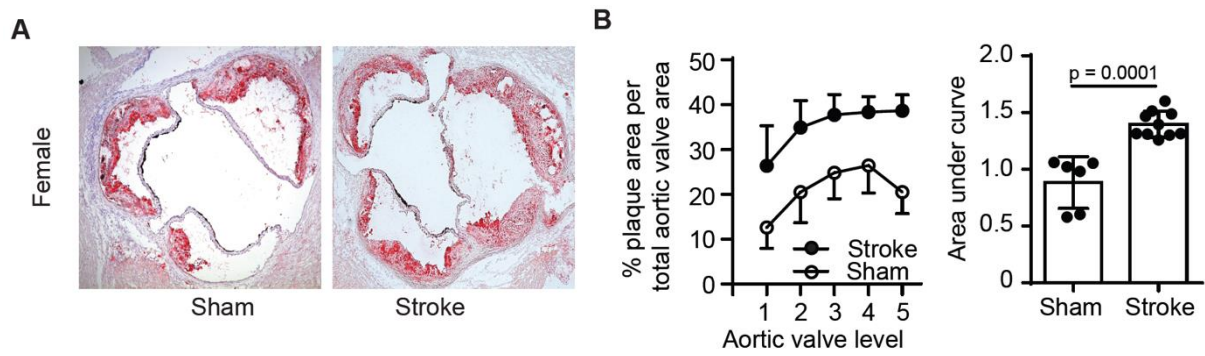


Figure S2. Exacerbation of atherosclerotic lesions in aortic valves of male and female HCD-fed *ApoE*^{-/-} mice 1 month after fMCAo surgery. (A) Representative images of Oil Red O aortic valve quantification of female HCD-fed *ApoE*^{-/-} mice one month after stroke or sham surgery. (B) Plaque area quantification of 5 consecutive levels in aortic valves (left) and area under curve (AUC, right) analysis in stroke and sham-operated mice one month after surgery (U Test, 8-10 per group). All data in panel B are shown as mean with error bars indicating s.d.

Figure S3

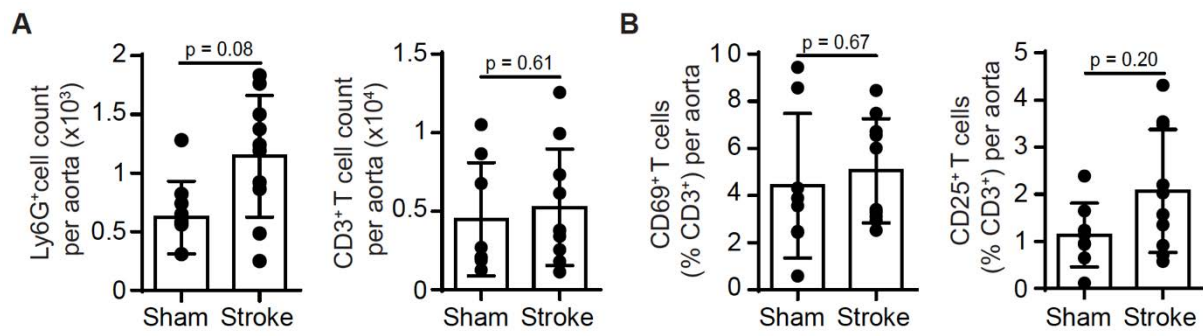


Figure S3. Immune cell counts in aorta of HCD-fed *ApoE*^{-/-} mice 1 month after experimental stroke. (A) CD45⁺Ly6G⁺ granulocytes (left) and CD45⁺CD3⁺ T cells (right) cell counts after sham or stroke surgery. (B) Percentage of CD69⁺ (left) and CD25⁺ (right) T cell subsets after sham or stroke surgery. (U Test, n= 8-10 per group).

Figure S4

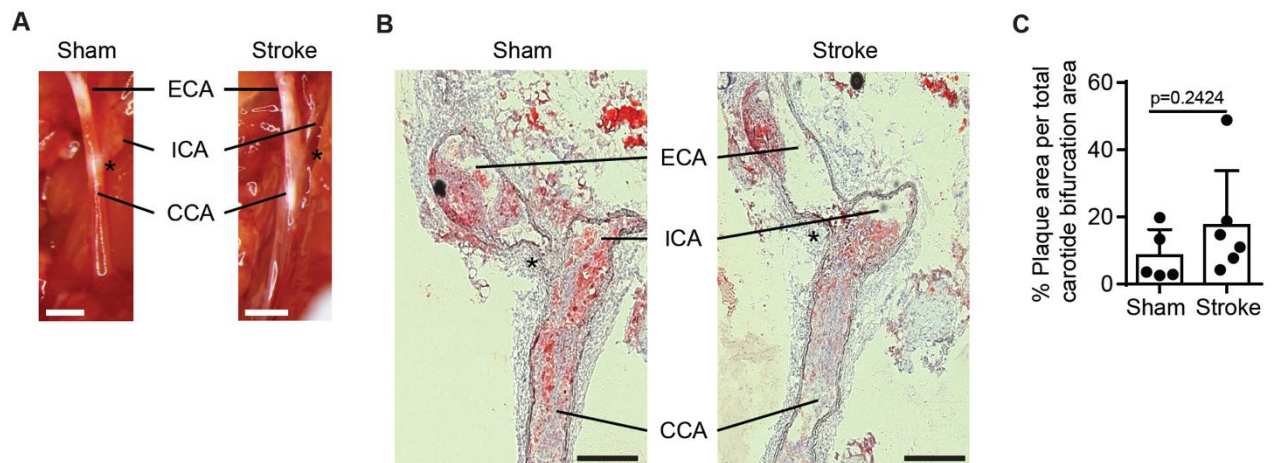


Figure S4. Analysis of atherosclerotic plaque load at the common carotid artery bifurcation in HCD-fed *ApoE*^{-/-} mice. (A) Representative microphotographs of the common carotid artery bifurcation on the contralateral side 7 days after stroke or sham surgery (scale bar = 1mm, * indicates bifurcation). (B) Representative Oil Red O stained longitudinal common carotid artery bifurcation sections (scale bar = 500 μ m, * indicates bifurcation). (C) Quantification of Oil Red O+ plaque load in the contralateral common carotid artery lumen 7 days after stroke or sham surgery (U Test, n= 5-6 per group). CCA = common carotid artery, ICA = internal carotid artery, ECA = external carotid artery.

Figure S5

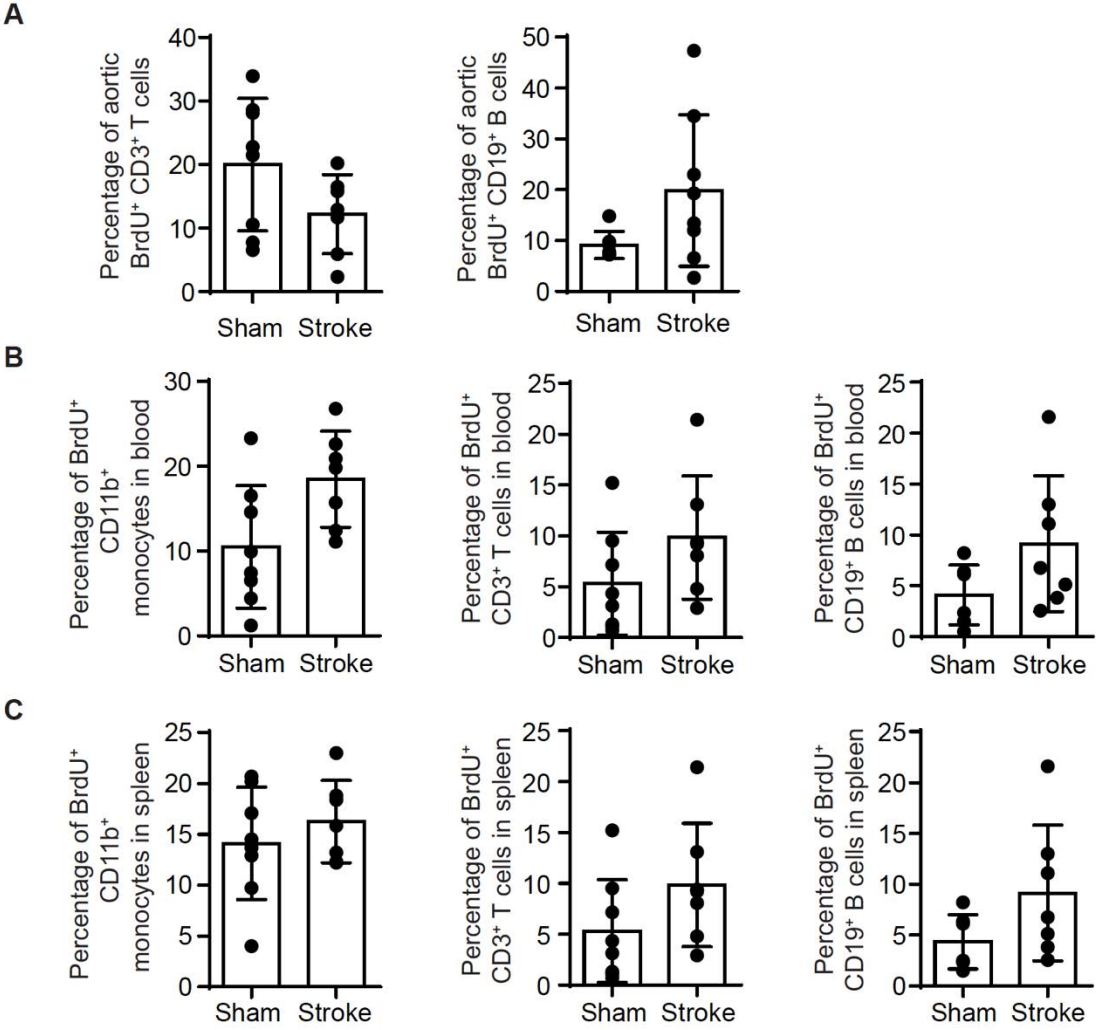
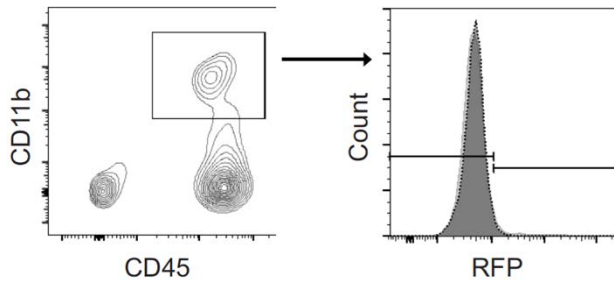


Figure S5. Comparison of BrdU incorporation in aorta, blood, and spleen 1 week after experimental stroke surgery. (A) Percentage of BrdU⁺ CD3⁺ T cells (left) and BrdU⁺ CD19⁺ B cells in aorta after stroke or sham surgery. (B, C) Percentage of BrdU⁺ cells in blood (B) and spleen (C) after experimental stroke or sham surgery (U Test, n= 6-8 mice per group). All bar graphs are shown as mean ± s.d.

Figure S6

A



B

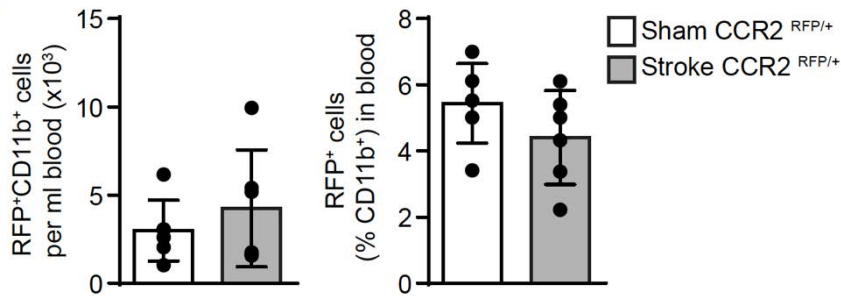


Figure S6. RFP⁺CD11b⁺ cell counts in blood after experimental stroke surgery. HCD-fed ApoE^{-/-} mice underwent sham or stroke surgery received CCR2RFP/+ bone marrow cell (BMC) transplantation (10⁷ cells) immediately after surgery. One week later mice were sacrificed and blood analyzed. **(A)** Flow cytometric gating strategy to analyze RFP⁺CD11b⁺ cells in blood. **(B)** Quantification of total RFP⁺CD11b⁺ cell counts in blood one week after sham or stroke surgery (left). Percentage of RFP⁺CD11b⁺ cells in blood one week after sham or stroke surgery (right, U Test, n= 5-6 mice per group). All bar graphs are shown as mean ± s.d.

Figure S7

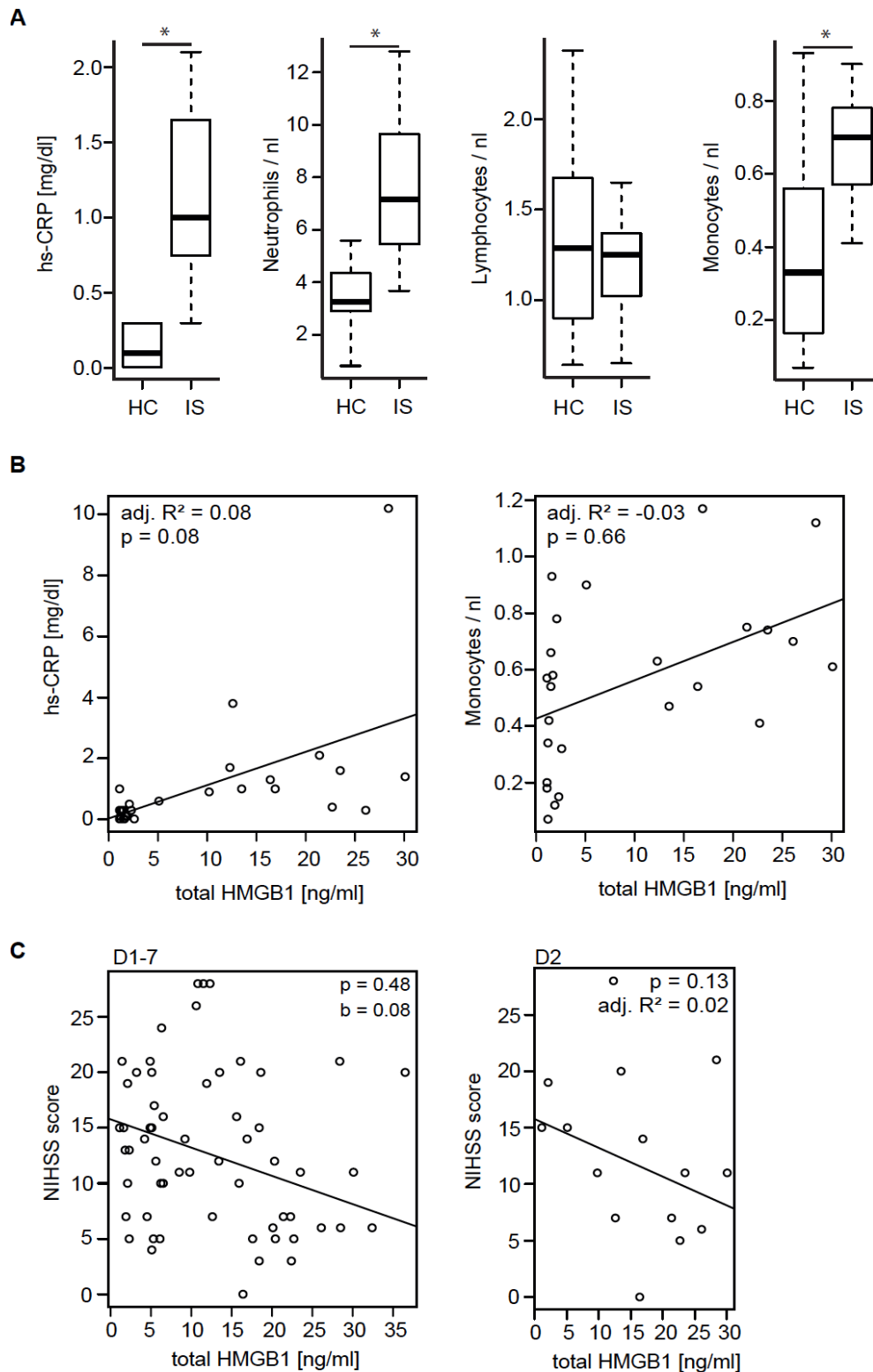


Figure S7. Immunological data of stroke patients. (A) Comparison of hs-CRP and leukocyte subpopulations between HCs and patients with IS at day 2 (Wilcoxon rank sum test) (B) Regression of total HMGB1 levels with hs-CRP or monocytes/nl of HCs and IS patients at day 2 after stroke (Linear regression analysis with adjustment for groups). (C) Regression analysis of NIHSS scores and total HMGB1 levels in patients with IS from admission to day 7 after stroke (Linear mixed model with day as random effect). Abbreviations: NIHSS, National Institute of Health stroke scale; IS, ischemic stroke.

Figure S8

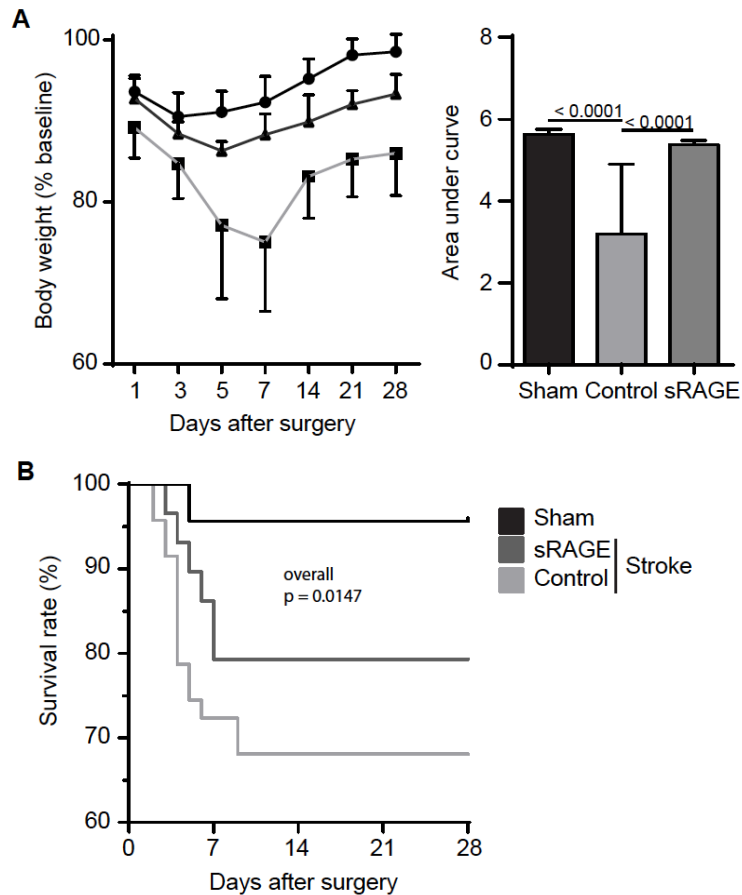


Figure S8. Body weight and mortality in sRAGE treatment mice after stroke. (A) Body weight curves (left, indicated as % body weight to individual baseline before stroke) after sham and stroke surgery with vehicle or sRAGE treatment. Area under curve analysis (right) for statistical analysis of indicated groups (U Test, $n = 10-15$ mice per group, graphs shown as mean \pm s.d.). (B) Kaplan-Meier curves of post-stroke survival within one month after stroke in vehicle or sRAGE treated and sham-operated mice (Comparison of differences between curves by Mantel-Cox Test, $n = 28-47$).

Figure S9

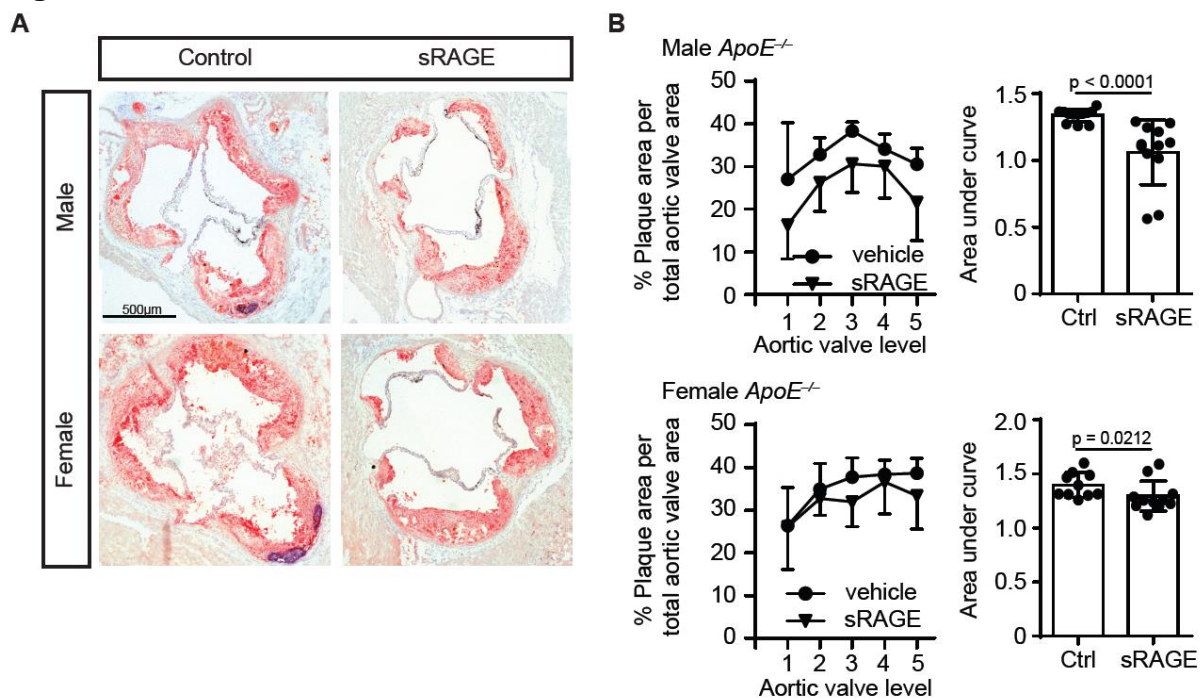


Figure S9. Atherosclerotic lesions in aortic valves of male and female HCD-fed $ApoE^{-/-}$ mice 1 month after experimental stroke and sRAGE treatment. (A) Representative images of Oil Red O aortic valve sections of male and female HCD-fed $ApoE^{-/-}$ mice with vehicle or sRAGE treatment 4 weeks after stroke surgery. (B) Plaque area quantification of 5 consecutive levels in aortic valves and area under curve (AUC) analysis of stroke (\pm sRAGE) for male and female mice (U Test, $n = 8-10$ mice per group). All graphs are shown as mean with error bars indicating s.d.

Figure S10

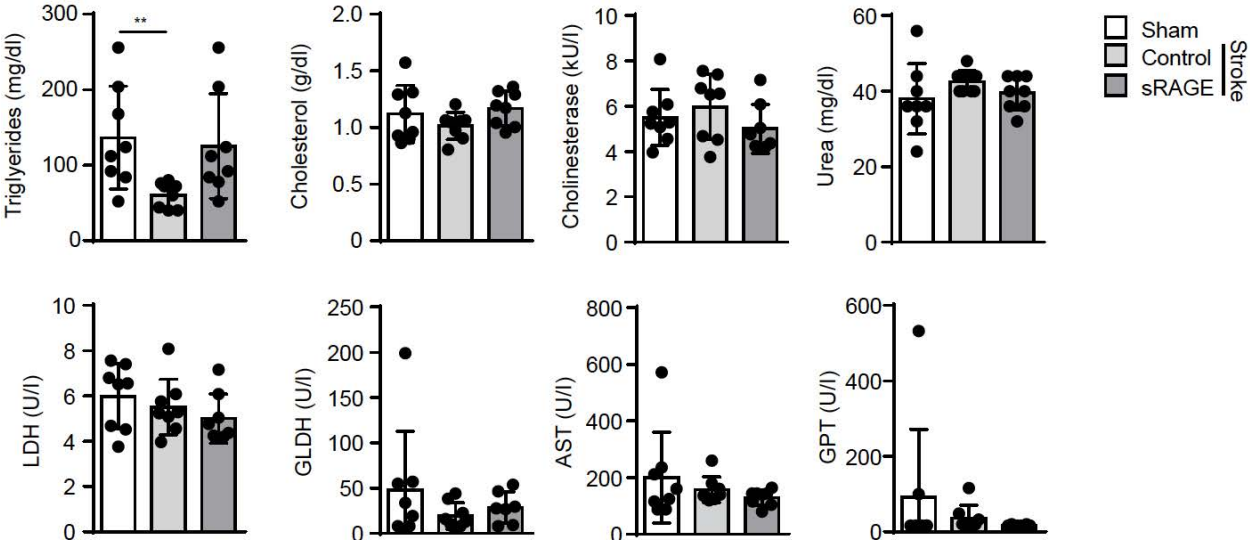


Figure S10. Lipid profile of plasma samples 1 month after experimental stroke surgery and sRAGE treatment. Triglycerides, cholesterol, cholinesterase, urea, lactate dehydrogenase (LDH), glutamate dehydrogenase (GLDH), aspartate aminotransferase (AST) and glutamic pyruvic transaminase (GPT) concentrations after experimental stroke or sham surgery (\pm sRAGE) in HCD-fed ApoE^{-/-} mice. (One way-ANOVA; n= 8-9 mice per group). All bar graphs are shown as mean \pm s.d.

Figure S11

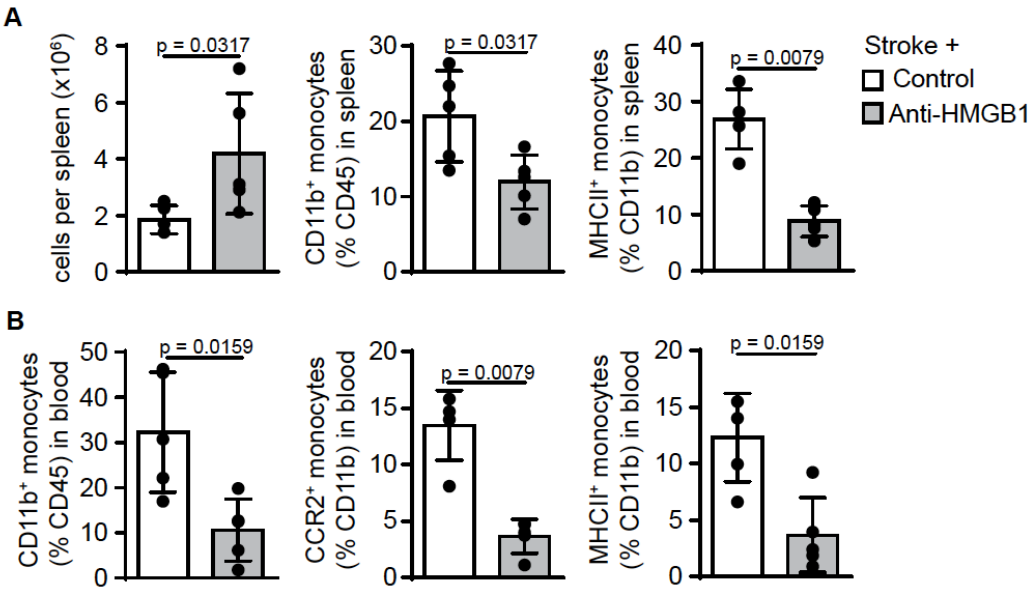


Figure S11. Flow cytometric analysis of spleen and blood 24 hours after experimental stroke with anti-HMGB1 treatment. (A) Flow cytometric analysis of WT mice treated with IgG control or HMGB1-specific monoclonal antibodies (anti-HMGB1) 24 h after stroke surgery. Whole CD45⁺ spleen cell counts (left) and percentages of CD11b⁺ (middle) and CD11b⁺MHCII⁺ (right) cells were measured. **(B)** Flow cytometric analysis of CD45⁺CD11b⁺ (left), CD11b⁺CCR2⁺ (middle) and CD11b⁺MHCII⁺ (right) cell percentages from blood 24 h after stroke ± anti-HMGB1 treatment (U Test, n= 5-8 mice per group). All bar graphs are shown as mean ± s.d.

Figure S12

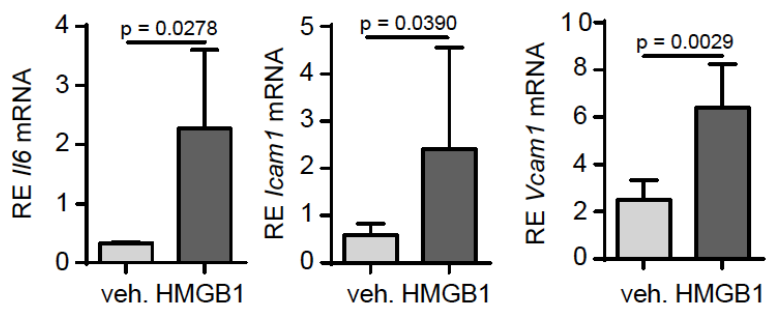


Figure S12. Recombinant HMGB1 in vivo administration exacerbates atherosclerosis. HCD-fed ApoE^{-/-} mice received i.p. injection of a single bolus of 10 μ g rHMGB1. After one week mice were sacrificed and aorta and aortic valve were analyzed. Expression of *Il-6* (left), *Icam-1* (middle) and *Vcam-1* (right) (RE, relative expression) was analyzed from aorta lysates (U Test, n= 5 per group). All graphs are shown as mean \pm s.d.

Figure S13

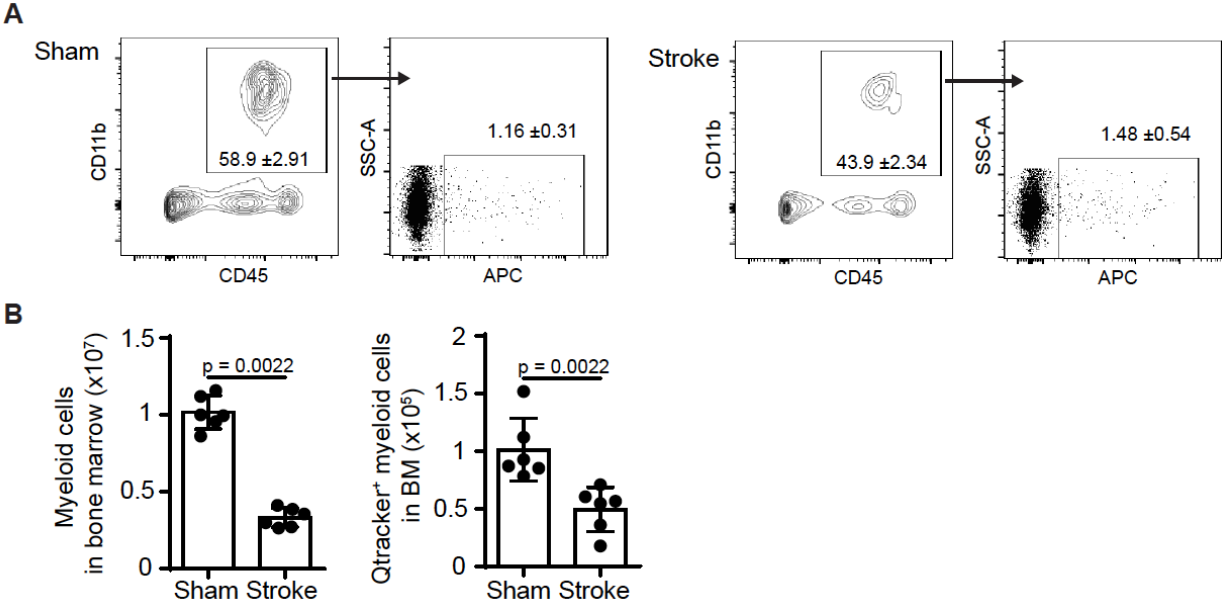


Figure S13. Quantification of in vivo Qdot labeling of femoral bone marrow 24 hours after experimental stroke. WT mice received Qdot administration in the femoral bone marrow 2h before sham or stroke surgery and were sacrificed 24 h later. (A) Representative gating strategy for CD45⁺CD11b⁺ monocytes and Qdot⁺ monocytes in femoral bone marrow after stroke or sham surgery. (B) Quantification of myeloid cells (left) and Qdot⁺ monocytes (right) in femoral bone marrow (U Test, n= 6 per group). All graphs are shown as mean \pm s.d.

Figure S14

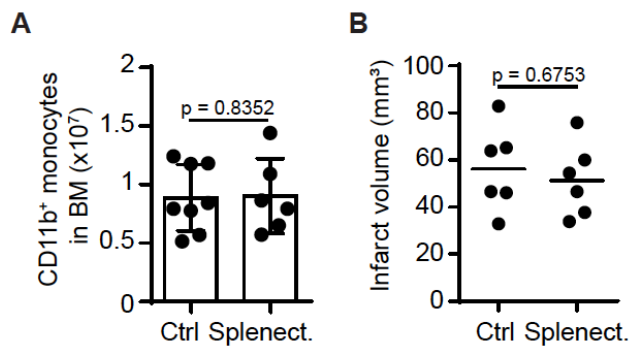


Figure S14. Myeloid cell count in femoral bone marrow and brain infarct volumetry after splenectomy. Spleen of HCD-fed ApoE^{-/-} mice were removed surgically or sham surgery was performed before experimental stroke was induced. One week later mice were sacrificed and analyzed for myeloid cell counts and infarct volumetry. **(A)** Flow cytometric analysis of bone marrow from either splenectomized or sham operated mice after experimental stroke (U Test, n= 6-8 per group). **(B)** Cresyl violet histology of infarcted brains from stroked mice with either splenectomy or sham surgery (U Test, n=6 per group). All graphs shown as mean ± s.d.

Figure S15

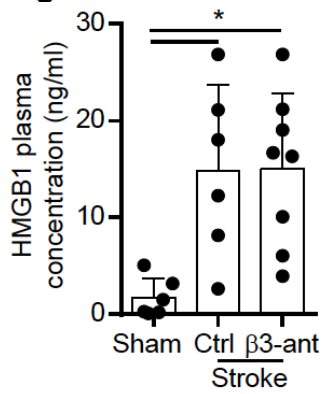


Figure S15. Impact of β 3-adrenoreceptor blockage on HMGB1 plasma levels after experimental stroke. HMGB1 plasma concentrations were measured by ELISA in sham and stroke-operated (\pm SR59230A treatment) HCD-fed ApoE^{-/-} mice 7d after surgery (H Test, n= 6-8 per group). Graph is shown as mean \pm s.d. (* = p value <0.05).

Figure S16

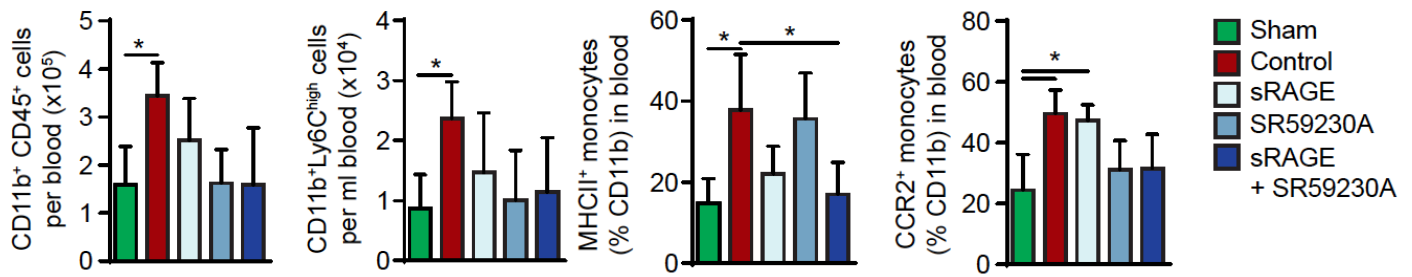


Figure S16. Impact of β 3-adrenoreceptor blockage (SR59230A), alarmin blockage (sRAGE), and combined treatment on blood immune cells in WT mice. WT mice received either SR59230A, sRAGE, both combined or control treatment immediately after stroke and blood was analyzed by flow cytometry 24 h later for total myeloid (CD45⁺CD11b⁺), CD11b⁺Ly6C^{high}, MHCII and CCR2 expressing cells (H Test, n= 6-8 per group). All graphs are shown as mean \pm s.d. (*: p < 0.05)

Figure S17

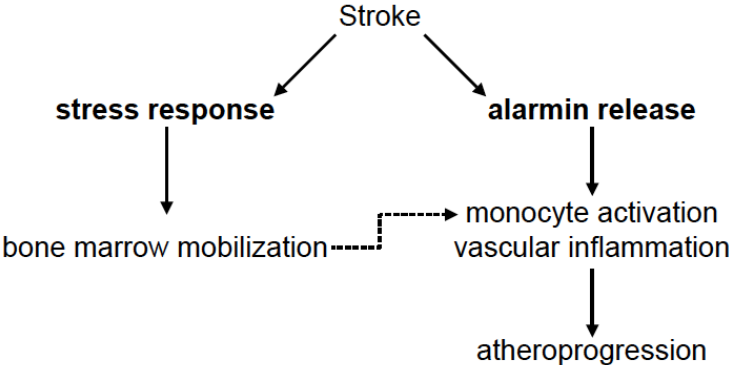


Figure S17. Schematic overview of proposed mechanism of atheroprotection after stroke.

Table S1. Primer list for quantitative PCR array (mouse chemokines and receptors).

Symbol	Description
C5ar1	Complement component 5a receptor 1
Ackr2	Chemokine binding protein 2
Ccl1	Chemokine (C-C motif) ligand 1
Ccl11	Chemokine (C-C motif) ligand 11
Ccl12	Chemokine (C-C motif) ligand 12
Ccl17	Chemokine (C-C motif) ligand 17
Ccl19	Chemokine (C-C motif) ligand 19
Ccl2	Chemokine (C-C motif) ligand 2
Ccl20	Chemokine (C-C motif) ligand 20
Ccl22	Chemokine (C-C motif) ligand 22
Ccl24	Chemokine (C-C motif) ligand 24
Ccl25	Chemokine (C-C motif) ligand 25
Ccl26	Chemokine (C-C motif) ligand 26
Ccl28	Chemokine (C-C motif) ligand 28
Ccl3	Chemokine (C-C motif) ligand 3
Ccl4	Chemokine (C-C motif) ligand 4
Ccl5	Chemokine (C-C motif) ligand 5
Ccl6	Chemokine (C-C motif) ligand 6
Ccl7	Chemokine (C-C motif) ligand 7
Ccl8	Chemokine (C-C motif) ligand 8
Ccl9	Chemokine (C-C motif) ligand 9
Ccr1	Chemokine (C-C motif) receptor 1
Ccr10	Chemokine (C-C motif) receptor 10
Ccr11	Chemokine (C-C motif) receptor 1-like 1
Ccr2	Chemokine (C-C motif) receptor 2
Ccr3	Chemokine (C-C motif) receptor 3
Ccr4	Chemokine (C-C motif) receptor 4
Ccr5	Chemokine (C-C motif) receptor 5
Ccr6	Chemokine (C-C motif) receptor 6
Ccr7	Chemokine (C-C motif) receptor 7
Ccr8	Chemokine (C-C motif) receptor 8
Ccr9	Chemokine (C-C motif) receptor 9
Ackr4	Chemokine (C-C motif) receptor-like 1
Ccr12	Chemokine (C-C motif) receptor-like 2
Cmklr1	Chemokine-like receptor 1
Cmtm2a	CKLF-like MARVEL transmembrane domain containing 2A
Cmtm3	CKLF-like MARVEL transmembrane domain containing 3
Cmtm4	CKLF-like MARVEL transmembrane domain containing 4
Cmtm5	CKLF-like MARVEL transmembrane domain containing 5
Cmtm6	CKLF-like MARVEL transmembrane domain containing 6
Cx3cl1	Chemokine (C-X3-C motif) ligand 1
Cx3cr1	Chemokine (C-X3-C) receptor 1
Cxcl1	Chemokine (C-X-C motif) ligand 1
Cxcl10	Chemokine (C-X-C motif) ligand 10
Cxcl11	Chemokine (C-X-C motif) ligand 11
Cxcl12	Chemokine (C-X-C motif) ligand 12
Cxcl13	Chemokine (C-X-C motif) ligand 13
Cxcl14	Chemokine (C-X-C motif) ligand 14
Cxcl15	Chemokine (C-X-C motif) ligand 15
Cxcl16	Chemokine (C-X-C motif) ligand 16
Cxcl2	Chemokine (C-X-C motif) ligand 2
Cxcl3	Chemokine (C-X-C motif) ligand 3
Cxcl5	Chemokine (C-X-C motif) ligand 5
Cxcl9	Chemokine (C-X-C motif) ligand 9
Cxcr1	Chemokine (C-X-C motif) receptor 1
Cxcr2	Chemokine (C-X-C motif) receptor 2
Cxcr3	Chemokine (C-X-C motif) receptor 3

Cxcr4	Chemokine (C-X-C motif) receptor 4
Cxcr5	Chemokine (C-X-C motif) receptor 5
Cxcr6	Chemokine (C-X-C motif) receptor 6
Ackr3	Chemokine (C-X-C motif) receptor 7
Ackr1	Duffy blood group, chemokine receptor
Fpr1	Formyl peptide receptor 1
Gpr17	G protein-coupled receptor 17
Hif1a	Hypoxia inducible factor 1, alpha subunit
Ifng	Interferon gamma
Il16	Interleukin 16
Il1b	Interleukin 1 beta
Il4	Interleukin 4
Il6	Interleukin 6
Itgam	Integrin alpha M
Itgb2	Integrin beta 2
Mapk1	Mitogen-activated protein kinase 1
Mapk14	Mitogen-activated protein kinase 14
Pf4	Platelet factor 4
Ppbp	Pro-platelet basic protein
Slit2	Slit homolog 2 (Drosophila)
Tgfb1	Transforming growth factor, beta 1
Tlr2	Toll-like receptor 2
Tlr4	Toll-like receptor 4
Tnf	Tumor necrosis factor
Tymp	Thymidine phosphorylase
Xcl1	Chemokine (C motif) ligand 1
Xcr1	Chemokine (C motif) receptor 1
Actb	Actin, beta
B2m	Beta-2 microglobulin
Gapdh	Glyceraldehyde-3-phosphate dehydrogenase
Gusb	Glucuronidase, beta
Hsp90ab1	Heat shock protein 90 alpha (cytosolic), class B member 1

Table S2. Demographic and clinical characteristics of the study population.

Characteristics	Stroke	Control
Demographic characteristics		
Total, n	18	12
Age, mean (SD) [years]	72.7 (14.3)	72.1 (5.9)
Female, n (%)	7 (38.9)	8 (66.7)
Vascular risk factors, n (%)		
Hypertension	15 (83.3)	4 (33.3)
Smoking history	8 (47.1)	3 (25)
Hypercholesterolemia	2 (11.8)	1 (8.3)
Obesity	4 (26.7)	1 (8.3)
Diabetes mellitus	1 (5.6)	0 (0)
Previous TIA/stroke/MI	5 (27.8)	0 (0)
ΔT , mean (SD) [hours]	5.5 (5.6)	n/a
Infarct volumes, mean (SD) [ml]	74.4 (48.0)	n/a

SD, standard deviation; TIA, transient ischemic attack; MI, myocardial infarction; ΔT , time from symptom onset until hospital arrival; n/a, not available.

5 REFERENCES

1. Strong, K., Mathers, C. & Bonita, R. Preventing stroke: saving lives around the world. *The Lancet. Neurology* **6**, 182-187 (2007).
2. Benjamin, E.J., *et al.* Heart Disease and Stroke Statistics-2017 Update: A Report From the American Heart Association. *Circulation* **135**, e146-e603 (2017).
3. Lopez, A.D., Mathers, C.D., Ezzati, M., Jamison, D.T. & Murray, C.J. Global and regional burden of disease and risk factors, 2001: systematic analysis of population health data. *Lancet* **367**, 1747-1757 (2006).
4. Feigin, V.L., *et al.* Global and regional burden of stroke during 1990-2010: findings from the Global Burden of Disease Study 2010. *Lancet* **383**, 245-254 (2014).
5. Murray, C.J., *et al.* Disability-adjusted life years (DALYs) for 291 diseases and injuries in 21 regions, 1990-2010: a systematic analysis for the Global Burden of Disease Study 2010. *Lancet* **380**, 2197-2223 (2012).
6. Olesen, J., *et al.* The economic cost of brain disorders in Europe. *European journal of neurology* **19**, 155-162 (2012).
7. Feng, W., Hendry, R.M. & Adams, R.J. Risk of recurrent stroke, myocardial infarction, or death in hospitalized stroke patients. *Neurology* **74**, 588-593 (2010).
8. Lovett, J.K., Coull, A.J. & Rothwell, P.M. Early risk of recurrence by subtype of ischemic stroke in population-based incidence studies. *Neurology* **62**, 569-573 (2004).
9. Lee, B.I., Nam, H.S., Heo, J.H., Kim, D.I. & Yonsei Stroke, T. Yonsei Stroke Registry. Analysis of 1,000 patients with acute cerebral infarctions. *Cerebrovascular diseases* **12**, 145-151 (2001).
10. Roth, S. & Liesz, A. Stroke research at the crossroads - where are we heading? *Swiss medical weekly* **146**, w14329 (2016).
11. Roger, V.L., *et al.* Heart disease and stroke statistics--2012 update: a report from the American Heart Association. *Circulation* **125**, e2-e220 (2012).
12. Adams, H.P., Jr., *et al.* Classification of subtype of acute ischemic stroke. Definitions for use in a multicenter clinical trial. TOAST. Trial of Org 10172 in Acute Stroke Treatment. *Stroke* **24**, 35-41 (1993).
13. National Institute of Neurological, D. & Stroke rt, P.A.S.S.G. Tissue plasminogen activator for acute ischemic stroke. *The New England journal of medicine* **333**, 1581-1587 (1995).
14. Jovin, T.G., *et al.* Thrombectomy within 8 hours after symptom onset in ischemic stroke. *The New England journal of medicine* **372**, 2296-2306 (2015).
15. Saver, J.L., *et al.* Stent-retriever thrombectomy after intravenous t-PA vs. t-PA alone in stroke. *The New England journal of medicine* **372**, 2285-2295 (2015).
16. Jauch, E.C., *et al.* Guidelines for the early management of patients with acute ischemic stroke: a guideline for healthcare professionals from the American Heart Association/American Stroke Association. *Stroke* **44**, 870-947 (2013).
17. O'Collins, V.E., *et al.* 1,026 experimental treatments in acute stroke. *Annals of neurology* **59**, 467-477 (2006).
18. van der Worp, H.B., *et al.* Can animal models of disease reliably inform human studies? *PLoS medicine* **7**, e1000245 (2010).
19. Muhammad, S., *et al.* The HMGB1 receptor RAGE mediates ischemic brain damage. *The Journal of neuroscience : the official journal of the Society for Neuroscience* **28**, 12023-12031 (2008).
20. Iadecola, C. & Anrather, J. The immunology of stroke: from mechanisms to translation. *Nature medicine* **17**, 796-808 (2011).
21. Singh, V., Roth, S., Veltkamp, R. & Liesz, A. HMGB1 as a Key Mediator of Immune Mechanisms in Ischemic Stroke. *Antioxidants & redox signaling* **24**, 635-651 (2016).
22. Liesz, A., *et al.* Inhibition of lymphocyte trafficking shields the brain against deleterious neuroinflammation after stroke. *Brain : a journal of neurology* **134**, 704-720 (2011).

23. Andersson, U., Erlandsson-Harris, H., Yang, H. & Tracey, K.J. HMGB1 as a DNA-binding cytokine. *Journal of leukocyte biology* **72**, 1084-1091 (2002).
24. Bustin, M. Regulation of DNA-dependent activities by the functional motifs of the high-mobility-group chromosomal proteins. *Molecular and cellular biology* **19**, 5237-5246 (1999).
25. Schiraldi, M., *et al.* HMGB1 promotes recruitment of inflammatory cells to damaged tissues by forming a complex with CXCL12 and signaling via CXCR4. *The Journal of experimental medicine* **209**, 551-563 (2012).
26. Yang, H., *et al.* Redox modification of cysteine residues regulates the cytokine activity of high mobility group box-1 (HMGB1). *Molecular medicine* **18**, 250-259 (2012).
27. Kazama, H., *et al.* Induction of immunological tolerance by apoptotic cells requires caspase-dependent oxidation of high-mobility group box-1 protein. *Immunity* **29**, 21-32 (2008).
28. Liesz, A., *et al.* DAMP signaling is a key pathway inducing immune modulation after brain injury. *The Journal of neuroscience : the official journal of the Society for Neuroscience* **35**, 583-598 (2015).
29. Roth, S., *et al.* Brain-released alarmins and stress response synergize in accelerating atherosclerosis progression after stroke. *Science Translational Medicine* **10**(2018).
30. Andersson, U. & Tracey, K.J. HMGB1 Is a Therapeutic Target for Sterile Inflammation and Infection. *Annu Rev Immunol* **29**, 139-162 (2011).
31. Courties, G., *et al.* Ischemic stroke activates hematopoietic bone marrow stem cells. *Circulation research* **116**, 407-417 (2015).
32. Offner, H., *et al.* Experimental stroke induces massive, rapid activation of the peripheral immune system. *J Cereb Blood Flow Metab* **26**, 654-665 (2006).
33. Prass, K., *et al.* Stroke-induced immunodeficiency promotes spontaneous bacterial infections and is mediated by sympathetic activation reversal by poststroke T helper cell type 1-like immunostimulation. *J Exp Med* **198**, 725-736 (2003).
34. Aslanyan, S., *et al.* Pneumonia and urinary tract infection after acute ischaemic stroke: a tertiary analysis of the GAIN International trial. *European journal of neurology* **11**, 49-53 (2004).
35. Liesz, A., *et al.* Stress mediators and immune dysfunction in patients with acute cerebrovascular diseases. *PLoS One* **8**, e74839 (2013).
36. Schulze, J., *et al.* Severe stroke induces long-lasting alterations of high-mobility group box 1. *Stroke* **44**, 246-248 (2013).
37. Chen, Y.C., *et al.* A novel mouse model of atherosclerotic plaque instability for drug testing and mechanistic/therapeutic discoveries using gene and microRNA expression profiling. *Circulation research* **113**, 252-265 (2013).
38. Weber, C. & Noels, H. Atherosclerosis: current pathogenesis and therapeutic options. *Nature medicine* **17**, 1410-1422 (2011).
39. Kwon, G.P., Schroeder, J.L., Amar, M.J., Remaley, A.T. & Balaban, R.S. Contribution of macromolecular structure to the retention of low-density lipoprotein at arterial branch points. *Circulation* **117**, 2919-2927 (2008).
40. Lusis, A.J. Atherosclerosis. *Nature* **407**, 233-241 (2000).
41. Chen, M., Masaki, T. & Sawamura, T. LOX-1, the receptor for oxidized low-density lipoprotein identified from endothelial cells: implications in endothelial dysfunction and atherosclerosis. *Pharmacology & therapeutics* **95**, 89-100 (2002).
42. Libby, P. Inflammation in atherosclerosis. *Nature* **420**, 868-874 (2002).
43. Hansson, G.K. & Hermansson, A. The immune system in atherosclerosis. *Nature immunology* **12**, 204-212 (2011).
44. Weber, C., Zernecke, A. & Libby, P. The multifaceted contributions of leukocyte subsets to atherosclerosis: lessons from mouse models. *Nature reviews. Immunology* **8**, 802-815 (2008).
45. Moore, K.J. & Tabas, I. Macrophages in the pathogenesis of atherosclerosis. *Cell* **145**, 341-355 (2011).
46. Ross, R. & Harker, L. Hyperlipidemia and atherosclerosis. *Science* **193**, 1094-1100 (1976).
47. Ross, R., Glomset, J. & Harker, L. Response to injury and atherogenesis. *The American journal of pathology* **86**, 675-684 (1977).

48. Bjorkbacka, H., *et al.* Reduced atherosclerosis in MyD88-null mice links elevated serum cholesterol levels to activation of innate immunity signaling pathways. *Nature medicine* **10**, 416-421 (2004).
49. Michelsen, K.S., *et al.* Lack of Toll-like receptor 4 or myeloid differentiation factor 88 reduces atherosclerosis and alters plaque phenotype in mice deficient in apolipoprotein E. *Proceedings of the National Academy of Sciences of the United States of America* **101**, 10679-10684 (2004).
50. Fiuza, C., *et al.* Inflammation-promoting activity of HMGB1 on human microvascular endothelial cells. *Blood* **101**, 2652-2660 (2003).
51. Guo, J., *et al.* Transplantation of monocyte CC-chemokine receptor 2-deficient bone marrow into ApoE3-Leiden mice inhibits atherogenesis. *Arteriosclerosis, thrombosis, and vascular biology* **23**, 447-453 (2003).
52. Llovera, G., *et al.* The choroid plexus is a key cerebral invasion route for T cells after stroke. *Acta neuropathologica* **134**, 851-868 (2017).
53. Zhu, Y., Liao, H.L., Lin, J.H., Verna, L. & Stemerman, M.B. Low-density lipoprotein augments interleukin-1-induced vascular adhesion molecule expression in human endothelial cells. *Atherosclerosis* **144**, 357-365 (1999).
54. van Dinther-Janssen, A.C., *et al.* The VLA-4/VCAM-1 pathway is involved in lymphocyte adhesion to endothelium in rheumatoid synovium. *J Immunol* **147**, 4207-4210 (1991).
55. Meerschaert, J. & Furie, M.B. The adhesion molecules used by monocytes for migration across endothelium include CD11a/CD18, CD11b/CD18, and VLA-4 on monocytes and ICAM-1, VCAM-1, and other ligands on endothelium. *Journal of immunology* **154**, 4099-4112 (1995).
56. Woollard, K.J. & Geissmann, F. Monocytes in atherosclerosis: subsets and functions. *Nature reviews. Cardiology* **7**, 77-86 (2010).
57. Serbina, N.V. & Pamer, E.G. Monocyte emigration from bone marrow during bacterial infection requires signals mediated by chemokine receptor CCR2. *Nature immunology* **7**, 311-317 (2006).
58. Shi, C. & Pamer, E.G. Monocyte recruitment during infection and inflammation. *Nature reviews. Immunology* **11**, 762-774 (2011).
59. Ziegler-Heitbrock, L. The CD14⁺ CD16⁺ blood monocytes: their role in infection and inflammation. *Journal of leukocyte biology* **81**, 584-592 (2007).
60. Rajavashisth, T.B., *et al.* Induction of endothelial cell expression of granulocyte and macrophage colony-stimulating factors by modified low-density lipoproteins. *Nature* **344**, 254-257 (1990).
61. Robbins, C.S., *et al.* Local proliferation dominates lesional macrophage accumulation in atherosclerosis. *Nature medicine* **19**, 1166-1172 (2013).
62. Moulton, K.S., *et al.* Inhibition of plaque neovascularization reduces macrophage accumulation and progression of advanced atherosclerosis. *Proceedings of the National Academy of Sciences of the United States of America* **100**, 4736-4741 (2003).
63. Newby, A.C. Dual role of matrix metalloproteinases (matrixins) in intimal thickening and atherosclerotic plaque rupture. *Physiological reviews* **85**, 1-31 (2005).
64. Moore, K.J., Sheedy, F.J. & Fisher, E.A. Macrophages in atherosclerosis: a dynamic balance. *Nature reviews. Immunology* **13**, 709-721 (2013).
65. Galkina, E. & Ley, K. Immune and inflammatory mechanisms of atherosclerosis (*). *Annual review of immunology* **27**, 165-197 (2009).
66. Zhou, X., Nicoletti, A., Elhage, R. & Hansson, G.K. Transfer of CD4(+) T cells aggravates atherosclerosis in immunodeficient apolipoprotein E knockout mice. *Circulation* **102**, 2919-2922 (2000).
67. Hansson, G.K., Robertson, A.K. & Soderberg-Naucler, C. Inflammation and atherosclerosis. *Annual review of pathology* **1**, 297-329 (2006).
68. Robertson, A.K. & Hansson, G.K. T cells in atherogenesis: for better or for worse? *Arteriosclerosis, thrombosis, and vascular biology* **26**, 2421-2432 (2006).
69. Koltsova, E.K., *et al.* Dynamic T cell-APC interactions sustain chronic inflammation in atherosclerosis. *The Journal of clinical investigation* **122**, 3114-3126 (2012).

70. Frostegard, J., *et al.* Cytokine expression in advanced human atherosclerotic plaques: dominance of pro-inflammatory (Th1) and macrophage-stimulating cytokines. *Atherosclerosis* **145**, 33-43 (1999).
71. Roselaar, S.E., Kakkanathu, P.X. & Daugherty, A. Lymphocyte populations in atherosclerotic lesions of apoE *-/-* and LDL receptor *-/-* mice. Decreasing density with disease progression. *Arteriosclerosis, thrombosis, and vascular biology* **16**, 1013-1018 (1996).
72. Tedgui, A. & Mallat, Z. Cytokines in atherosclerosis: pathogenic and regulatory pathways. *Physiological reviews* **86**, 515-581 (2006).
73. Gupta, S., *et al.* IFN-gamma potentiates atherosclerosis in ApoE knock-out mice. *The Journal of clinical investigation* **99**, 2752-2761 (1997).
74. Hauer, A.D., *et al.* Blockade of interleukin-12 function by protein vaccination attenuates atherosclerosis. *Circulation* **112**, 1054-1062 (2005).
75. Buono, C., *et al.* T-bet deficiency reduces atherosclerosis and alters plaque antigen-specific immune responses. *Proceedings of the National Academy of Sciences of the United States of America* **102**, 1596-1601 (2005).
76. Eid, R.E., *et al.* Interleukin-17 and interferon-gamma are produced concomitantly by human coronary artery-infiltrating T cells and act synergistically on vascular smooth muscle cells. *Circulation* **119**, 1424-1432 (2009).
77. Ait-Oufella, H., *et al.* Natural regulatory T cells control the development of atherosclerosis in mice. *Nature medicine* **12**, 178-180 (2006).
78. Ait-Oufella, H., *et al.* B cell depletion reduces the development of atherosclerosis in mice. *The Journal of experimental medicine* **207**, 1579-1587 (2010).
79. Binder, C.J., *et al.* IL-5 links adaptive and natural immunity specific for epitopes of oxidized LDL and protects from atherosclerosis. *The Journal of clinical investigation* **114**, 427-437 (2004).
80. Novikova, D.S., Popkova, T.V. & Nasonov, E.L. The effect of anti-B-cell therapy on the development of atherosclerosis in patients with rheumatoid arthritis. *Current pharmaceutical design* **18**, 1512-1518 (2012).
81. Nilsson, J., Hansson, G.K. & Shah, P.K. Immunomodulation of atherosclerosis: implications for vaccine development. *Arteriosclerosis, thrombosis, and vascular biology* **25**, 18-28 (2005).
82. Getz, G.S. & Reardon, C.A. Animal models of atherosclerosis. *Arteriosclerosis, thrombosis, and vascular biology* **32**, 1104-1115 (2012).
83. Goldstein, J.L. & Brown, M.S. The LDL receptor. *Arteriosclerosis, thrombosis, and vascular biology* **29**, 431-438 (2009).
84. Wouters, K., Shiri-Sverdlov, R., van Gorp, P.J., van Bilsen, M. & Hofker, M.H. Understanding hyperlipidemia and atherosclerosis: lessons from genetically modified apoE and ldlr mice. *Clinical chemistry and laboratory medicine* **43**, 470-479 (2005).
85. Ishibashi, S. [LDL-receptor-related protein]. *Nihon rinsho. Japanese journal of clinical medicine* **52**, 3177-3183 (1994).
86. Plump, A.S., *et al.* Severe hypercholesterolemia and atherosclerosis in apolipoprotein E-deficient mice created by homologous recombination in ES cells. *Cell* **71**, 343-353 (1992).
87. van Ree, J.H., *et al.* Diet-induced hypercholesterolemia and atherosclerosis in heterozygous apolipoprotein E-deficient mice. *Atherosclerosis* **111**, 25-37 (1994).
88. Gough, P.J., Gomez, I.G., Wille, P.T. & Raines, E.W. Macrophage expression of active MMP-9 induces acute plaque disruption in apoE-deficient mice. *The Journal of clinical investigation* **116**, 59-69 (2006).
89. Sato, K., *et al.* Dietary cholesterol oxidation products accelerate plaque destabilization and rupture associated with monocyte infiltration/activation via the MCP-1-CCR2 pathway in mouse brachiocephalic arteries: therapeutic effects of ezetimibe. *Journal of atherosclerosis and thrombosis* **19**, 986-998 (2012).
90. Hug, A., *et al.* Infarct volume is a major determiner of post-stroke immune cell function and susceptibility to infection. *Stroke* **40**, 3226-3232 (2009).
91. Lotze, M.T. & Tracey, K.J. High-mobility group box 1 protein (HMGB1): nuclear weapon in the immune arsenal. *Nature reviews. Immunology* **5**, 331-342 (2005).
92. Burn, J., *et al.* Long-term risk of recurrent stroke after a first-ever stroke. The Oxfordshire Community Stroke Project. *Stroke* **25**, 333-337 (1994).

6 ACKNOWLEDGEMENTS

I would deeply like to thank all the people who helped me and contributed to the completion of my thesis.

First and most importantly, I like to thank my supervisors PD Dr. Arthur Liesz and PD Dr. Christof Haffner. I am very thankful for the great guidance, motivation and patience during the last years. They always provided me an open door and time for fruitful discussions about our projects. I appreciated their trust in me and the given possibility to expand my horizon in the field of neuroscience, immunology and vascular diseases. I am grateful for the opportunity they gave me to work together with them in such a stimulating, scientific environment.

A special thanks to Prof. Dr. Martin Dichgans for the possibility to work in the Institute for Stroke and Dementia Research, which provided me opportunity to get to know great scientists and magnificent colleagues which showed and taught me a plethora of techniques and new ideas.

I am happy to acknowledge my collaboration partners (Lisa Schindler & Jürgen Bernhagen, Steffen Tiedt & Martin Dichgans, Antoine Anfray, Antoine Fournier, Maxime Gauberti, Cyrille Orset and Denis Vivien, Daniel J. Antoine, Georg Huber and Arie Geerlof, Marco Bianchi, Helena Erlandsson Harris, Britta Engelhardt) for providing critical input, precious data and teaching me new techniques. They made this project possible and successful.

There are not enough words to thank every single member in the Lab for Stroke Immunology:

I am very thankful to Arthur who gave me the opportunity to become a member of his Lab – his guidance and scientific curiosity gave me the possibility to work on various great projects in the last years.

Special thanks to Kerstin for all the support she gave me, for her helping hands at the bench which made laboratory work much easier, her advice and daily encouragement.

Thanks to Gemma, with whom I started at ISD and enjoyed daily lab work within the last 5 years. Thanks to Vikram, Julia, Becky, Jun, Steffi and Corinne, my colleagues and friends in the lab for stroke immunology.

I would like to express my deepest gratitude to my colleagues Matilde, Farida and Thanasis without their critical input, guidance, knowhow in techniques, motivation and most importantly, their friendship I would not have been able to finish this thesis.

I want to thank all my dear colleagues in the laboratories of the Center for Stroke and Dementia in Munich for their help, knowhow, guidance and support.

Special thanks to Uta, Barbara, Melanie and Natalie who gave me a lot of technical support and their great help in daily laboratory routine.

Thanks to the animal facility of the ISD/CSD (Dr. Manuela Schneider, Dr. Anne von Thaden, Peggy Kunath, Stefanie Wurster and Tamara Voss) for their help with the experimental animal work and management of my mice lines.

I am grateful to my friends and colleagues Josh, Andreas, Severin, Carmelo, Steffen, Matthias, Yaw, Lee, Kathrin, Burcu and Rainer for conversations in a coffee break, their motivation and support.

Thanks to my beloved parents and my brother. I am thankful for their support, motivation and love. Without them, nothing would have been possible.

Thanks to my friends Benni, Tino, Hannes, Jens, Thomas, Ecki, Felix and Jurek for supporting me and reminding me that there is a world outside the lab.

And last but definitely not least, there is not enough space to express the gratefulness and love to my partner, my friend, my wife, and the loving mother of our little Maja, Sabine. Thank you for giving me new perspectives and having the patience to discuss with me about my work. Thank you for understanding my scientific ambition and the weird working hours which come with that.